

## THE SDSS-III BARYON OSCILLATION SPECTROSCOPIC SURVEY: QUASAR TARGET SELECTION FOR DATA RELEASE NINE

NICHOLAS P. ROSS<sup>1,2</sup>, ADAM D. MYERS<sup>3,4</sup>, ERIN S. SHELDON<sup>5</sup>, CHRISTOPHE YÈCHE<sup>6</sup>, MICHAEL A. STRAUSS<sup>7</sup>, JO BOVY<sup>8</sup>,  
JESSICA A. KIRKPATRICK<sup>1,9</sup>, GORDON T. RICHARDS<sup>10</sup>, ÉRIC AUBOURG<sup>6,11</sup>, MICHAEL R. BLANTON<sup>8</sup>, W. N. BRANDT<sup>2</sup>,  
WILLIAM C. CARITHERS<sup>1</sup>, RUPERT A.C. CROFT<sup>12</sup>, ROBERT DA SILVA<sup>13</sup>, KYLE DAWSON<sup>14</sup>, DANIEL J. EISENSTEIN<sup>15,16</sup>,  
JOSEPH F. HENNAWI<sup>17</sup>, SHIRLEY HO<sup>1</sup>, DAVID W. HOGG<sup>8</sup>, KHEE-GAN LEE<sup>7</sup>, BRITT LUNDGREN<sup>18</sup>, RICHARD G. MCMAHON<sup>19</sup>,  
JORDI MIRALDA-ESCUDE<sup>20,21</sup>, NATHALIE PALANQUE-DELABROUILLE<sup>6</sup>, ISABELLE PÂRIS<sup>22</sup>, PATRICK PETITJEAN<sup>22</sup>, MATTHEW  
M. PIERI<sup>23,24</sup>, JAMES RICH<sup>6</sup>, NATALIE A. ROE<sup>1</sup>, DAVID SCHIMINOVICH<sup>25</sup>, DAVID J. SCHLEGEL<sup>1</sup>, DONALD P. SCHNEIDER<sup>2</sup>,  
ANŽE SLOSAR<sup>5</sup>, NAO SUZUKI<sup>1</sup>, JEREMY L. TINKER<sup>1,8</sup>, DAVID H. WEINBERG<sup>23</sup>, ANYA WEYANT<sup>26</sup>, MARTIN WHITE<sup>1,9</sup>, W.  
MICHAEL WOOD-VASEY<sup>26</sup>

(Dated: October 8, 2018)  
Draft version October 8, 2018

### ABSTRACT

The SDSS-III Baryon Oscillation Spectroscopic Survey (BOSS), a five-year spectroscopic survey of 10,000 deg<sup>2</sup>, achieved first light in late 2009. One of the key goals of BOSS is to measure the signature of baryon acoustic oscillations in the distribution of Ly $\alpha$  absorption from the spectra of a sample of  $\sim 150,000$   $z > 2.2$  quasars. Along with measuring the angular diameter distance at  $z \approx 2.5$ , BOSS will provide the first direct measurement of the expansion rate of the Universe at  $z > 2$ . One of the biggest challenges in achieving this goal is an efficient target selection algorithm for quasars in the redshift range  $2.2 < z < 3.5$ , where their colors tend to overlap those of the far more numerous stars. During the first year of the BOSS survey, quasar target selection methods were developed and tested to meet the requirement of delivering at least 15 quasars deg<sup>-2</sup> in this redshift range, with a goal of 20, out of 40 targets deg<sup>-2</sup> allocated to the quasar survey. To achieve these surface densities, the magnitude limit of the quasar targets was set at  $g \leq 22.0$  or  $r \leq 21.85$ . While detection of the BAO signature in the distribution of Ly $\alpha$  absorption in quasar spectra does not require a uniform target selection algorithm, many other astrophysical studies do. We have therefore defined a uniformly-selected subsample of 20 targets deg<sup>-2</sup>, for which the selection efficiency is just over 50% ( $\sim 10$   $z > 2.20$  quasars deg<sup>-2</sup>). This “CORE” subsample will be fixed for Years Two through Five of the survey. For the remaining 20 targets deg<sup>-2</sup>, we will continue to develop improved selection techniques, including the use of additional data sets beyond the SDSS imaging data. In this paper we describe the evolution and implementation of the BOSS quasar target selection algorithms during the first two years of BOSS operations (through July 2011), in support of the science investigations based on these data, and we analyze the spectra obtained during the first year. During this year, 11,263 new  $z > 2.20$  quasars were spectroscopically confirmed by the BOSS, roughly double the number of previously known quasars with  $z > 2.20$ . Our current algorithms select an average of 15  $z > 2.20$  quasars deg<sup>-2</sup> from 40 targets deg<sup>-2</sup> using single-epoch SDSS imaging. Multi-epoch optical data and data at other wavelengths can further improve the efficiency and completeness of BOSS quasar target selection.

*Subject headings:* surveys - quasars: Lyman- $\alpha$  forest, cosmology: classification techniques

Electronic address: npross@lbl.gov

<sup>1</sup> Lawrence Berkeley National Laboratory, 1 Cyclotron Road, Berkeley, CA 92420, USA

<sup>2</sup> Department of Astronomy and Astrophysics, The Pennsylvania State University, 525 Davey Laboratory, University Park, PA 16802, USA

<sup>3</sup> Department of Astronomy, MC-221, University of Illinois, 1002 West Green Street, Urbana, IL 61801, USA

<sup>4</sup> Department of Physics and Astronomy, University of Wyoming, Laramie, WY 82071, USA

<sup>5</sup> Brookhaven National Laboratory, Bldg 510, Upton, NY 11375, USA

<sup>6</sup> CEA, Centre de Saclay, IRFU, 91191 Gif-sur-Yvette, France

<sup>7</sup> Department of Astrophysical Sciences, Princeton University, Princeton, NJ 08544, USA

<sup>8</sup> Center for Cosmology and Particle Physics, New York University, 4 Washington Place, New York, NY 10003, USA

<sup>9</sup> Department of Physics, 366 LeConte Hall, University of California, Berkeley, CA 94720, USA

<sup>10</sup> Department of Physics, Drexel University, 3141 Chestnut Street, Philadelphia, PA 19104, U.S.A

<sup>11</sup> APC, Université Paris Diderot-Paris 7, CNRS/IN2P3, CEA,

Observatoire de Paris, 10, rue A. Domon & L. Duquet, Paris, France.

<sup>12</sup> Bruce and Astrid McWilliams Center for Cosmology, Carnegie Mellon University, Pittsburgh, PA 15213, USA

<sup>13</sup> Department of Astronomy & Astrophysics, University of California, Santa Cruz, Santa Cruz, CA, 95064, USA

<sup>14</sup> Department of Physics and Astronomy, University of Utah, UT, USA

<sup>15</sup> Steward Observatory, 933 North Cherry Avenue, Tucson, AZ 85721, USA

<sup>16</sup> Harvard College Observatory, 60 Garden St., Cambridge, MA 02138, USA

<sup>17</sup> Max-Planck-Institut für Astronomie, Königstuhl 17, 69117 Heidelberg, Germany

<sup>18</sup> Department of Physics, Yale University, New Haven, CT 06511, USA

<sup>19</sup> Institute of Astronomy, University of Cambridge, Madingley Road, Cambridge CB3 0HA, UK

<sup>20</sup> Institutió Catalana de Recerca i Estudis Avançats, Barcelona, Catalonia, Spain

<sup>21</sup> Institut de Ciències del Cosmos, Universitat de

## 1. INTRODUCTION

1.1. *The Baryon Oscillation Spectroscopic Survey*

The current Cosmic Microwave Background (CMB) data are in excellent agreement with the theoretical predictions of a flat cosmological model with cold dark matter which is dominated by dark energy with an equation of state parameter,  $w = -1$  ( $\Lambda$ CDM; Komatsu et al. 2011; Larson et al. 2011). Acoustic peaks in the CMB anisotropy power spectrum are generated by cosmological perturbations exciting sound waves in the relativistic plasma of the early universe (Sunyaev & Zeldovich 1970; Peebles & Yu 1970; Bond & Efstathiou 1984, 1987; Holtzman 1989; Meiksin et al. 1999). The scale of these peaks, which is set by the sound horizon at last scattering (Eisenstein & Hu 1998; Blake & Glazebrook 2003; Seo & Eisenstein 2003), can be used as a cosmological standard ruler. These baryon acoustic oscillations (BAO) are present in the distribution of matter at late times as well, and were first measured in the large-scale distribution of galaxies by Eisenstein et al. (2005) and Cole et al. (2005).

BAO should also be present in the distribution of neutral hydrogen gas in the intergalactic medium, and thus should be observable in the Lyman- $\alpha$  forest (Ly $\alpha$ F) absorption spectra of distant quasars (White 2003; McDonald & Eisenstein 2007; Slosar et al. 2009; Norman et al. 2009; Barenboim et al. 2010; White et al. 2010; McQuinn & White 2011). Measurements of BAO in the Ly $\alpha$ F would provide the first measurements of cosmic expansion and the angular diameter distance at redshift  $z > 2$  (other than the CMB itself), a regime not constrained by current data, thus giving important constraints on, and tests of, the standard cosmological model.

The Sloan Digital Sky Survey (York et al. 2000) is now in its third phase (SDSS-III; Eisenstein et al. 2011), and is carrying out a combination of four interleaved surveys that will continue until the summer of 2014. One of those surveys, the Baryon Oscillation Spectroscopic Survey (BOSS<sup>27</sup>) commenced operations in late 2009, and is using essentially all the dark time for SDSS-III. The key goal of the BOSS is to measure the absolute cosmic distance scale and expansion rate to an accuracy of a few percent from the signature of BAO in the distribution of galaxies and neutral hydrogen (Schlegel et al. 2007, 2009). This will be achieved by measuring spectroscopic redshifts for  $\approx 1.5$  million luminous red galaxies and, simultaneously, the Ly $\alpha$ F towards  $\approx 150,000$  high-redshift quasars<sup>28</sup>. Both samples aim to constrain the equation

| Quantity/units                                | Year One | Full Survey*   |
|---|----------|----------------|
| Area (deg <sup>2</sup> )                      | 880      | 10,200         |
| Target density in NGC (deg <sup>-2</sup> )    | 80       | $\approx 50$   |
| Target density in SGC (deg <sup>-2</sup> )    | 70       | $\approx 40$   |
| Total number of Targets / $1 \times 10^3$     | 133      | $\sim 440$     |
| Efficiency                                    | 0.26     | $\gtrsim 0.40$ |
| Number of $z > 2.2$ quasars / $1 \times 10^3$ | 13.5     | 175            |

TABLE 1

\*PROJECTION BASED ON OBSERVATIONS THROUGH APRIL 2011 AND DR9 TARGET SELECTION.

of state of dark energy by measuring the angular diameter distance,  $d_A$ , and the Hubble Parameter,  $H(z)$ , at  $z = 0.3, 0.6$  and  $\sim 2.5$ . In addition to the cosmology goals, the unprecedented dataset of  $z \sim 2.5$  quasars will enable tests of black hole growth, wind and feedback models and provide insights into the links between galaxy formation, evolution and luminous AGN activity. Using data from the original SDSS quasar survey will also allow studies of spectroscopic variability. BOSS uses the same 2.5m Sloan Foundation telescope (Gunn et al. 2006) that was used in SDSS-I/II, but since BOSS will observe fainter targets, the fiber-fed spectrographs have been significantly upgraded. These upgrades include: new CCDs with improved blue and red response; 1000 2" instead of 640 3" optical diameter fibers; higher throughput gratings over a spectral range of 3600–10000Å at a resolution of about 2000, and improved optics.

1.2. *Quasar Target Selection in BOSS*

Quasars have colors distinct from those of the much more numerous stars in the five-color photometry of the SDSS (Fan 1999). Unobscured quasars have very blue continua, without any breaks redward of the Ly $\alpha$  emission line, and so can be distinguished from hot stars which have a strong Balmer break in the  $u - g, g - r$  color-color diagram (Figure 1). In particular, at  $z < 2.2$ , quasars have a UV excess (as measured by  $u - g$ ) that distinguishes them from most stars, and they lie well away from the stellar locus at most higher redshifts (but see below). SDSS-I/II targeted quasars for spectroscopy (Richards et al. 2002) by selecting point sources which lie far from the locus of stars in color-color space (and all extended sources with a strong UV excess), as well as point sources with radio emission from the Faint Radio Sources at Twenty cm (FIRST) survey (Becker et al. 1995). The majority of the more than 100,000 quasars spectroscopically observed by SDSS (Schneider et al. 2010) were targeted in this way.

The Ly $\alpha$  forest enters the sensitive range of the BOSS spectrographs at  $z > 2.2$ , and the number density of quasars falls dramatically at  $z > 3$  (Osmer 1982; Schmidt et al. 1995; Richards et al. 2006), so BOSS quasar target selection is designed to focus on the range  $2.2 < z < 3.5$ . However, at  $z \sim 2.7$ , SDSS quasar colors are very similar to those of A stars and blue horizontal branch stars (Fan 1999), thus the optimal quasars for studying the Ly $\alpha$  forest are the most difficult ones for BOSS to target. Indeed, the SDSS-I/II quasar target selection algorithm deliberately sparse-sampled objects in the region of color space where  $z = 2.7$  quasars should lie (Richards et al. 2002), in an attempt to minimize the contamination by

Barcelona/IEEC, Barcelona 08028, Catalonia, Spain

<sup>22</sup> Université Paris 6 et CNRS, Institut d'Astrophysique de Paris, 98bis blvd. Arago, 75014 Paris, France

<sup>23</sup> Astronomy Department and Center for Cosmology and AstroParticle Physics, Ohio State University, 140 West 18th Avenue, Columbus, OH 43210, USA

<sup>24</sup> Center for Astrophysics and Space Astronomy, University of Colorado, 389 UCB, Boulder, CO 80309, USA

<sup>25</sup> Department of Astronomy, Columbia University, 550 West 120th Street, New York, NY 10027, USA

<sup>26</sup> Department of Physics and Astronomy, University of Pittsburgh, 100 Allen Hall, 3941 O'Hara St, Pittsburgh PA 15260, USA

<sup>27</sup> <http://www.sdss3.org/surveys/boss.php>

<sup>28</sup> In this paper we will use the language "low" and "high" redshift to indicate objects with  $z < 2.2$  and  $z > 2.2$ , respectively. The term "mid- $z$ " will be used to explicitly refer to quasars with  $2.2 < z < 3.5$ .

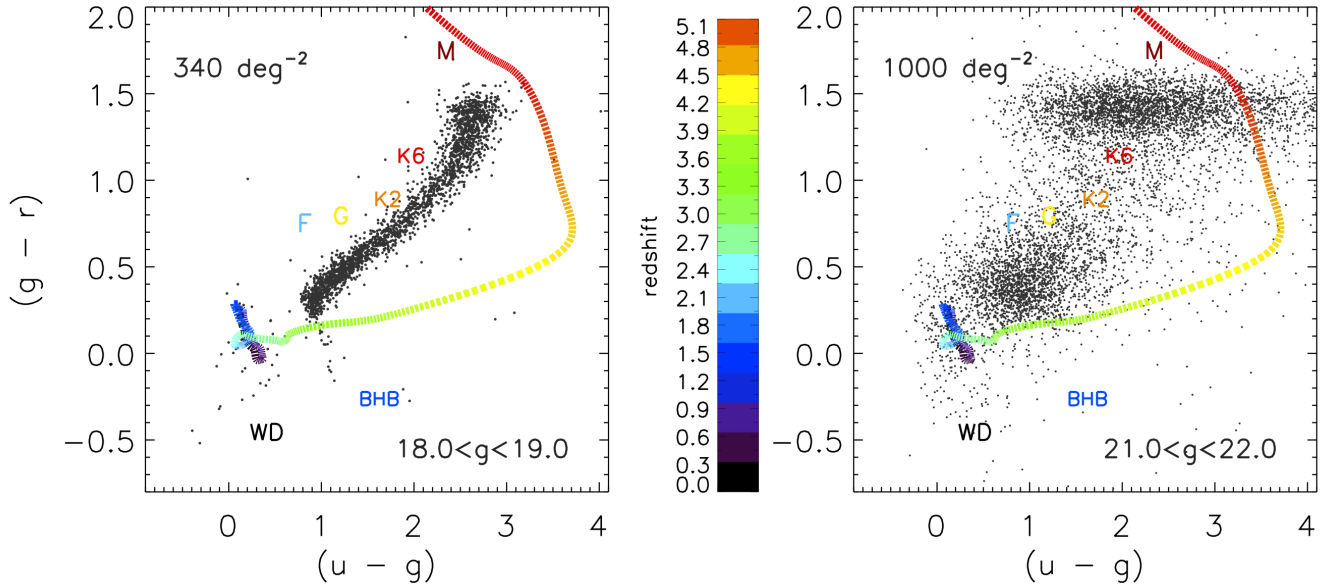


FIG. 1.— Color-color diagrams of point sources drawn from  $7 \text{ deg}^2$  (the BOSS spectrograph field of view) in the SDSS photometric database. (Left) 2,400 objects with  $18.0 < g < 19.0$ , and (Right) 7,000 objects with  $21.0 < g < 22.0$ . Most of the objects shown are stars; low-redshift ( $z < 2.2$ ) quasars lie preferentially in the region  $u - g < 0.6, g - r > 0$  where very few stars are found. At  $z > 2.2$ , quasars become systematically redder in  $u - g$  as the Ly $\alpha$  forest moves into the  $u$ -band and Ly $\alpha$  emission moves into  $g$ . At  $z \sim 2.7$ , quasars have colors similar to those of blue horizontal branch (BHB) stars. The larger photometric errors at faint magnitudes broaden the stellar locus considerably (especially in the  $u$ -band for the reddest stars, which gives rise to the spread at  $g - r \sim 1.5$ ), illustrating the challenges involved in selecting faint objects by their colors. Tracks for the quasar locus, as presented in Bovy et al. (2011b, in prep.) are also shown, with the corresponding redshift given by the color-bar legend. Approximate surface densities are quoted, and stellar classifications are given as a guide.

stars.

The BOSS survey requirements are for spectroscopy of 15 or more  $z > 2.2$  quasars  $\text{deg}^{-2}$  (150,000 quasars over the BOSS footprint of  $10,000 \text{ deg}^2$ ; Eisenstein et al. 2011). Combining calculations from McDonald & Eisenstein (2007) and McQuinn & White (2011) with the luminosity function given by Jiang et al. (2006), we find that targeting to a magnitude of  $g < 22$  with perfect completeness will provide a surface density of 20  $z > 2.2$  quasars  $\text{deg}^{-2}$ . This magnitude limit is approaching the detection limit of SDSS photometry (Abazajian et al. 2004), meaning that photometric errors will significantly broaden the stellar locus (Figure 1) and star-galaxy separation will be a factor. Contamination at both the bright and the faint end of the BOSS target range is mainly from metal-poor halo A and F stars, faint lower redshift ( $z \sim 0.8$ ) quasars, and compact galaxies. To put these requirements into perspective, the final quasar catalog from the original SDSS-I/II quasar survey (Schneider et al. 2010) contained 17,582  $z > 2.2$  objects over  $9380 \text{ deg}^2$ , while the 2dF-SDSS LRG And QSO (2SLAQ) survey (Croom et al. 2009), which observed to  $g < 21.85$  and concentrated on UV-excess objects, contained 1,110 such quasars selected over  $192 \text{ deg}^2$ . The original 2dF QSO redshift survey (2QZ; Croom et al. 2004) focused on the redshift range  $z < 2.1$ .

These challenges required a new approach to quasar target selection. The first year of the BOSS survey (“Year One”; 2009 September through July 2010) was devoted in part to refining our algorithms for selecting these objects. The resulting sample of quasars at  $z > 2.2$  is comparable in size to the SDSS high-redshift quasar

sample, and of course reaches much fainter magnitudes with much higher surface density. Thus the new sample itself represents the best test of our selection algorithms, and we modified those algorithms multiple times through the year. Year One included roughly three months of commissioning of the upgraded BOSS spectrographs and instrument control software as well as a steady ramp-up to full efficiency operations, so it includes well under 20% of the anticipated final sample for the five-year BOSS survey. As of April 2011, BOSS is on track to complete its intended  $10,000 \text{ deg}^2$  of spectroscopic survey area assuming historical weather patterns and continuation of the current observing efficiency.

Motivated by the first science investigations based on Year One data (e.g., Slosar et al. 2011), this paper presents the methods and performance of the quasar target selection during this year. In what follows, “Year Two” will refer both to the spectroscopic observations carried out during BOSS’ second year, 2010 August to 2011 July, and the results of the quasar target selection presented in this paper over the entire  $10,000 \text{ deg}^2$  BOSS footprint; the distinction should be clear from context. Data from spectroscopic observations in Years One and Two will be included in SDSS Data Release Nine (DR9<sup>29</sup>). The final SDSS-III quasar target selection algorithm will appear in a separate paper.

Background quasars have no causal influence on structure in the Ly $\alpha$ F at the BAO scale<sup>30</sup>. Hence the sample

<sup>29</sup> <http://www.sdss3.org/surveys/>

<sup>30</sup> There may however be some measurement bias at the 0.1 – 1% level for the flux power spectrum, optical depth and the flux probability distribution, due to gravitational lensing effects, (see

of quasars we use for Ly $\alpha$ F cosmological studies may be quite heterogeneous, with the only consequence that the window function of the survey will depend on the distribution of the quasars for which we have spectra. Since the precision of the BAO measurement improves rapidly with the surface density of quasars (at fixed spectroscopic signal-to-noise ratio (S/N)), we have implemented a target selection scheme in BOSS that can maximize the number of quasars found at  $z > 2.2$  in any area of the sky, taking advantage of any available information (e.g., auxiliary data). In Year One, we explored a variety of methods, settling on our final target selection algorithms late in the year.

At the same time, in order to use the quasars themselves for statistical studies (such as luminosity functions or clustering analyses), we must also produce a uniformly selected sample, which we refer to hereafter as CORE (§ 3.1). However, we changed the definition of the CORE sample several times over Year One, as we tested various algorithms. Therefore, our fully uniform quasar sample will not include data from this first year of the survey. However, statistical studies (luminosity functions, clustering, and so forth) can utilize all five years of BOSS data by including moderate incompleteness corrections for Year One selection relative to the final CORE algorithm (see §6). We describe the evolution of our algorithms in detail in this paper, concluding with a description of the method we finally adopted. We give the target selection for both Years One and Two, and thus for the DR9, and analyze our performance from spectra obtained in Year One. By the end of Year Two, quasar target selection (QTS) had been performed over the whole 10,000 deg<sup>2</sup> BOSS footprint. Data from Year One were gathered over 880 deg<sup>2</sup>; see Table 1.

This paper is organized as follows. In § 2 we describe the SDSS photometry on which the target selection algorithms are most heavily based. Section 3 describes our methods for selecting quasars (Richards et al. 2009a; Yèche et al. 2010; Kirkpatrick et al. 2011; Bovy et al. 2011). These four papers suggest different, but complementary, methods, and we have used a union of these techniques in different combinations through the survey. In Section 4 we describe the implementation of these targeting methods through the first year. In Section 5, we report on the global properties of the resulting sample, including high- $z$  quasar targeting efficiency, from the data gathered during the first year of the BOSS, and we compare the effectiveness of the various methods. In Section 6 we discuss the production of a statistical quasar sample. We conclude in Section 7 and suggest improvements to BOSS quasar target selection for the remainder (Years Three, Four and Five) of the survey. Appendix A tabulates the logical cuts used on the input imaging data. Appendix B gives more detail about Year One target selection, while Appendix C describes a pre-BOSS pilot survey using the MMT. Appendix D characterizes the redshift completeness of our spectroscopic data.

We assume a cosmological model throughout with  $\Omega_b = 0.046$ ,  $\Omega_m = 0.228$ ,  $\Omega_\Lambda = 0.725$  (Komatsu et al. 2011). All optical magnitudes are quoted in, and based upon, the SDSS approximation to the AB zero-point system (Oke & Gunn 1983; Adelman-McCarthy et al. 2006),

e.g., Loverde et al. 2010).

while all near-infrared (NIR) magnitudes are based on the Vega system. Throughout the paper, “magnitude” refers to SDSS Point Spread Function (PSF) magnitudes (Stoughton et al. 2002).

## 2. SDSS PHOTOMETRY

### 2.1. Imaging Data

BOSS uses the same imaging data as that of the original SDSS-I/II survey, with an extension in the South Galactic Cap (SGC). These data were gathered using a dedicated 2.5 m wide-field telescope (Gunn et al. 2006) to collect light for a camera with 30 2k $\times$ 2k CCDs (Gunn et al. 1998) over five broad bands - *ugriz* (Fukugita et al. 1996); this camera has imaged 14,555 unique deg<sup>2</sup> of the sky, including 7,500 deg<sup>2</sup> in the North Galactic Cap (NGC) and 3,100 deg<sup>2</sup> in the SGC (Aihara et al. 2011). The imaging data were taken on dark photometric nights of good seeing (Hogg et al. 2001), and objects were detected and their properties were measured (Lupton et al. 2001; Stoughton et al. 2002) and calibrated photometrically (Smith et al. 2002; Ivezić et al. 2004; Tucker et al. 2006; Padmanabhan et al. 2008), and astrometrically (Pier et al. 2003).

Padmanabhan et al. (2008) present an algorithm which uses overlaps between SDSS imaging scans to photometrically calibrate the SDSS imaging data. BOSS target selection uses data calibrated using this algorithm from the SDSS Data Release Eight (DR8) database (Sec. 3.3; Aihara et al. 2011). The 2.5°-wide stripe along the celestial equator in the Southern Galactic Cap, commonly referred to as “Stripe 82” was imaged multiple times, with up to 80 epochs at each point along the stripe spanning a 10-year baseline (Abazajian et al. 2009). In Section 4 we will discuss how the commissioning phase of BOSS used coadded catalogs in SDSS Stripe 82, generated by averaging the photometric measurements from  $\sim 20$  individual repeat scans; the details are discussed in Appendix A.6 and in Kirkpatrick et al. (2011).

Roughly 50% of the SDSS footprint has been imaged more than once (Aihara et al. 2011); combining the photometric measurements in these overlap regions reduces the flux errors.

Using the imaging data, BOSS quasar target candidates are selected for spectroscopic observation based on their PSF fluxes and colors in SDSS bands. Fluxes that are used for quasar target selection are corrected for Galactic dust extinction according to the maps of Schlegel et al. (1998). All objects classified as point-like (OBJC\_TYPE = 6) and are brighter than  $g = 22$  or  $r = 21.85$  are passed to the various quasar target selection algorithms. The joint magnitude limit was imposed due to concerns of the Ly $\alpha$ F moving into the  $g$ -band at  $z \approx 2.3$  resulting in suppressed flux at redshifts greater than this. In practice, almost all our targets satisfy both these conditions. Throughout this paper, magnitudes use the asinh scale at low flux levels, as described by Lupton et al. (1999).

### 2.2. Photometric Pipeline Flag and Logic Cuts

During processing of the imaging data by the SDSS photometric pipeline, a number of photometric flags are set for each detected object (Stoughton et al. 2002). These are generated by the SDSS photometric pipeline



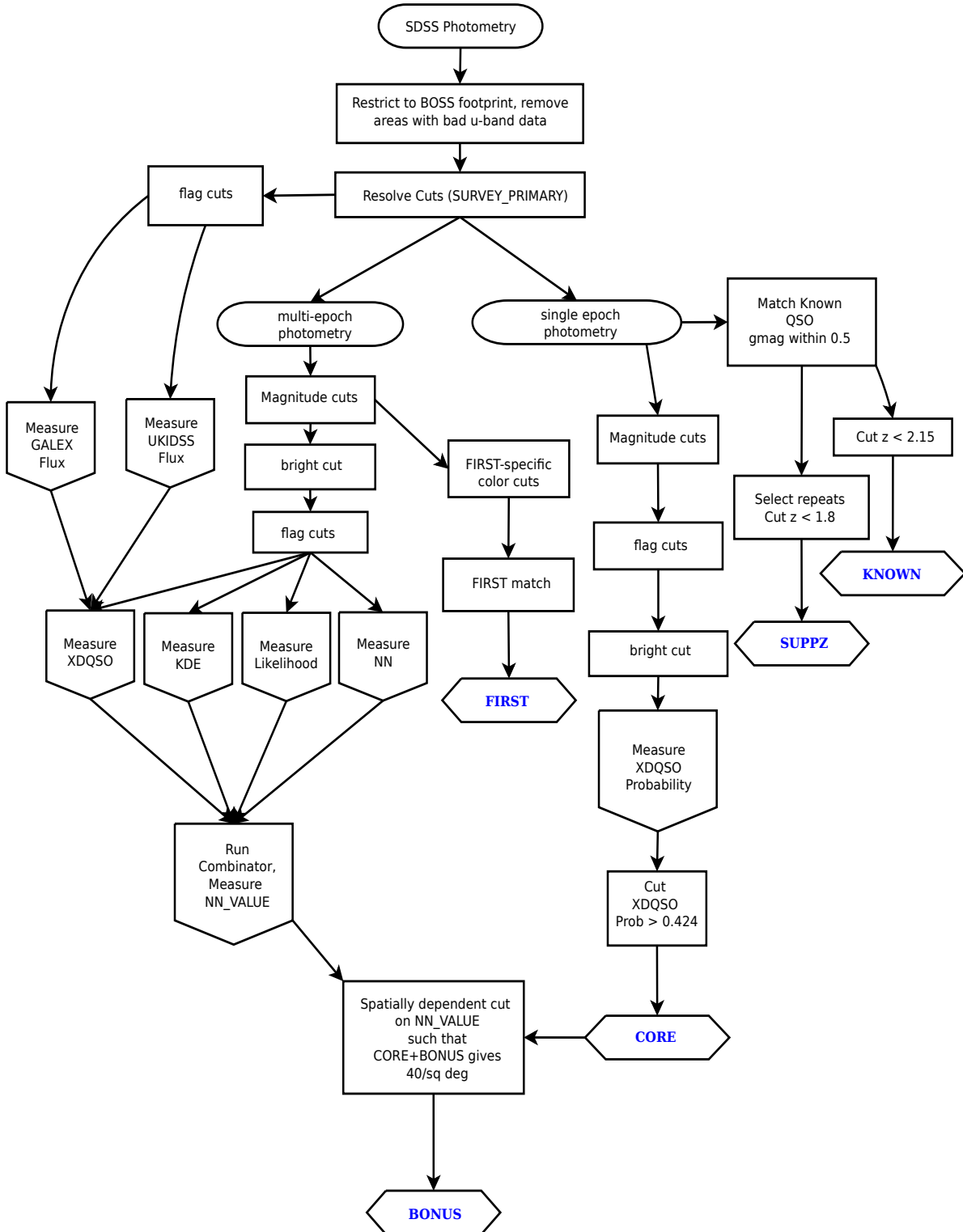


FIG. 2.— Flowchart for the BOSS quasar target selection, as implemented from the beginning of the second year of BOSS observations. The various broad categories of targets, including CORE, BONUS, KNOWN objects, and those detected by the FIRST survey, are indicated, and are described in detail in Section 3; SUPPZ refers to a small number of lower-redshift objects targeted to study the effects of metal line absorption (§ 4.6). The flowchart for the first year of BOSS target selection is given in Appendix B. The CORE sample is fixed for DR9 and the remainder of the BOSS. Objects which satisfy the XDQSO probability cut of  $P(XDQSO) > 0.424$  are selected as CORE, and the QSO\_CORE\_MAIN target flag bit is set. CORE selection is based on single-epoch SDSS photometry, but other selections use multi-epoch photometry where it is available (e.g., in regions where SDSS imaging stripes overlap).

(Lupton et al. 2001), the *Resolve* algorithm (Aihara et al. 2011), and by photometric calibration (Padmanabhan et al. 2008). Some of these flags indicate problems with the de-blending of close pairs of objects. Other flags are set due to poor or unreliable photometry, e.g., if an object was saturated due to a bright star’s diffraction spike or an object was too close to the edge of a frame. If these flags are ignored, they can lead to artifacts in the imaging data being selected as quasar targets. Details of these flags are given in Stoughton et al. (2002) and have been updated in DR8 (Aihara et al. 2011).

There are four distinct sets of quasars targeted by BOSS: targets selected by a uniform method, targets selected in a non-uniform way, matches to previously known  $z > 2.2$  quasars, and matches to objects in the FIRST survey. We refer to these subsets of targets in this paper as CORE, BONUS, KNOWN and FIRST, respectively.

Each of our targeting algorithms has different imaging flag cuts, as well as different flux limits imposed. We refer to these criteria collectively as “logic cuts.” All such cuts are applied using single-epoch data with one exception: color cuts made on FIRST targets use coadded, multi-epoch data wherever these are available. FIRST objects are thus not considered to be part of the CORE statistical sample, unless they independently meet the CORE selection criteria. The logic cuts are described in detail in Appendix A.

### 3. METHODS FOR BOSS QUASAR TARGET SELECTION

#### 3.1. *Philosophy of CORE and BONUS*

The methods, data and logic flag cuts for BOSS Quasar Target Selection (QTS) are summarized in Fig. 2. During Year One, we carried out QTS and designed spectroscopic plates on areas of  $\sim 100\text{--}300 \text{ deg}^2$  at a time. We refer to these areas, within which all the algorithms used in QTS are uniform, as “chunks”. Once QTS was more settled in Year Two, the areas of chunks could be, and sometimes were, more than  $1000 \text{ deg}^2$ . For guidance in the following discussion, Chunks 1 through 9, inclusive, constitute Year One, and Chunks 10 through 18, Year Two. Stripe 82 was targeted twice with different targeting algorithms: once in Year One (Chunk 1) and once in Year Two (Chunk 11).

If an object satisfies the selection criteria of one or more of our methods outlined below, bits in the BOSS.TARGET1 target flag are set. Table 2 gives the flag name, the bit value and the short description of the different target selection flags.

As discussed in the introduction, we wish to define a CORE sample that is uniformly selected over the BOSS footprint, for statistical studies of quasars, such as measurements of the luminosity function and the clustering of quasars. While these goals do not drive our technical requirements, the survey we have designed to measure the BAO signal will also provide an unprecedented spectroscopic dataset for studies of quasars themselves. Thus, design choices that are roughly neutral with regard to cost and impact on the cosmology goals are guided by these additional science considerations.

This is the motivation for dividing our quasar targets into two broad classes. Since the one (imaging) dataset

that we have over the entire BOSS footprint is the SDSS single-epoch photometry (including the new coverage in the SGC; Aihara et al. 2011), we define quasar CORE targets as a sample of  $20 \text{ targets deg}^{-2}$ , which are selected *only from this single-epoch imaging data, using a uniform algorithm*. As we shall see, the efficiency of the CORE sample is near our goal of 50% (i.e.  $\sim 10$  out of 20 CORE targets  $\text{deg}^{-2}$  are  $z > 2.2$  quasars). The CORE sample is designed to have a well understood, uniform, and reproducible selection function.

In contrast, the “BONUS” sample is selected using as many methods and additional data as deemed necessary to achieve our desired quasar density. The BONUS sample has a target density of  $20 \text{ deg}^{-2}$ . The number of BONUS targets added in each region of sky is adjusted to assure that the total density of targets, CORE + BONUS, is uniform across the sky, as we will show in § 4.7 below. However, as we detail below, the number of BONUS targets was extended up to  $60 \text{ targets deg}^{-2}$  (and then  $40 \text{ targets deg}^{-2}$ ), during the BOSS Commissioning and early science phases, for a total (CORE+BONUS) of  $80$  (and then  $60$ )  $\text{targets deg}^{-2}$ . The efficiency of BONUS selection is generally lower than that of CORE, despite the use of multiple algorithms and auxiliary data, simply because the relatively “easy” targets have already been picked by CORE and are therefore not included in BONUS.

Prior to BOSS, there was no extant survey that successfully targeted  $z > 2.2$  quasars to the depth and surface density and with the efficiency we needed. The first year of BOSS spectroscopy was therefore largely a commissioning year for quasar target selection, during which we gathered the quasar sample needed to test our various algorithms. In particular, it was only at the end of the year that we settled on the final CORE and BONUS algorithms. Thus, the nominal CORE-selected objects from the first year are *not* a uniformly selected sample. Sec. 6 describes the completeness of the final CORE sample in Year One spectroscopy.

Through this first year, we worked on and refined a variety of algorithms for BOSS target selection, as it was not clear from the outset that any single method could meet our scientific goals. These methods include:

- The Non-parametric Bayesian Classification and Kernel Density Estimator (KDE; Richards et al. 2004, 2009a), which measures the densities of quasars and stars in color-color space from training sets. Richards et al. (2009a) showed that this was able to identify quasars at  $2.2 < z < 3.5$  from SDSS photometry with an efficiency of  $46.4 \pm 5.8\%$ , down to a magnitude limit of  $i = 21.3$ , approximately  $\sim 0.5$  magnitudes brighter than the BOSS limit.
- A likelihood approach (Kirkpatrick et al. 2011), which determines the likelihood that each object is a quasar, given its photometry and models for the stellar and quasar loci.
- A Neural Network (NN) approach from Yèche et al. (2010), which takes as input the SDSS photometry and errors.
- A variant of the likelihood approach, which accounts for the observational errors more properly

| BOSS.TARGET1 flag                   | bit       | Description                               | Used in Year Two? |
|-------------------------------------|-----------|---|-------------------|
| QSO_CORE <sup>a</sup>               | 10        | Restrictive quasar selection              | No                |
| QSO_BONUS <sup>a</sup>              | 11        | Permissive quasar selection               | No                |
| QSO_KNOWN_MIDZ                      | 12        | Known quasar with $z > 2.15$              | Yes               |
| QSO_KNOWN_LOHIZ <sup>b</sup>        | 13        | Known quasar with $z < 2.15$              | Yes               |
| QSO_NN <sup>c</sup>                 | 14        | Neural Net                                | Yes               |
| QSO_UKIDSS <sup>d</sup>             | 15        | K-excess targets                          | No                |
| QSO_KDE.COADD                       | 16        | KDE targets from the Stripe82 coadd       | No                |
| QSO_LIKE                            | 17        | Likelihood method                         | Yes               |
| QSO_FIRST_BOSS                      | 18        | FIRST radio match                         | Yes               |
| QSO_KDE                             | 19        | Selected by KDE+ $\chi^2$                 | Yes               |
| <b>QSO_CORE_MAIN<sup>e</sup></b>    | <b>40</b> | <b>Main survey CORE sample</b>            | <b>Yes</b>        |
| <b>QSO_BONUS_MAIN<sup>e,f</sup></b> | <b>41</b> | <b>Main survey BONUS sample</b>           | <b>Yes</b>        |
| QSO_CORE_ED                         | 42        | Extreme Deconvolution in CORE             | Yes               |
| QSO_CORE_LIKE                       | 43        | Likelihood objects that make it into CORE | Yes               |
| QSO_KNOWN_SUPPZ                     | 44        | Known quasars with $1.80 < z < 2.15$      | Yes               |

TABLE 2

THE FLAG NAME, BIT VALUE AND THE SHORT DESCRIPTION OF THE DIFFERENT TARGET SELECTION FLAGS.

<sup>a</sup>QSO\_CORE AND QSO\_BONUS WERE SET ONLY FOR CHUNKS 1 AND 2, AFTER WHICH THE DEFINITION OF CORE AND BONUS CHANGED.

<sup>b</sup>THESE OBJECTS ARE NOT TARGETED.

<sup>c</sup>SET IF AN OBJECT IS SELECTED BY THE FIRST STAGE NEURAL NETWORK (§ 3.4).

<sup>d</sup>THESE OBJECTS WERE ONLY TARGETED ON CHUNK 1.

<sup>e</sup> QSO\_CORE\_MAIN AND QSO\_BONUS\_MAIN WERE INTRODUCED WITH CHUNK 3, AND IDENTIFY THE CORE AND BONUS SAMPLES. THEY APPEAR IN TANDEM WITH ANOTHER FLAG INDICATING THE SPECIFIC METHOD THAT SELECTED EACH OBJECT.

<sup>f</sup>SET IF AN OBJECT IS SELECTED BY THE NN-COMBINATOR.

when determining the stellar locus, called “Extreme Deconvolution” (XD; Bovy et al. 2009). Bovy et al. (2011) present full details on how the XD method can be used to describe a probabilistic quasar target selection technique, called “XDQSO”, that uses density estimation in flux space to assign quasar probabilities to all SDSS point sources. XDQSO was not used in Year One target selection, but it did become the CORE method in Year Two.

Each of the methods described above has one, or more, key parameters; these are summarized in Table 3, and Table 2 gives the associated bitwise target flags. We now describe each of these methods in turn, leaving the details for the cited papers. We also introduce a variant of the NN, the “Combined Neural Network” (a.k.a. the NN-Combinator), which incorporates information from all the methods and produces the BONUS sample. We also describe several ancillary methods of selection, including objects associated with FIRST radio sources (§ 3.6) and repeat observations of previously known  $z > 2.2$  quasars (§ 3.7).

### 3.2. Kernel Density Estimation and $\chi^2$ cuts

Gray & Moore (2003), Gray & Riegel (2006), and Riegel et al. (2008) describe the KDE classification scheme. Richards et al. (2004) and Richards et al. (2009a) have applied it to the SDSS imaging data to produce photometric quasar catalogs with  $\approx 10^6$  quasars. The principles of the KDE are as follows. A sample of objects of known classification (stars and quasars) serves as a training set, from which the smoothed distributions of quasar and star probability as a function of color are constructed. This allows one to compute the probability that any object of interest from the test set is a star, “KDE star density”, or quasar, “KDE quasar density” (e.g. Fig. 8 in Richards et al. 2009a). Based on these probabilities, we define the “KDE

probability” (see Fig. 2 and Table 3) as:

$$\text{KDE}_{Prob} = \frac{\text{KDE quasar density}}{\text{KDE quasar density} + \text{KDE star density}}, \quad (1)$$

which can be used to decide whether a given object should be targeted as a quasar. As described in Section 3.5 of Richards et al. (2009a), for our purposes, we define the quasar density just for those objects with  $2.2 < z < 3.5$ ; all other quasars are put into the “star” category.

Richards et al. (2004, 2009a) actually define two KDEs, split at  $g = 21$ , with separate color loci (different “trainings”) for the bright and faint estimations. This approach crudely accounts for the very different photometric errors of the two sets, given that the KDE method, as implemented, does not take errors explicitly into account.

Roughly 45% of objects in the KDE catalog of Richards et al. (2009a) in the “mid- $z$ ” range (i.e. the redshift range of interest to BOSS) are not stars (Table 4, Richards et al. 2009a), based on an analysis of the classification efficiency using clustering (e.g., Myers et al. 2006). In the absence of significant contamination by galaxies at the faint end of the KDE catalog, the KDE algorithm is thus about 45% efficient at the Richards et al. (2009a) target density of 18.6 mid- $z$  quasars  $\text{deg}^{-2}$ .

We need a higher efficiency for BOSS, so we have applied an additional cut beyond that of the Richards et al. papers to improve the efficiency of the KDE method. This cut is based on the  $\chi^2_{star}$  statistic introduced by Hennawi et al. (2010), which quantifies how far a given object is from the stellar locus:

$$\chi^2_{star} = \sum_{m=ugriz} \frac{[f_{data}^m - Af_{model}^m]^2}{[\sigma_{data}^m]^2 + A^2[\sigma_{model}^m]^2} \quad (2)$$

where  $f$  is the flux in each of the five SDSS bands ( $m = ugriz$ ) for the data and for the model,  $\sigma_{data}^m$  is the flux error in each band,  $\sigma_{model}^m$  is the model uncer-

| Method         | Key Parameter(s) | Variable name in target files | References                |
|----------------|------------------|-------------------------------|---------------------------|
| Likelihood     | $\mathcal{P}$    | LIKE_RATIO                    | Kirkpatrick et al. (2011) |
| KDE            | $KDE_{prob}$     | KDE_Prob                      | Richards et al. (2009a)   |
|                | $\chi_{star}^2$  | chi2_star                     | Hennawi et al. (2010)     |
| Neural Network | $y_{NN}$         | NN_XNN                        | Yèche et al. (2010)       |
|                | $z_{pNN}$        | NN_ZNN_phot                   | Yèche et al. (2010)       |
| XDQSO          | $P(XDQSO)$       | QSOED_PROB                    | Bovy et al. (2011)        |
| Combined-NN    | NN Value         | NN_VALUE                      | this paper                |

TABLE 3  
KEY PARAMETERS FOR THE VARIOUS METHODS AND THE VARIABLE NAME IN THE OUTPUT TARGET FILES.

tainty in each band, and  $A$  is a normalization. Following Hennawi et al. (2010), the stellar locus is defined by a set of  $\approx 14,000$  stars with accurate photometry from SDSS spectroscopic plates, on which all point sources were targeted above a flux limit of  $i < 19.1$  regardless of color (Adelman-McCarthy et al. 2006). The minimum distance to the stellar locus,  $\chi_{star}^2$ , can be computed by minimizing the value  $\chi^2(A, g - i)$ , where  $A$  is the normalization constant relating the data to a model,  $f_{data}^m = Af_{model}^m$ , and  $g - i$  is the color chosen as a proxy for stellar temperature. The distribution of the minimum distance to the stellar locus, i.e. range of  $\chi_{star}^2$ , is shown in Fig. 3 of Hennawi et al. (2010). The crucial strength that the  $\chi_{star}^2$  cut adds to our KDE selection is the rejection of objects that have colors consistent with those of quasars, but have flux errors that make them consistent with the stellar locus as well.

The key parameters (Fig. 2) for the KDE method are the minimum thresholds for selection in both  $KDE_{prob}$  and  $\chi_{star}^2$ . Early in Year One, CORE objects were selected solely by the KDE algorithm (Section 4); at that time, we applied a limit  $\chi_{star}^2 \geq 7$ . Later, when KDE was no longer the CORE algorithm, we relaxed this criterion to  $\chi_{star}^2 \geq 3$ . Objects selected by the KDE method have the QSO\_KDE target flag set.

### 3.3. Likelihood Method

Full details of the Likelihood method, including an in-depth analysis of its performance, are presented in Kirkpatrick et al. (2011). We summarize it briefly here.

Like KDE, the Likelihood method starts with a sample of known quasars, and a sample of “Everything Else” (EE in what follows), i.e., stars and galaxies, with  $ugriz$  photometry and errors. One defines likelihoods that a given object with fluxes  $f^m$  and errors  $\sigma^m$  ( $m = ugriz$ ) is drawn from the quasar or EE catalog by summing a  $\chi^2$ -like statistic over the full training set:

$$\mathcal{L}_{quasar} = \sum_i \prod_m \sqrt{\frac{1}{2\pi(\sigma_i^m)^2}} \exp\left(-\frac{[f^m - quasar_i^m]^2}{2(\sigma^m)^2}\right) \quad (3)$$

$$\mathcal{L}_{EE} = \sum_i \prod_m \sqrt{\frac{1}{2\pi(\sigma_i^m)^2}} \exp\left(-\frac{[f^m - EE_i^m]^2}{2(\sigma^m)^2}\right). \quad (4)$$

The sums are over all objects  $i$  in the training set. By restricting the sum to those training-set quasars in a specific redshift range, one can define an equivalent likelihood that the object in question is in this redshift range; in Year One, this was done by summing over those

quasars with  $z > 2.2$ . Given these likelihoods, one defines a probability that the object is a quasar to be targeted (compare with equation 1):

$$\mathcal{P} = \frac{\mathcal{L}_{quasar}(z > 2.2)/A_{quasar}}{\mathcal{L}_{EE}/A_{EE} + \mathcal{L}_{quasar}(\text{all } z)/A_{quasar}}, \quad (5)$$

where the  $A$ s normalize for the possibly different effective solid angles of the quasar and  $EE$  training sets. In the denominator, the likelihood sum is over quasars at all redshifts, not just those at  $z > 2.2$ .

Like the KDE method above, this method makes use of the varying densities of objects in color space, and includes a  $\chi^2$  selection. Note that it correctly utilizes the flux errors in determining whether a given object belongs to the quasar or EE class. Potential quasar targets can be ranked by their probability  $\mathcal{P}$ . We define a threshold ( $\mathcal{P} \geq 0.234$ ); for  $\mathcal{P}$  above this value, we target all objects as quasars. The Likelihood method was chosen as the CORE algorithm near the end of Year One (section 4.4). Objects selected by the Likelihood method have the QSO\_LIKE target flag set.

### 3.4. Artificial Neural Network

We use an Artificial Neural Network (NN) at two stages of the selection process. Full details of this algorithm may be found in Yèche et al. (2010). As in the previous methods, we define training sets of known quasars, and objects that are not quasars.

For the first stage, we use the NN with 10 inputs for each object (the SDSS  $g$ -band magnitude, the five SDSS magnitude errors and the four SDSS colors). The training set for non-quasars is a set of  $\sim 30,000$  SDSS point sources from SDSS DR7 (Abazajian et al. 2009), selected over the magnitude range  $18.0 < g < 22.0$  and with Galactic latitude  $b \approx 45^\circ$  to average the effects of Galactic extinction. The training set for quasars consisted of spectroscopically confirmed quasars from the 2QZ (Croom et al. 2004), 2SLAQ (Croom et al. 2009), and the SDSS (Schneider et al. 2010) quasar catalogs.

The NN developed for target selection has four layers of “neurons” (see Fig. 3 of Yèche et al. 2010). The fourth layer only has one neuron, providing a single output parameter,  $y_{NN}$ . The quantity  $y_{NN}$  quantifies the probability that an input object is a quasar, although since  $y_{NN}$  can be greater than 1, it is not a probability in the formal sense. A photometric redshift estimate,  $z_{pNN}$ , is also generated (see Section 5 of Yèche et al. 2010), with a cut placed on this photometric redshift estimate,  $z_{pNN} > 2.1$ . Objects selected by the NN method have the QSO\_NN target flag set.

### 3.5. Extreme Deconvolution

Extreme deconvolution (XD; Bovy et al. 2009) is a method to describe the underlying distribution function of a series of points in parameter space (e.g., quasars in color space), by modeling that distribution as a sum of Gaussians convolved with measurement errors. Bovy et al. (2011) apply XD to the problem of quasar target selection, using flux data from the SDSS DR8. The so-called “XDQSO” method is conceptually similar to the Likelihood method, but explicitly models the non-uniform errors of the training set from which the quasars and stellar/EE loci are derived. Indeed, the Likelihood method effectively double-counts the errors of the training set, since the *observed* distribution of fluxes from which the Likelihood training set is built is the true *underlying* distribution convolved with the uncertainty distribution. XD avoids this double-counting by deconvolving the underlying distribution of the training set.

XDQSO constructs a model of the distribution of the fluxes of stars and quasars in different redshift ranges based on training samples of known stars and quasars. XDQSO then builds a model of the relative-flux distribution as a mixture of 20 Gaussian components and fits this model to the training data, taking the heteroscedastic nature of the SDSS flux uncertainties fully into account. The XD model for the relative-flux distribution is fit in narrow bins in *i*-band magnitude and combined with an apparent-magnitude dependent prior based on star counts in Stripe 82 and the Hopkins et al. (2007) quasar luminosity function. The probability for an object to be a mid-redshift quasar ( $2.2 < z < 3.5$ ) is given by the ratio between the number density of mid-redshift quasars and that of stars plus all quasars at the object’s fluxes (in the spirit of equation 5). The probability that a given object is a mid-*z* quasar is then:

$$P(\text{QSO}_{\text{midz}} | \{f^m\}) \propto P(\{f^m / f^i\} | \text{QSO}_{\text{midz}}) P(f^i | \text{QSO}_{\text{midz}}) P(\text{QSO}_{\text{midz}}), \quad (6)$$

where *m* indexes the fluxes and  $f^i$  is the SDSS *i*-band flux. The first factor on the right is given by the XD model for the relative-flux (i.e., color) distribution of quasars, while the second and third factors are obtained from the quasar luminosity function. The underlying relative-flux distribution is convolved with the object’s flux uncertainties before evaluation. The expressions for stars and high/low redshift quasars are similar. Probabilities are normalized assuming that these classes exhaust the possibilities ( $P(\text{QSO}_{\text{midz}}) + P(\text{QSO}_{\text{hilo}}) + P(\text{star}) = 1$ ). Objects are ranked on their mid-redshift quasar probability for targeting.

Since XDQSO target selection properly takes the flux uncertainties into account both in the training and the evaluation stage, it can be trained and evaluated on data of low signal-to-noise ratio. It can also incorporate data from surveys other than SDSS in a straightforward way, as we describe for near-infrared and ultraviolet surveys below. The performance of XDQSO, using Stripe 82 data is given in Bovy et al. (2011) and its performance in Year Two will be described in a future paper. The catalog of SDSS objects selected by XDQSO is available through

the SDSS-III DR8 Science Archive Server<sup>31</sup>.

The XDQSO method was not used during Year One, but we then set, **and fixed**, XDQSO as CORE for Year Two and the remainder of the BOSS. In Section 6 we detail how to replicate the CORE selection using XDQSO for the BOSS quasars. Objects selected by the XDQSO method have the QSO\_CORE\_MAIN, and sometimes the QSO\_CORE\_ED, target flag set (see Section 6).

#### 3.5.1. The UKIRT Infrared Deep Sky Survey

Lawrence et al. (2007) presents an overview of the United Kingdom Infrared Telescope (UKIRT) Infrared Deep Sky Survey (UKIDSS). The UKIDSS is a collection of five surveys of different coverage and depth using the Wide-Field Camera (WFCAM, Casali et al. 2007) on UKIRT. WFCAM has an instantaneous field of view of 0.21 deg<sup>2</sup>, and the various surveys employ up to five filters, *ZYJHK*, covering the wavelength range 0.83-2.37 μm. The photometric system and calibration are described in Hewett et al. (2006) and Hodgkin et al. (2009), respectively. The pipeline processing is described in Irwin et al. (2011, in prep.) and the WFCAM Science Archive (WSA) by Hambly et al. (2008). The astrometry is accurate to 0.1″.

The UKIDSS Large Area Survey (ULAS) aims to map ~ 4,000 deg<sup>2</sup> of the Northern Sky, which, when combined with the SDSS, produces an atlas covering almost an octave in wavelength. The target point-source depths of the survey are  $Y = 20.3, J = 19.5, H = 18.6, K = 18.2$  (Vega); the ULAS does not image in the WFCAM *Z*-band. Unlike the SDSS, the ULAS multiband photometry is not taken simultaneously (e.g. Sec. 5.2 of Dye et al. 2006; Lawrence et al. 2007, Sec. 4.2), so the four bands have different coverage maps, with the *H* and *K* bands obtained together, and *Y* and *J* obtained separately. For example, the ULAS “DR8Plus”<sup>32</sup> coverage is 2,670 deg<sup>2</sup>, 2,685 deg<sup>2</sup>, 2,795 deg<sup>2</sup> and 2,810 deg<sup>2</sup>, in *Y, J, H* and *K* respectively.

We use the UKIDSS NIR photometry to improve target selection in two complementary techniques. The first is to classify quasars by their “K-excess” (“KX”; e.g., Warren et al. 2000; Croom et al. 2001; Sharp et al. 2002; Chiu et al. 2007; Maddox et al. 2008; Smail et al. 2008; Wu & Jia 2010; Peth et al. 2011). The power-law quasar SED has an excess in the *K*-band over a blackbody stellar SED, allowing quasars to be identified (and stars rejected) that would be normally excluded from an optical color-only quasar selection algorithm - even for dust reddened quasars. Peth et al. (2011) investigated the KX method and provided an SDSS-UKIDSS matched quasar catalog. For BOSS, KX-selected objects were selected early in commissioning and had the QSO\_UKIDSS target flag set. However, the very low yield (from admittedly a small target sample) caused us to drop this method.

The second method of inclusion of NIR photometry is to improve quasar classification, and of particular importance for BOSS, photometric redshift estimation, in the XDQSO method. Including the NIR flux information removes many of the optically-based redshift degeneracies known for quasars (see Bovy et al. 2011b, in prep.). Models were trained for SDSS-only fluxes and various

<sup>31</sup> <http://data.sdss3.org/sas/dr8/groups/boss/photoObj/xdqso/xdcore/>

<sup>32</sup> <http://surveys.roe.ac.uk/wsa/dr8.las.html>

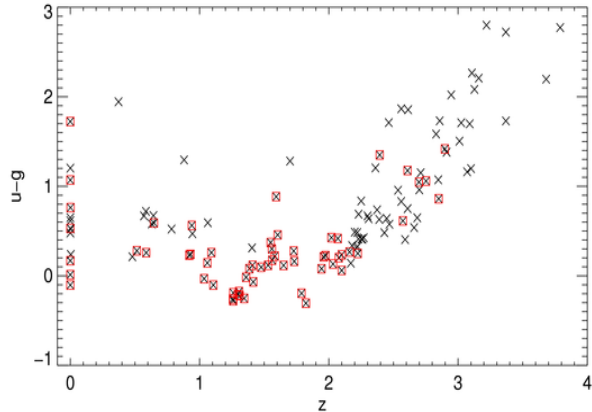


FIG. 3.— Redshift versus  $(u - g)$  color for BOSS FIRST quasar targets. Objects from the BOSS commissioning were either targeted by FIRST, and also a optical selection, (black) crosses, or, they were targeted *only* as FIRST sources, (red) squares. These early findings inspired our  $(u - g) > 0.4$  cut to minimize contamination from  $z < 2.2$  quasars.

combinations of SDSS+UKIDSS data.  $z \sim 2.5$  quasars have  $(i - K) \sim 2.1$  (e.g., Peth et al. 2011); thus given the BOSS quasar survey magnitude limit of  $i \sim 21.8$ , the ULAS catalog is too shallow to guarantee  $5\sigma$  detections of all sources. We therefore measure aperture magnitudes in the UKIDSS images at the positions of SDSS object counterparts; even low-significance detections can be used by XDQSO. Bovy et al. (2011b, in prep) give technical details. The SDSS (optical) only model is used by XDQSO to generate targets for CORE, where the upper limit of the mid- $z$  bin is  $z = 3.5$ . For BONUS, the SDSS+UKIDSS model is used to generate targets as an input to the NN-Combinator with an upper limit of the mid- $z$  bin extended to  $z = 4.0$ . This was implemented in BONUS from the middle of Year Two (Chunk 16) onwards, with significant gains in the yield of  $z > 2.2$  quasars.

### 3.5.2. GALEX: The Far and Near UV

The Far (1350 - 1750Å) and Near (1750 - 2750Å) ultraviolet (FUV and NUV respectively) photometry from the GALEX Small Explorer mission (Martin et al. 2005) also provide information that could help discriminate between hot stars and  $z \sim 0.8$  quasars, both of which should have considerably more flux in the UV than a  $z > 2$  quasar because of Ly $\alpha$  absorption along the line of sight in the latter.

We have trained the XDQSO technique on SDSS, UKIDSS and GALEX input data. Thus we can now perform 11-dimensional quasar target selection using the *FUV/NUVgrizYJHK* bands. The relevant GALEX surveys are relatively shallow, e.g.  $m_{UV} \approx 20.5$  AB, so most potential BOSS quasar targets are not detected at high significance. Despite this, our tests (detailed in Section 5) confirmed that GALEX measurements—even at low significance—do help with target selection.

We had access to medium-deep GALEX data on Stripe 82 at the start of Year Two, when we targeted the Stripe for the second time (Chunk 11; § 4.4). We therefore incorporated the GALEX FUV and NUV fluxes in the XDQSO probabilities.

### 3.6. Radio Selection

As in the SDSS-I/II quasar survey, objects that are detected in the FIRST radio survey (Becker et al. 1995) are also incorporated in target selection. Radio stars are rare, thus most radio sources with faint, unresolved optical counterparts are quasars. Optical stellar objects with  $g \leq 22.00$  or  $r \leq 21.85$  which have FIRST counterparts within  $1''$  are considered as potential quasar targets, irrespective of the radio morphology.

In the early BOSS commissioning data (§ 4), we simply selected all such radio matches. This approach targeted a substantial number of quasars with  $z < 2.2$ , and thus we placed an additional color cut,  $(u - g) > 0.4$ , to exclude UV-excess sources at lower redshift (Fig. 3). Thus the QSO\_FIRST flag designates objects with  $(u - g) > 0.4$  that matched a FIRST source. Bluer FIRST sources are not rejected outright, but are required to pass one of the regular optical color selections to be selected. Section 4 describes when in Year One this  $(u - g) > 0.4$  cut was implemented.

### 3.7. Previously Known Objects

The density of  $z > 2.2$  quasars known before BOSS started was  $\sim 2$  objects  $\text{deg}^{-2}$ . Given the superior throughput of the BOSS spectrographs over those of SDSS-I/II, we decided to re-observe these objects for improved Ly $\alpha$  forest clustering signal. Moreover, this allows vital checks of survey quality and uniformity, and the data can be used to study the spectroscopic variability of quasars. We thus target previously known spectroscopically confirmed  $z > 2.15$  quasars from the literature. We include such objects as targets if they match a point source in the target imaging to within  $1.5''$ , or if they match a point source in the target imaging to within  $2''$  and match the magnitude of that object to within 0.5.

The catalogs of previously known quasars we use include the SDSS DR7 quasar catalog (Schneider et al. 2010), the 2SLAQ quasar catalog (Croom et al. 2009), the 2QZ survey (Croom et al. 2004), the AAT-UKIDSS-SDSS (AUS) survey (Croom et al., in prep), and the MMT-BOSS pilot survey (Appendix C).

To compare and check our moderate resolution spectra of generally fainter quasars to those taken by 10m class telescopes using high-resolution spectrographs (e.g. KECK-HIRES and VLT-UVES), we also mined the data archives (the NED<sup>33</sup>, the Keck Observatory Archive<sup>34</sup> and the ESO Science Archive Facility<sup>35</sup>) and added those quasars with  $z > 2.15$  that were not included from the above catalogs.

The full sample of known quasars contains  $\sim 18,000$   $z > 2.15$  objects. We assign those objects in the BOSS footprint the QSO\_KNOWN\_MIDZ flag and give them highest targeting priority in tiling (Blanton et al. 2003).

We also veto previously known low ( $z < 2.15$ ) redshift quasars identified from the SDSS-I/II, 2QZ, 2SLAQ and MMT surveys, labeling them with the QSO\_KNOWN\_LOHIZ target flag and never assigning them spectroscopic fibers<sup>36</sup>. We are confident that we

<sup>33</sup> <http://nedwww.ipac.caltech.edu/>

<sup>34</sup> <http://www2.keck.hawaii.edu/koa/public/koa.php>

<sup>35</sup> <http://archive.eso.org/>

<sup>36</sup> The name for this flag, QSO\_KNOWN\_LOHIZ, is misleading, in that it does not explicitly flag high- $z$  quasars.



are not inadvertently rejecting any real  $z > 2.2$  quasars, since the vast majority of these objects were visually inspected and identified in the SDSS, 2QZ and MMT surveys (Schneider et al. 2010; Croom et al. 2005). A veto of objects with known stellar spectra, again from the SDSS-I/II, 2QZ, 2SLAQ and MMT surveys, was not implemented until Chunk 5, because we were not initially confident that shallower surveys, at their faint end, would have sufficient S/N to correctly identify stars, and that our initial matching procedures were not discarding some quasars of utility to BOSS.

### 3.8. Combinations of Methods

Combining results from several of the methods described above in target selection requires a method to merge the (overlapping) ranked lists from these methods into a single ranked catalog. The challenge is shown in Fig. 4, which shows the surface density of the union of those objects selected by the KDE, Likelihood, and NN methods with no further refinement, to yield an average target density of  $\sim 60$  targets  $\text{deg}^{-2}$ . The tidal stream of the Sagittarius dwarf spheroidal galaxy (Ibata et al. 1995; Belokurov et al. 2006) is quite striking in this figure, spanning  $180^\circ < \alpha < 240^\circ$  and  $0^\circ < \delta < +15^\circ$ . The target density in Figure 4 varies from 35 to 70  $\text{deg}^{-2}$ .

#### 3.8.1. Tuning and Ranking

In the early stages of commissioning, the target density was tuned to 80  $\text{deg}^{-2}$  using the KDE method (and its  $\chi_{\text{star}}^2$  parameter). The three main Year One algorithms (KDE, Likelihood and NN) were then trained on regions where very early BOSS spectroscopy was obtained. This was mainly in Stripe 82 (observed in Chunk 1; see § 4.1), but also some of Chunk 2, yielding  $\sim 650$   $z > 2.2$  quasars from  $\sim 2000$  targets. For these initial tests, the limiting parameters of the KDE, Likelihood and NN methods were chosen to give target densities of 80  $\text{deg}^{-2}$  each, and each produced a ranked list (based on the value of their respective output probability parameter) of targets. These three lists were then combined to generate the list of the 60 targets  $\text{deg}^{-2}$  most likely to be high- $z$  quasars, finding the interleaving (without repeating objects selected by more than one algorithm) of the combined list of objects that led to the highest yield of  $z > 2.2$  quasars. That is, we first took the first-ranked object from each of the three methods, then the second-ranked object, and so on, of course not double-counting objects which were selected by more than one method. Each of these objects is associated with a ranking parameter (as listed in Table 3), giving us a relative ranking of the three methods which we can use for combining other data in which one didn't know a priori which objects were actually  $z > 2.2$  quasars. This technique was tested by splitting the initial data in half and running the ranking algorithm to find the thresholds required for each of the three methods. Observed targets from the second half of the data were also chosen using these calculated thresholds, and the yield of  $z > 2.2$  quasars was consistent. The result of the combined rankings was to allocate targets to the three methods in approximately equal quantity and priority.

#### 3.8.2. NN-Combinator

We found that the outputs of the three methods could be used as inputs into a neural net to improve the yield of  $z > 2.2$  quasars. We refer to this approach in what follows as the NN-Combinator. This approach can easily be expanded to allow input from additional selection techniques.

The key output parameter of the NN-Combinator is designated as the “NN value”, which is, by design, allowed to change from chunk to chunk. The NN-Combinator used the data from Stripe 82 obtained by BOSS (Chunk 1, see Section 4.1 below) as an input training set. The NN-Combinator was the selection method for BONUS from Chunk 7 onwards in the survey, drawing on the inputs of KDE, Likelihood, and NN. This replaced the interleaving method described in §3.8.1.

In Year Two, with the advent of the XDQSO method, we added the results of this method to the NN Combinator. In particular, near the end of Year Two, we used a version of XDQSO that included data from UKIDSS (§ 3.5.1) which selected targets to  $z = 4$ ; the version of XDQSO used for CORE used SDSS single-epoch photometry only and did not incorporate UKIDSS data.

### 3.9. Rationale and Summary

As the above makes clear, BOSS quasar selection has been through a complex series of changes during its first two years. Here we recall the reasons for this complexity and summarize the main points of this history.

BOSS quasar target selection is complex because

- for the survey’s defining science goal, measurement of BAO in the Ly $\alpha$  forest, the primary requirement is a high surface density of quasars in the relevant redshift range, not simplicity or homogeneity of selection,
- selection of quasars in the desired redshift range from single-epoch SDSS imaging is difficult because of proximity to the stellar locus and substantial photometric errors near the magnitude limit for BOSS selection,
- pre-BOSS quasar samples provided inadequate training sets in our desired magnitude and redshift range, so the quasars we discovered in this first year allowed us to refine our algorithms as the year proceeded.

Roughly speaking, the effective survey volume for measurement of Ly $\alpha$  forest clustering is quadratic in the number of quasars, so even modest gains in efficiency have a significant science impact.

As discussed in §3.1, the goal of CORE selection *is* to provide a homogeneously selected sample suitable for quasar science. Ideally, we would have frozen the CORE algorithm at the very beginning of BOSS, but the higher imperative of maximizing efficiency has led us to alter CORE as our algorithms improved. We started by using KDE+ $\chi^2$  as the CORE algorithm but switched to Likelihood based on its greater flexibility and simplicity. Finally, we switched from Likelihood to XDQSO based on its better performance (at a level of  $\sim$ one additional high- $z$  quasar  $\text{deg}^{-2}$ ). The chunk-by-chunk history of these changes is given in §4 below. We intend to maintain a fixed CORE algorithm for Years 2–5 of the survey,

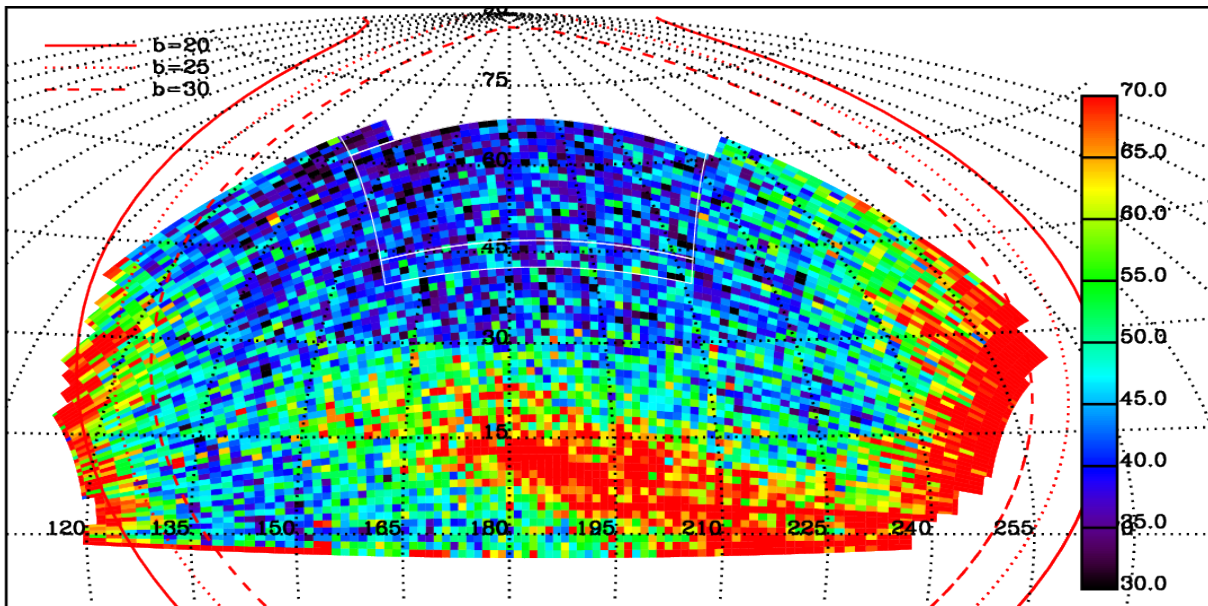


FIG. 4.— The BOSS quasar target surface density in Equatorial coordinates in the NGC, from a run of the BOSS QTS with a selection made by combining the three Year One methods, KDE, Likelihood and NN, in such a way that the average target density over the full given NGC area was  $\sim 60$  quasar targets  $\text{deg}^{-2}$ . The color indicates the local number density of targets per square degree. The tidal stream of the Sagittarius dwarf spheroidal galaxy is prominent in the region  $180^\circ < \alpha < 240^\circ$ , and  $0^\circ < \delta < +15^\circ$ . The white lines show the “Blind Test Area”, described in § 5.5.

and for many purposes we anticipate that completeness corrections will allow use of Year One data in statistical studies of the quasar population (see §6).

Beyond CORE, we use whatever combinations of data and methods can maximize our targeting efficiency, including known quasars, FIRST candidates, and the BONUS sample. Because the methods described in §§3.2-3.5 have complementary strengths, we draw on all of them in creating the BONUS sample. We have tried different methods of forming a combined BONUS list during the first year, and we have now settled on the NN-combinator (§3.8.2) as our primary tool for doing so. The individual methods feeding into the NN-combinator use co-added SDSS photometry where it is available in overlap regions, in contrast to CORE, which relies on single-epoch photometry to ensure uniformity. Auxiliary data such as UKIDSS and GALEX photometry are fed into the XDQSO selection, which in turn is fed into the NN-combinator.

#### 4. BOSS QUASAR TARGET SELECTION FOR YEARS ONE AND TWO, CHUNK BY CHUNK

BOSS is a five year project running from 2009 August to the end of June 2014. Starting in 2009 September, target selection commissioning (both for the galaxies and quasars) ran alongside commissioning of the new hardware and reduction software. The hardware commissioning was essentially complete by 2009 December (data taken earlier were therefore not of survey quality), but QTS commissioning continued through 2010 April; during this period the quasar target density was set appreciably higher (60 or 80  $\text{deg}^{-2}$ ), than for the nominal survey (40  $\text{deg}^{-2}$ ). The bulk of the Year One observations from MJD=55176 (2009 December 11) to MJD=55383 (2010 July 6) were thus QTS commissioning data.

The targeting chunks into which the Year One and Year Two data were divided are detailed in Table 4 and

Figure 5. By the end of Year Two, we had run target selection over the whole 10,000  $\text{deg}^2$  imaging footprint, resulting in  $\approx 430,000$  tiled targets. This target list is not necessarily final – if we obtain data that could improve our target selection efficiency in later years of BOSS, we will rerun target selection for areas that have not yet been observed. Spectra collected during Years One and Two will constitute the DR9, and will include 150,000 quasar targets, a third to half of which will be  $z > 2.2$  quasars. By the end of Year Two, we will have observed all of the Year One chunks. The BOSS quasar target selection changed from chunk to chunk during the first year, as we gathered data and refined our algorithms. These changes in the algorithms are detailed in the following subsections.

##### 4.1. *Chunk 1*

The first area that we targeted and observed for BOSS was SDSS Stripe 82, along the celestial equator in the Southern Galactic Cap. The target field covered  $317.0^\circ \leq \alpha_{J2000} \leq 45.0^\circ$ ,  $-1.25^\circ \leq \delta_{J2000} \leq 1.25^\circ$ , for a total area of 220  $\text{deg}^2$  (smaller than the  $\sim 300 \text{deg}^2$  imaging coverage on the Stripe).

The KDE method, based on single-run data and with a cut at  $\chi_{\text{star}}^2 \geq 7.0$ , was used as the CORE (QSO\_CORE) selection for Chunk 1. The KDE method was one of the techniques used for BONUS, (QSO\_BONUS) with targets chosen using the coadded data described by Section 2, and given the flag QSO\_KDE\_COADD. Coadded data were not used in later chunks, thus the QSO\_KDE\_COADD flag was used only for Chunk 1. In Chunk 1, with the benefit of coadded data, the quasar and stellar loci were better defined than in the standard one-epoch SDSS data. Hence there was far more overlap between the samples of sources targeted by all of the methods, freeing fibers to be placed on lower-priority KDE targets. As most of these lower-priority targets

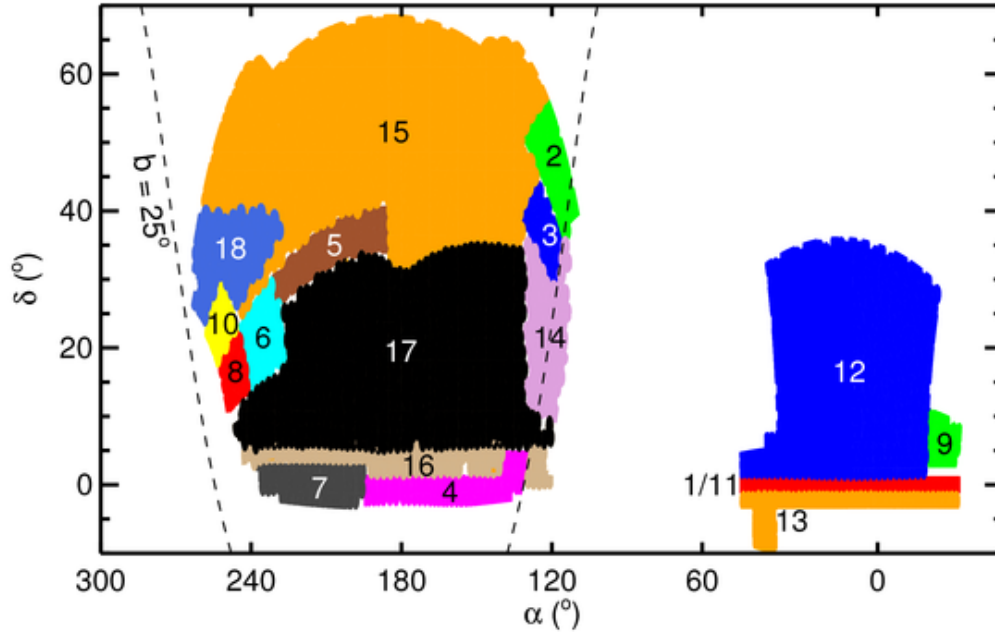


FIG. 5.— The targeting footprint for the SDSS-III:BOSS Ly $\alpha$  forest/Quasar Survey. The various chunks are indicated by different colors. Chunks 16, 17 and 18 lie within the footprint of Chunk 15. The full targeting footprint is 10,200 deg<sup>2</sup>, with a total of  $\approx$ 430,000 tiled targets. Roughly  $\sim$ 150,000 of these targets will have spectra by the end of Year Two observations. The global Year One quasar target density is 60.4 targets deg<sup>-2</sup>, and the mean target density over all chunks shown is 47.9 targets deg<sup>-2</sup>. The dashed line is at Galactic latitude  $b = 25^\circ$ .

| Area Name       | RA (2000) Range           | Dec (2000) Range | Area deg <sup>2</sup> | Total # targets (tiled)  | Galactic latitude cut? | quasar target density deg <sup>-2</sup> (tiled) | Method for CORE          |
|-----------------|---------------------------|------------------|-----------------------|--------------------------|------------------------|---|--------------------------|
| Chunk 1         | 317.0 - 45.0 <sup>a</sup> | -1.25 - +1.25    | 219.93                | 19,205 (18,657)          | no                     | 87.3 (84.8)                                     | KDE <sup>b</sup>         |
| Chunk 2         | 108.9 - 131.0             | 35.6 - 56.2      | 143.66                | 11,337 (11,024)          | no                     | 78.9 (76.7)                                     | KDE                      |
| Chunk 3         | 115.7 - 132.8             | 28.8 - 44.4      | 107.34                | 9,476 (6,949)            | $b > 25^\circ$         | 88.3 (64.7)                                     | — <sup>d</sup>           |
| Chunk 4         | 128.7 - 195.0             | -3.3 - 5.0       | 306.50                | 32,750 (20,679)          | $b > 25^\circ$         | 106.9 <sup>c</sup> (67.5)                       | — <sup>d</sup>           |
| Chunk 5         | 185.0 - 232.2             | 26.2 - 40.7      | 245.82                | 18,533 (13,418)          | no                     | 75.4 (54.6)                                     | — <sup>d</sup>           |
| Chunk 6         | 225.4 - 244.9             | 13.5 - 30.53     | 186.13                | 19,304 (13,130)          | no                     | 103.7 (70.5)                                    | — <sup>d</sup>           |
| Chunk 7         | 194.0 - 237.9             | -3.6 - 3.2       | 257.01                | 10,783 (9,596)           | no                     | 42.0 (37.3)                                     | Likelihood               |
| Chunk 8         | 240.2 - 253.1             | 10.5 - 22.9      | 97.82                 | 4,004 (3,500)            | no                     | 40.9 (35.8)                                     | Likelihood               |
| Chunk 9         | 316.3 - 330.0             | 2.5 - 11.1       | 97.54                 | 3,870 (3,360)            | $b < -25^\circ$        | 39.7 (34.4)                                     | Likelihood               |
| <b>Year One</b> |                           |                  | <b>1661.75</b>        | <b>132,923 (100,313)</b> |                        |   | <b>80.0 (60.4)</b>       |
| Chunk 10        | 245.0 - 258.6             | 17.1 - 30.0      | 91.14                 | 3,661 (3,325)            | no                     | 40.2 (36.5)                                     | Likelihood               |
| Chunk 11        | 317.0 - 45.0              | [1.25]           | (219.84)              | 8,820 (8,432)            | no                     | 40.1 (38.4)                                     | variability <sup>e</sup> |
| Chunk 12        | 324.6 - 45.1              | 0.55 - 36.2      | 2075.9                | 84,038 (77,447)          | no                     | 40.5 (37.3)                                     | Likelihood/XDQSO         |
| Chunk 13        | 317.0 - 45.0              | -9.9 - -0.8      | 281.7                 | 11,051 (10,072)          | no                     | 39.2 (35.8)                                     | Likelihood/XDQSO         |
| Chunk 14        | 111.8 - 131.5             | 9.0 - 36.3       | 347.43                | 14,165 (13,479)          | no                     | 40.8 (38.8)                                     | XDQSO                    |
| Chunk 15        | 118.9 - 263.9             | -0.8 - 68.7      | 5743.5                | 233,530 (220,029)        | no                     | 40.7 (38.3)                                     | XDQSO                    |
| Chunk 16        | 118.9 - 247.3             | -0.8 - 35.6      | (3108.3)              | [128,250 (120,905)]      | no                     | 41.3 (38.9)                                     | XDQSO                    |
| Chunk 17        | 118.9 - 247.3             | 4.4 - 35.6       | (2742.4)              | [116,471 (107,562)]      | no                     | 42.5 (39.2)                                     | XDQSO                    |
| Chunk 18        | 226.9 - 263.9             | 23.1 - 41.1      | (337.20)              | [13,372 (12,699)]        | no                     | 39.7 (37.7)                                     | XDQSO                    |
| <b>Year Two</b> |                           |                  | <b>8539.65</b>        | <b>355,265 (332,784)</b> |                        |   | <b>41.6 (39.0)</b>       |
| <b>Total *</b>  |                           |                  | <b>10,201.4</b>       | <b>488,188 (433,097)</b> |                        |   | <b>47.9 (42.5)</b>       |

TABLE 4

DETAILS OF THE 18 CHUNKS TARGETED FOR THE FIRST TWO YEARS OF BOSS OBSERVATIONS. SPECTRA FROM EACH OF THE 18 CHUNKS WILL BE TAKEN DURING THE FIRST TWO YEARS, BUT ONLY AN AREA OF  $\sim$ 3000 DEG<sup>2</sup> WILL BE COVERED FOR SPECTROSCOPY. HOWEVER, WE PLAN TO OBSERVE *all* OF THE YEAR ONE CHUNKS BY THE END OF THE YEAR TWO OBSERVATIONS. <sup>a</sup> THE RA AND DEC RANGES GIVE THE EXTREMITIES OF EACH CHUNK AREA, AND THUS DO NOT INDICATE THE COORDINATES OF THE CORNERS OF THE CHUNK FOOTPRINTS. CHUNKS 16, 17 AND 18 LIE WITHIN THE AREA OF CHUNK 15, HENCE THEIR AREAS AND TARGETS ARE NOT COUNTED TOWARDS THE TOTAL.

<sup>b</sup>FROM SINGLE-EPOCH DATA.

<sup>c</sup>CHUNK 4 USES IMAGING DATA IN WHICH PROBLEMS WITH THE  $u$ -BAND DATA LEAD TO AN EXCESS TARGET DENSITY ( $> 106$  TARGETS DEG<sup>-2</sup>).

<sup>d</sup>A RANKING SCHEME WAS USED; FOR CHUNKS 3-6, CORE INCLUDED A COMBINATION OF NN, LIKELIHOOD, AND KDE TARGETS (§ 4.3).

proved to be stars, the overall efficiency of selection of the KDE method is thus quite low in Chunk 1.

Likelihood targets were selected at a target density of  $\sim 35$  targets  $\text{deg}^{-2}$  using a threshold  $\mathcal{P} = 0.10$ , Neural Network targets at  $\sim 20$   $\text{deg}^{-2}$  with a threshold  $y_{NN} = 0.65$ , and KDE targets using the coadded data at  $\sim 50$   $\text{deg}^{-2}$ . The density of the coadded KDE targets was tuned on a *second*  $\chi_{\text{star}}^2$  value calculated from coadded data, to obtain the required total of 80 targets  $\text{deg}^{-2}$  total across all methods. This second  $\chi_{\text{star}}^2$  parameter is dependent on right ascension, but is always  $> 4.0$ .

The final Chunk 1 target densities were approximately 7, 2, 20, and 60 targets  $\text{deg}^{-2}$  for the Known, KX-selected (§ 3.5.1) CORE, and BONUS, respectively (with overlap between these categories). At tiling, *all* quasar targets were given priority over all other BOSS targets (such as galaxies) for Chunks 1 and 2. The tiling priorities for all the chunks are given in Appendix B (Table 12).

About 100  $\text{deg}^2$  of Chunk 1 was observed following hardware commissioning, i.e., after MJD 55176. Stripe 82 was re-observed in 2010 Fall as part of Chunk 11 (§ 4.4).

#### 4.2. Chunk 2

For this chunk in the NGC (Figure 5), the targeting algorithms were similar, but not identical, to Chunk 1, as coadded photometry was not available. The surface density of known quasars was lower than in Chunk 1 (since Stripe 82 contains more extensive spectroscopy from prior surveys), and with no UKIDSS coverage, there were no KX-selected targets. Unresolved optical objects that had a match to *any* FIRST source (§ 3.6) were included, and given the target flag QSO\_FIRST (bit 18). The CORE method remained the KDE. The Chunk 2 target densities were approximately 2, 2, and 20  $\text{deg}^{-2}$  for the Known, radio-selected and CORE objects, respectively.

Objects from the Likelihood, NN and KDE methods were targeted for BONUS, using single-epoch data to achieve  $\sim 35$ , 20 and 25 targets  $\text{deg}^{-2}$ , respectively. As in Chunk 1, the KDE was tuned on the  $\chi_{\text{star}}^2$  parameter to obtain a total of 80 targets  $\text{deg}^{-2}$  over all methods. In Chunk 2, flux errors are larger than in Chunk 1, due to the use of single-epoch data. Thus, the stellar locus is expanded and there is far less overlap between the targets chosen by various methods. The target density of QSO\_BONUS sources is thus approximately halved in Chunk 2.

As this chunk used single-epoch data with its larger photometric errors, the thresholds for the target selection algorithms were modified as follows, giving the target densities above:

- The Likelihood Probability threshold,  $\mathcal{P}$ , was changed from 0.10 to 0.24;
- The NN probability parameter,  $y_{NN}$ , was changed from 0.65 to 0.70;
- The KDE algorithm was retrained, using all available quasar spectroscopy to date.

At this stage, the list of quasars with high-resolution spectroscopy (Section 3.7) were added to the database of

known quasars, although few lie within the boundaries of Chunk 2.

#### 4.3. Chunks 3, 4, 5 and 6

We already had our initial spectroscopic results in hand from  $\sim 20$  plates from Chunks 1 and 2 when we identified targets in Chunk 3, and we used these results to refine our algorithms. In particular, we rejected FIRST sources with  $(u-g) < 0.4$ , greatly decreasing contamination from  $z < 2.2$  quasars, but decreasing the number of FIRST  $z > 2.2$  objects by only 10%. The resulting FIRST target density drops to  $\sim 1-2$   $\text{deg}^{-2}$ , 40% of which turn out to be  $2.2 < z < 3.5$  quasars (see Fig. 3).

In the first two chunks, we found that only 1 *new* bright ( $i \leq 17.7$ )  $z > 2.2$  quasar had been discovered from 486 bright targets. Thus, a bright limit of  $i > 17.8$  was set to reduce stellar contamination at the bright end. Due to the proximity of Chunk 3 to the Milky Way, we also imposed a Galactic latitude cut of  $b > 25^\circ$ .

There was a change in the target density and methodology from those in Chunks 1 and 2. For Chunks 3, 4, 5 and 6, the ranking method described in Section 3.8.1 was adopted, allowing us to combine Likelihood, KDE, and NN for CORE at 20 targets  $\text{deg}^{-2}$ . All remaining targets, to a total density of 60  $\text{deg}^{-2}$ , were designated as BONUS. To monitor the CORE and BONUS changes, two new target flags, QSO\_CORE\_MAIN (flag bit 40) and QSO\_BONUS\_MAIN (flag bit 41)<sup>37</sup> were introduced.

The final target densities for Chunks 3, 4, 5 and 6 were 2 and 1 targets  $\text{deg}^{-2}$  for Known quasar and FIRST targets, respectively. The CORE target density was  $\approx 19, 19, 16, 17$   $\text{deg}^{-2}$  in the four chunks respectively, and the BONUS target density was roughly 40  $\text{deg}^{-2}$ . To provide a more uniform galaxy sample, galaxy targets were given precedence over quasar targets in tiling (see Appendix B and Table 12).

#### 4.4. Chunks 7 - 11

Chunks 7, 8 and 9 were the first chunks which were targeted at the nominal survey target density of 40 quasar targets  $\text{deg}^{-2}$ . The area covered by Chunk 9 in the SGC was not in the original SDSS survey, and target selection was done from the DR8 imaging (Aihara et al. 2011), a region of sky where there were no previously known  $z > 2.2$  quasars in our catalog (§ 3.7). This change led to a lower efficiency (see Section 5).

For Chunks 7, 8 and 9, based on the tests described in Section 5.5, we set the CORE method to Likelihood, while BONUS targets were selected using the NN-Combinator (§ 3.8.2). In addition, previously known stars from SDSS or 2dF spectroscopy were now vetoed. The NN photometric redshift threshold was relaxed slightly, from  $z_{pNN} > 2.1$  to 2.0.

Chunk 9 was the last chunk to be observed in Year One, and thus the last data included in the spectroscopic sample presented in this paper. Target selection for Chunk 10 was performed in the first year of BOSS, but the Chunk 10 plates were not observed until the second year, after the Summer 2010 shutdown. Chunk 11, the re-observation of Stripe 82, was also observed at the start of the second year of BOSS observations. As described in detail by Palanque-Delabrouille et al. (2010),

<sup>37</sup> Now requiring Long64, or “LL” integer type.

a variability-based quasar selection was performed for Chunk 11. This led to a significantly higher high- $z$  quasar density than elsewhere in the survey, 24  $z > 2.15$  quasars  $\text{deg}^{-2}$  (Palanque-Delabrouille et al. 2010), as we describe further in Section 5.

#### 4.5. Chunks 12 and 13

The XDQSO method was introduced in Chunk 12 to test its efficiency. There is substantial overlap between the target list of XDQSO and Likelihood, and including the highest ranked 20 targets  $\text{deg}^{-2}$  from each yielded a total of 25 targets  $\text{deg}^{-2}$ . We thus defined CORE to be the union of all these targets. The NN-Combinator was retained as the method for BONUS.

#### 4.6. Chunks 14-18

The Chunk 12 and 13 spectroscopic results demonstrated the superiority of XDQSO for the core algorithm. Therefore, from Chunk 14 onwards, and for the rest of the BOSS, the ‘‘Extreme Deconvolution’’ algorithm (XDQSO), and that alone, was set to be CORE. This led to a gain of  $\sim 1$  high- $z$  quasar  $\text{deg}^{-2}$  in the CORE.

Various further improvements were implemented in BONUS starting with Chunk 14. For Chunk 14, a change in fiber collision prioritization (see Appendix B) led to a gain of  $\sim 1$  quasar  $\text{deg}^{-2}$ . In Chunk 15 we began a policy of re-observing previously known quasars in plate overlap regions, leading to a spectroscopic signal-to-noise ratio gain of  $\sim 15\%$  per quasar. In Chunk 16, we incorporated UKIDSS photometry into the training of XDQSO as an input to the NN-Combinator. This led to a gain of 2 – 3 high- $z$  quasars  $\text{deg}^{-2}$  where UKIDSS data were available. Overlap between adjacent imaging scans allowed improved photometry for objects observed more than once, (Sec. 2), leading to a gain of  $\sim 0.3 - 0.5$  quasars  $\text{deg}^{-2}$  in Chunk 16. In Chunk 17, an optical-only trained version of the XDQSO (essentially what is used for CORE) was also used as an input to the NN-Combinator used for BONUS, with a gain of  $\sim 0.5$  quasars  $\text{deg}^{-2}$ .

BOSS spectroscopic plates are designed by giving priority first to BOSS galaxy and quasar targets, followed by objects in various ancillary programs (Section 2 of Eisenstein et al. 2011). If additional fibers are available, we assign them to previously known  $1.8 < z < 2.15$  quasars; these are labeled as SUPPZ in Figure 2 and are flagged as QSO\_KNOWN\_SUPPZ in Table 2. Reobserving these objects allows a measurement of the spectral structure from metal lines along the line of sight and spectral artifacts that may contaminate Ly $\alpha$  structure measurements (McDonald et al. 2006).

#### 4.7. The Sky Distribution of BOSS Quasar Targets

The sky distribution of the BOSS quasar targets are shown in Figs. 6, 7, 8 and 9. In Figs. 6 and 7, we show the surface densities of BOSS quasar targets for the NGC and the SGC, respectively, as selected by the CORE method (XDQSO) for DR9. In Figs. 8 and 9, we show the surface densities of BOSS quasar targets for the NGC and the SGC, respectively, as selected by the CORE (XDQSO), BONUS (NN-Combinator) and FIRST methods, as well as the inclusion of all previously known  $z > 2.2$  quasars.

The CORE sample is designed to produce a mean surface density of 20 targets  $\text{deg}^{-2}$ , and although it is reasonably uniform, the density of targets ranges from 10 to 30 targets  $\text{deg}^{-2}$  over the footprint of the survey. The largest variations are associated with Galactic structure, with excesses visible at low Galactic latitudes and in the Sagittarius stream. The BONUS sample adds enough targets in each area of sky to give a much more uniform 40 targets  $\text{deg}^{-2}$ .

## 5. RESULTS

In this section, we present the results of spectroscopy carried out during Year One after the completion of hardware commissioning, from MJD 55176 (2009 December 11) through MJD 55383 (2010 July 06). The distribution of BOSS Year One quasars on the celestial sphere is shown in Fig. 10.

### 5.1. Global Properties and Efficiencies

Table 5 summarizes the results from the first year of BOSS quasar observations. BOSS quasar targets are those which have one of the target bit flags listed in Table 2 set. There were 54,909 spectra of objects targeted as quasars, of which 52,238 were unique objects. These were observed over over a footprint of 878  $\text{deg}^2$ , giving a mean surface density of 63.8 targets  $\text{deg}^{-2}$ .

Of the 54,909 (52,238 unique) spectra, 35,305 (33,556) had high-quality redshifts, as designated by the ‘‘zWarning’’ flag of the spectroscopic pipeline (Adelman-McCarthy et al. 2008; Aihara et al. 2011). From visual inspection of the data, the zWarning flag is reliable at the 90-95% level for the quasar target spectra; very few of the objects flagged as having high-quality redshifts (i.e., zWarning=0) are incorrect. We present the performance of zWarning as a function of magnitude and S/N in Appendix D; most objects with zWarning  $\neq 0$  are faint objects with low S/N spectra. Given the faint magnitude limit of BOSS, it is not surprising that many of the targets that are not quasars lack the clearly identified spectral features required to assign a high-confidence redshift. We will present a detailed examination of the performance of the reduction pipeline, the zWarning flag and the findings from the visual inspection of the data when we publish the BOSS Quasar DR9 Catalog in a separate paper.

Of the 33,556 unique objects with high-quality redshifts, 11,149 are stars, while 13,580 have  $z > 2.20$ . The remaining 8,827 objects are mostly quasars at  $z \sim 0.8$  and  $\sim 1.6$ , and low- $z$  compact galaxies; see Fig. 11. Of the 13,580 high redshift objects, 2,317 had the QSO\_KNOWN\_MIDZ flag set; thus the first year of BOSS observations resulted in the spectroscopic confirmation of 11,263 new  $z > 2.2$  quasars. A full breakdown of the number of objects associated with each target flag, the number of good (zWarning=0) redshifts and the number of  $z > 2.2$  quasars obtained is given in Table 6.

Figure 11 shows the redshift distribution of BOSS quasars from the first year, and compares it with that from the SDSS DR7 quasar sample (Schneider et al. 2010) and the 2SLAQ survey (Croom et al. 2009). This plot is very similar, but not identical, to that shown in the SDSS-III overview paper of Eisenstein et al. (2011).



| Chunk        | Observed Area (deg <sup>2</sup> ) | Total spectra        | CORE <sup>a</sup> spectra | # high-quality <sup>b</sup> (zWarning=0) | # high-quality z > 2.20 | # CORE high-quality z > 2.20 |
|--------------|-----------------------------------|----------------------|---------------------------|--|-------------------------|------------------------------|
| 1            | 37.4                              | 3811 ( 3174)         | 988 ( 849)                | 2313 (1909)                              | 1211 ( 986)             | 411 ( 355)                   |
| 2            | 117.6                             | 9865 ( 9018)         | 2639 (2409)               | 7052 (6461)                              | 2018 (1847)             | 880 ( 799)                   |
| 3            | 33.1                              | 2191 ( 2142)         | 630 ( 616)                | 1463 (1433)                              | 521 ( 513)              | 268 ( 264)                   |
| 4            | 168.3                             | 11879 (11362)        | 3275 (3126)               | 6603 (6302)                              | 2527 (2417)             | 1320 (1269)                  |
| 5            | 186.0                             | 10344 (10154)        | 2924 (2875)               | 7132 (7004)                              | 3376 (3323)             | 1714 (1691)                  |
| 6            | 121.7                             | 8733 ( 8582)         | 2063 (2023)               | 5091 (5003)                              | 1914 (1878)             | 915 ( 896)                   |
| 7            | 120.8                             | 4615 ( 4506)         | 2647 (2581)               | 3100 (3027)                              | 1635 (1595)             | 1188 (1160)                  |
| 8            | 67.0                              | 2565 ( 2400)         | 1697 (1591)               | 1891 (1762)                              | 834 ( 772)              | 657 ( 608)                   |
| 9            | 26.2                              | 906 ( 900)           | 742 ( 738)                | 660 ( 655)                               | 251 ( 249)              | 226 ( 224)                   |
| <b>TOTAL</b> | <b>878.14</b>                     | <b>54909 (52238)</b> | <b>17605 (16808)</b>      | <b>35305 (33556)</b>                     | <b>14287 (13580)</b>    | <b>7579 (7266)</b>           |

TABLE 5

SUMMARY OF THE RESULTS FROM THE FIRST YEAR OF BOSS QUASAR OBSERVATIONS, CHUNK BY CHUNK. NUMBERS IN PARENTHESES ARE FOR UNIQUE OBJECTS. <sup>a</sup>CORE DEFINED AS TARGET BIT 10 FOR CHUNKS 1 AND 2, BIT 40 FOR CHUNKS 3–9 (TABLE 2). <sup>b</sup>HIGH-QUALITY REDSHIFTS ARE THOSE FOR WHICH THE SPECTROSCOPIC PIPELINE zWARNING FLAG IS ZERO.

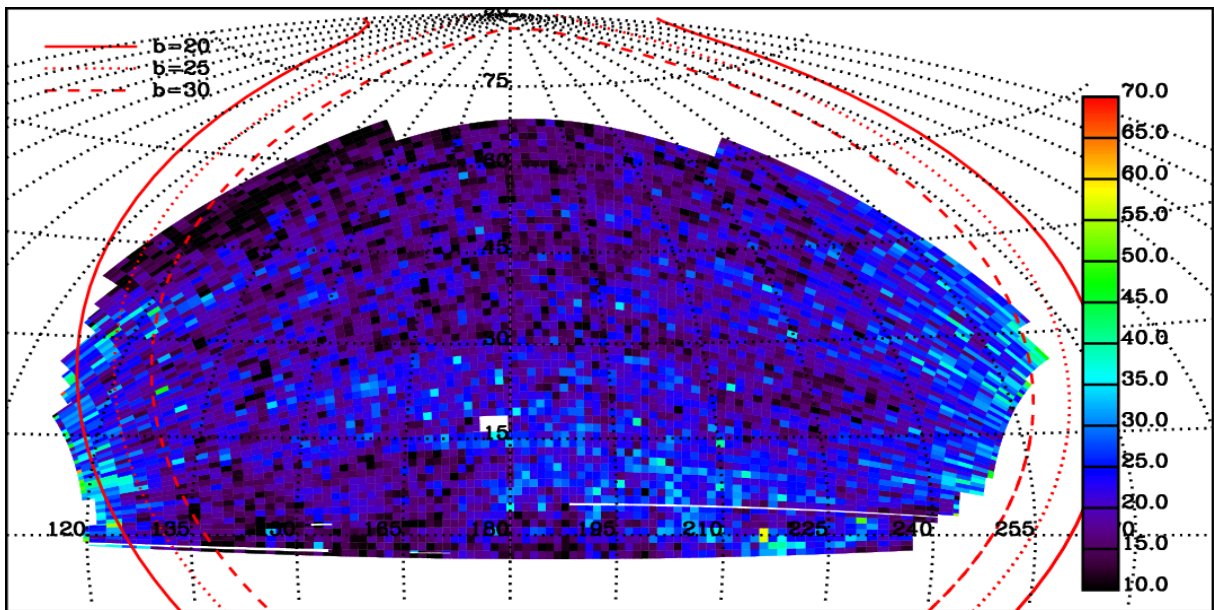


FIG. 6.— The quasar target density map in the NGC for the XDQSO CORE targets, displayed in equatorial coordinates. The units are targets deg<sup>-2</sup>.

| TARGET_FLAG | No. of targets (only) | No. of targets with zWarning=0 (only) | zWarning=0 and z > 2.20 (only) | zWarning=0 and stars (only) |
|-------------|-----------------------|---------------------------------------|--------------------------------|-----------------------------|
| CORE        | 3627 (1509)           | 2693 (890)                            | 1291 (89)                      | 1007 (619)                  |
| BONUS       | 4071 (2927)           | 2631 (1756)                           | 546 (131)                      | 1558 (1300)                 |
| KNOWN_MIDZ  | 2975 (529)            | 2831 (490)                            | 2520 (357)                     | 0 (0)                       |
| KNOWN_LOWZ  | 0 (0)                 | 0 (0)                                 | 0 (0)                          | 0 (0)                       |
| NN          | 17678 (1111)          | 13988 (791)                           | 8197 (152)                     | 3776 (562)                  |
| UKIDSS      | 139 (36)              | 119 (33)                              | 80 (6)                         | 22 (21)                     |
| KDE_COADD   | 2407 (860)            | 1517 (309)                            | 890 (31)                       | 324 (107)                   |
| LIKE        | 30534 (2541)          | 23022 (1779)                          | 11793 (479)                    | 4712 (794)                  |
| FIRST       | 986 (530)             | 791 (400)                             | 403 (104)                      | 35 (34)                     |
| KDE         | 27145 (0)             | 16068 (0)                             | 7313 (0)                       | 5330 (0)                    |
| CORE_MAIN   | 13978 (0)             | 10652 (0)                             | 6288 (0)                       | 2106 (0)                    |
| BONUS_MAIN  | 40363 (8)             | 25218 (2)                             | 10616 (0)                      | 7588 (2)                    |

TABLE 6

THE TOTAL NUMBER OF SPECTRA OF OBJECTS SELECTED WITH EACH TARGET FLAG FOR YEAR ONE OBSERVATIONS. OBJECTS CAN BE COUNTED MORE THAN ONCE; THE NUMBER OF OBJECTS IN ONLY ONE CATEGORY IS ALSO SHOWN. ALSO TABULATED ARE THE NUMBER OF GOOD (zWARNING=0) REDSHIFTS, THE NUMBER OF z > 2.2 QUASARS, AND THE NUMBER OF STELLAR SPECTRA OBTAINED.



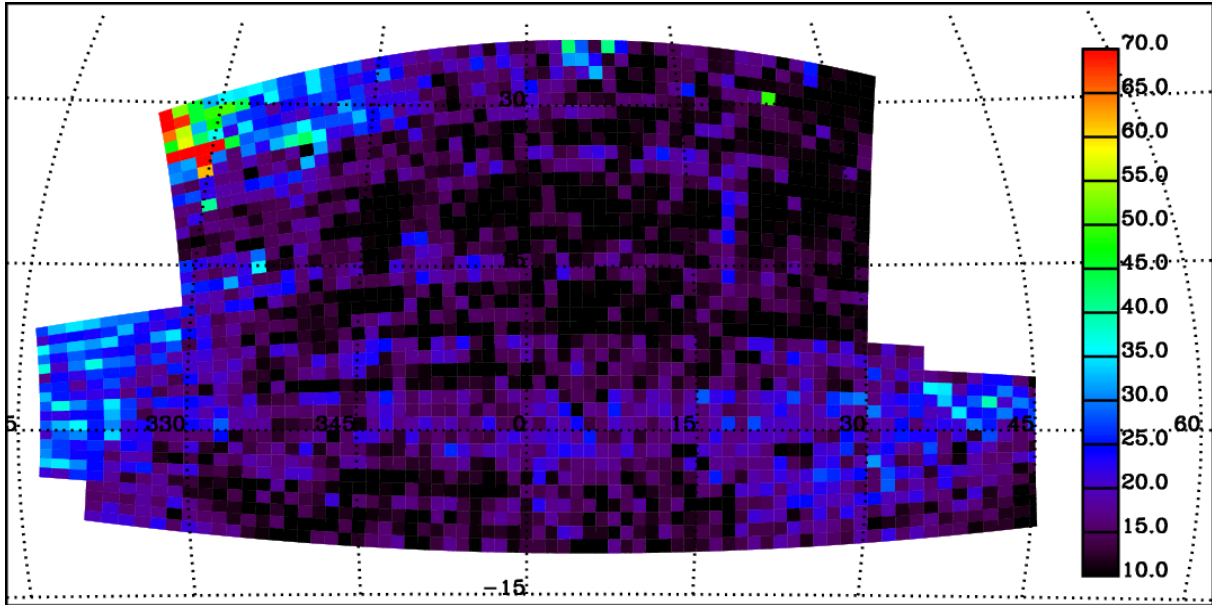


FIG. 7.— The quasar target density map in the SGC for the XDQSO CORE targets, displayed in equatorial coordinates. The units are targets  $\text{deg}^{-2}$ .

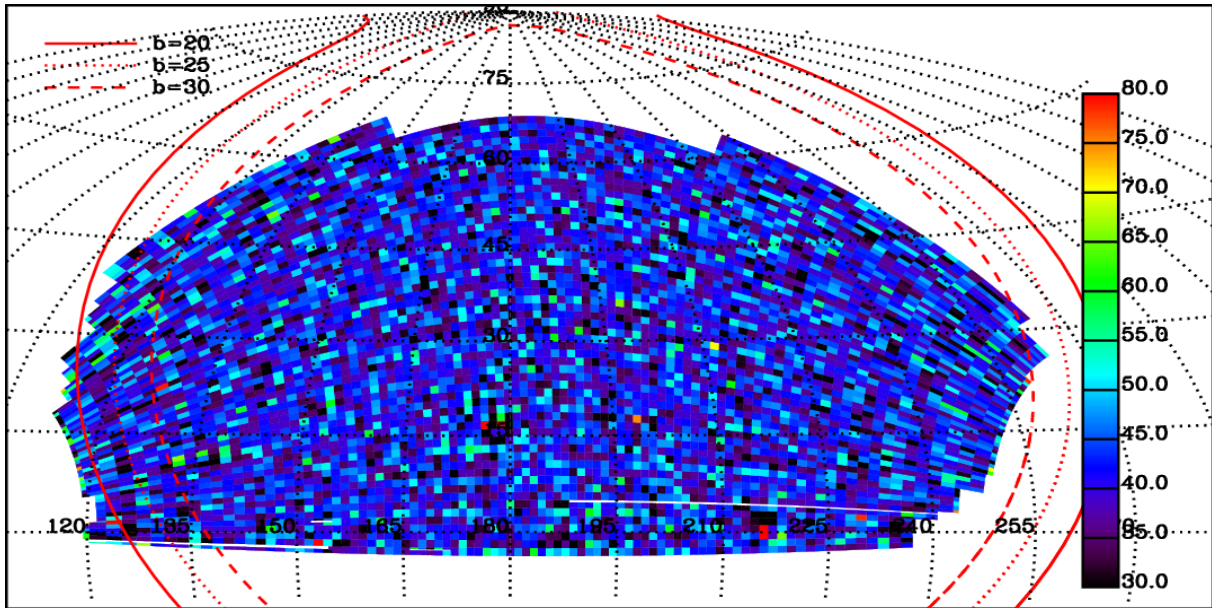


FIG. 8.— The quasar target density map in the NGC for all our targets, CORE+BONUS+KNOWN+FIRST, displayed in equatorial coordinates. The units are targets  $\text{deg}^{-2}$ .

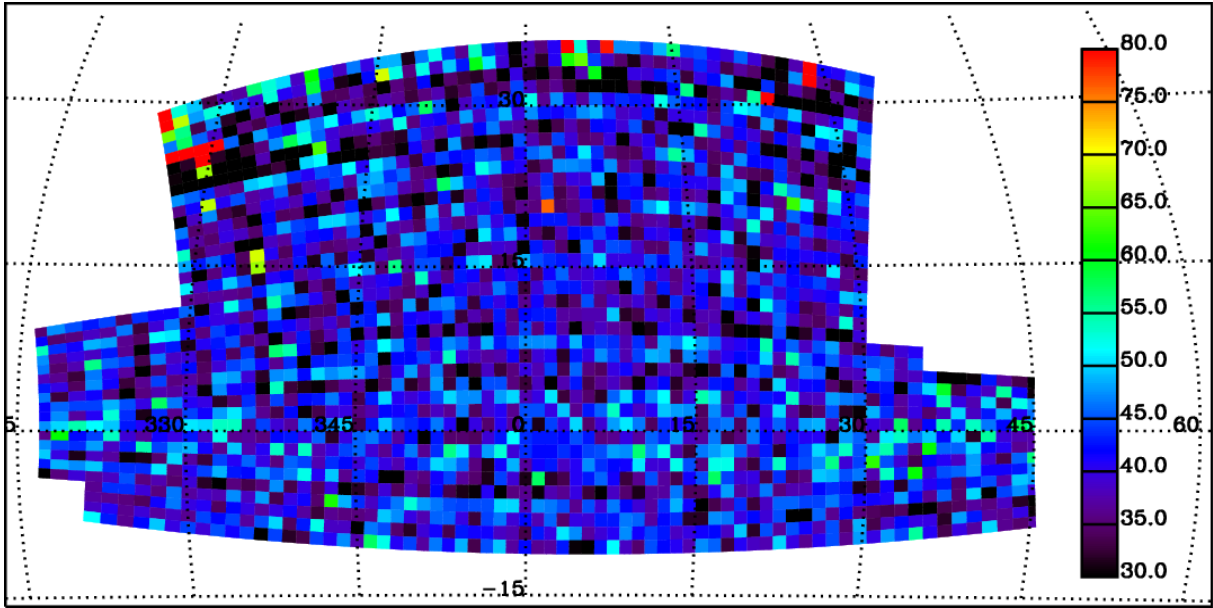


FIG. 9.— The quasar target density map in the SGC for all our targets, CORE+BONUS+KNOWN+FIRST, displayed in equatorial coordinates. The units are targets  $\text{deg}^{-2}$ .

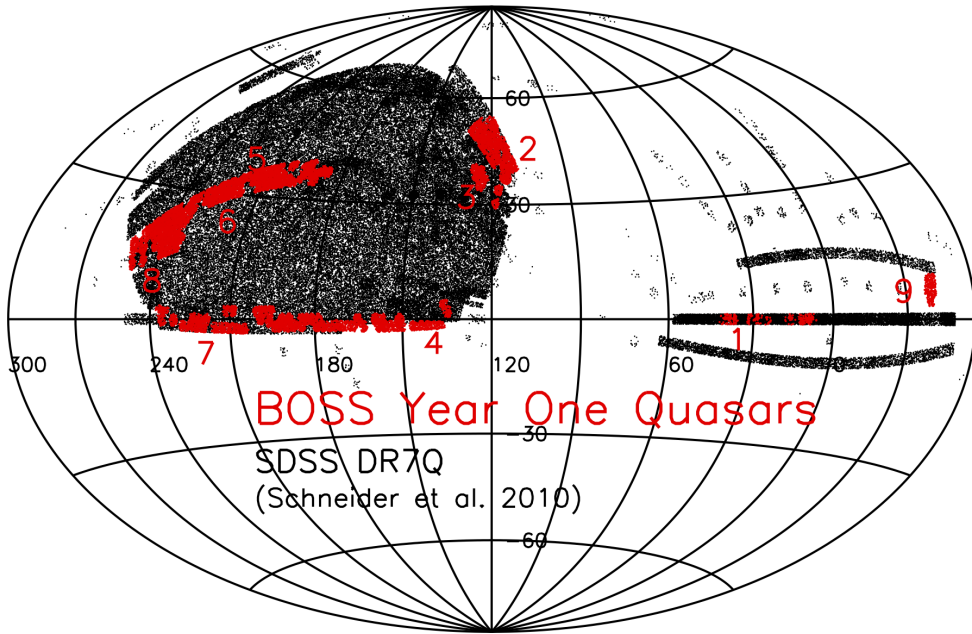


FIG. 10.— Sky distribution of the 14,287 quasars in the BOSS Year One quasar survey (J2000 equatorial coordinates), in red. The nine chunks are labeled accordingly, and the dotted lines are drawn at Galactic latitudes  $b = \pm 25^\circ$ . The spectroscopically confirmed SDSS-I/II DR7 quasar catalog (Schneider et al. 2010) is shown for comparison in black.

Of course, the DR7 sample is selected over the full SDSS-II imaging area, approximately  $9,380 \text{ deg}^2$ , while the BOSS Year One data come from observations of  $880 \text{ deg}^2$ . Already BOSS has slightly more quasars in the  $z = 2.2 - 2.8$  range, while at higher redshifts the DR7 sample remains larger.

Degeneracies in the color-redshift relation of quasars lead to the selection of low- $z$  quasars in BOSS. The quasars at  $z \sim 0.8$  have  $\text{Mg II } \lambda 2800 \text{ \AA}$  at the same wave-

length as  $\text{Ly}\alpha$  at redshift  $z \sim 3.1$ , giving these objects similar broad-band colors, while the large number of objects at  $z \sim 1.6$  is due to the confusion between  $\lambda 1549 \text{ C IV}$  and  $\text{Ly}\alpha$  at  $z \approx 2.3$ . We shall come back to this feature when comparing the performance of the NN, KDE, and Likelihood methods in § 5.4. The tail of objects at  $z \gtrsim 3.5$  includes a significant contribution from re-observations of previously known quasars.

Figures 12 and 13 present our key results, the efficiency

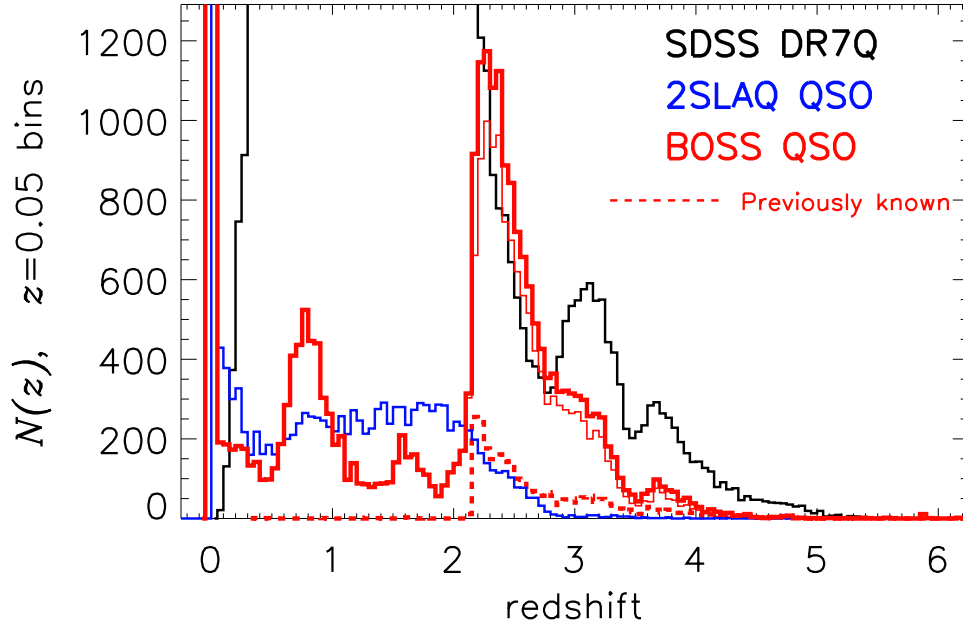


FIG. 11.— The redshift histogram of BOSS Year One quasars (solid red thick histogram). The dashed red line represents those objects known prior to BOSS observations, while the distribution of newly confirmed quasars is given by the thin red line. For comparison the SDSS DR7 quasars from Schneider et al. (2010) (selected over a much larger sky area) are shown by the black histogram, while the 2SLAQ quasar data (Croom et al. 2009), are in blue.

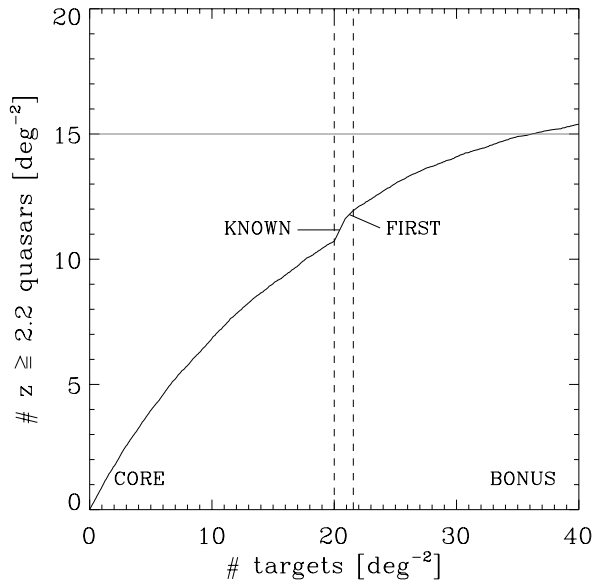


FIG. 12.— Cumulative number of quasars with  $z > 2.2$  as a function of the rank of the target for the Stripe 82 control sample with single-epoch photometry. At 20 fibers  $\text{deg}^{-2}$ , the XDQSO CORE algorithm selects  $10.7 \text{ quasars deg}^{-2}$ , while previously known and FIRST sources add an average of  $1.5 \text{ quasars deg}^{-2}$ . At 40 fibers  $\text{deg}^{-2}$ , the total surface density of  $z > 2.2$  quasars selected by our current algorithms from single-epoch SDSS photometry is  $15.4 \text{ deg}^{-2}$ . Note that these numbers represent an average over a wide range of Galactic latitude, and therefore stellar contamination.

of the current target selection algorithms. For these tests, we have constructed a control sample of targets on Stripe 82, where our spectroscopy is more complete than anywhere else on the sky, albeit still not perfect. Here we include data from Year Two from Chunk 11, where Stripe 82 was retargeted using a variability selection for quasars

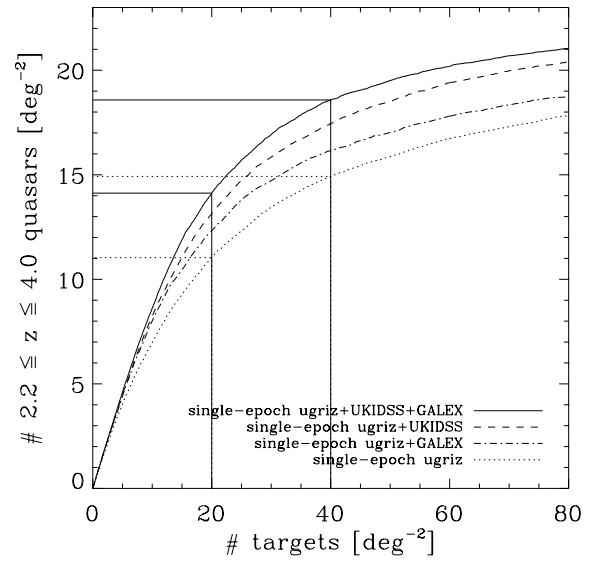


FIG. 13.— Similar to Figure 12, but showing the impact of adding GALEX photometry, UKIDSS photometry, or both to SDSS single-epoch photometry. This Figure is based on Stripe 82 data and XDQSO selection for all targets.

(Palanque-Delabrouille et al. 2010). Stripe 82 also has high completeness because quasars are selected from co-added photometry, with much smaller photometric errors.

For Figure 12, we select the quasar targets in our normal way from *single-epoch* data, with the first 20 targets  $\text{deg}^{-2}$  selected by the XDQSO CORE algorithm. Targets are ranked in order of probability, and the plot shows the number of  $z > 2.2$  quasars  $\text{deg}^{-2}$  vs. the number of targets  $\text{deg}^{-2}$ , with the slope of the curve

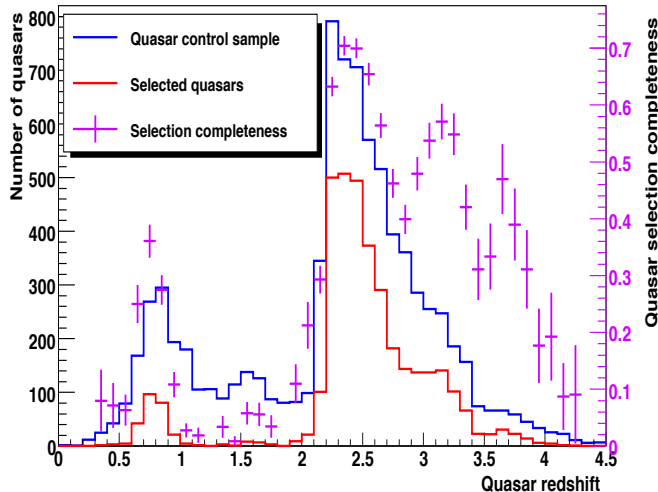


FIG. 14.— Completeness of BOSS single-epoch target selection vs. redshift, on Stripe 82. The blue histogram shows the redshift distribution of all spectroscopically confirmed quasars on Stripe 82. The red histogram is for those quasars that pass the BOSS single-epoch target selection for a threshold tuned to produce 40 targets  $\text{deg}^{-2}$ . Purple points with Poisson error bars show the ratio of the two, i.e., the selection completeness (right-hand scale).

indicating the efficiency of selection. The CORE algorithm selects  $10.7 z > 2.2$  quasars  $\text{deg}^{-2}$  from its 20 targets. We then show the average contribution of KNOWN and FIRST quasars, totaling  $1.6$  high- $z$  quasars  $\text{deg}^{-2}$ . This increment assumes a surface density of  $0.9$  known high- $z$  quasars  $\text{deg}^{-2}$  (and  $0.7 \text{ deg}^{-2}$  from FIRST), which is consistent with our Year One data (see Table 6) but lower than the surface density of known pre-BOSS high- $z$  quasars on Stripe 82, which is unusually well studied. Finally, we add the BONUS targets from the NN-combinator, again in rank order. At  $40$  targets  $\text{deg}^{-2}$ , we are just above the minimum BOSS goal, with a mean density of  $15.4 z > 2.2$  quasars  $\text{deg}^{-2}$ . Stripe 82 samples a wide range of Galactic latitude and thus stellar density; we therefore anticipate that this test should be representative of selection efficiency averaged over the full BOSS survey region. We also found from observations of early chunks, that adding additional fibers beyond the nominal  $40 \text{ deg}^{-2}$ , led to only very minimal gains in yield.

Figure 13 shows the impact of adding UKIDSS and GALEX data to single-epoch SDSS photometry. For this test we use the XDQSO algorithm alone, since this is where these auxiliary data sets currently enter our selection procedures, and we extend the efficiency curves up to  $80$  targets  $\text{deg}^{-2}$ . At  $40$  targets  $\text{deg}^{-2}$ , the efficiency for XDQSO with single-epoch SDSS imaging alone is  $15.0 z > 2.2$  quasars  $\text{deg}^{-2}$ . Adding GALEX data improves the efficiency to  $16.2 \text{ deg}^{-2}$ , adding UKIDSS improves it to  $17.3 \text{ deg}^{-2}$ , and adding both improves it to  $18.6 \text{ deg}^{-2}$ . Thus, both of these data sets can significantly enhance the efficiency of BOSS quasar target selection in regions where they are available. Stripe 82 has medium-deep (“MIS”) GALEX data, and the improvement with shallower (“AIS”) coverage will be smaller, but our tests indicate that GALEX addition will still improve the selection.

Fig. 14 shows the redshift distribution of all known quasars on Stripe 82 as a function of redshift, as well

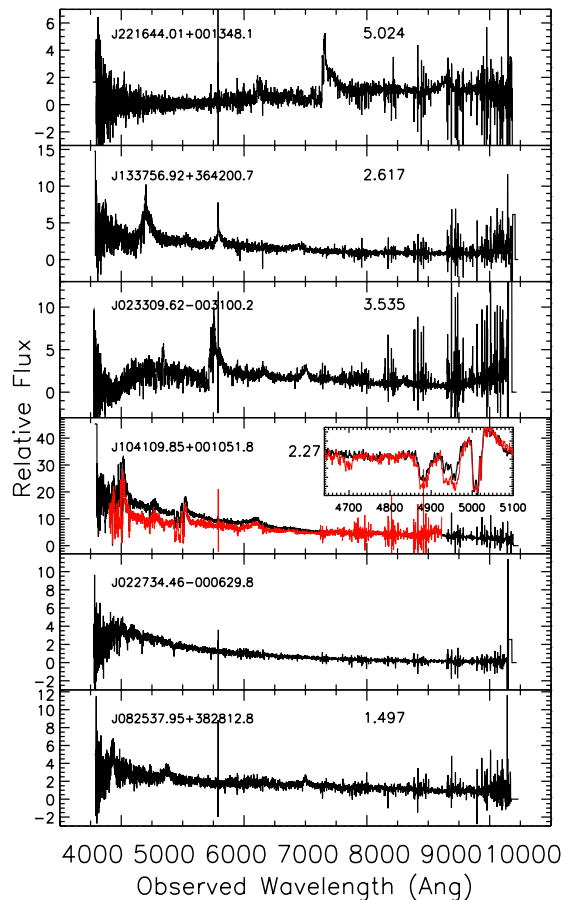


FIG. 15.— Examples of spectra of BOSS quasar targets. The SDSS object name and pipeline redshift are given in each panel (except for the star). From top to bottom: a  $z > 5$  quasar found by the Likelihood method; a newly discovered  $z = 2.6$  quasar at the typical S/N; a  $z = 3.5$  quasar selected only by the KX method (§ 3.5.1); a re-observed BAL quasar showing spectroscopic variability (black line is the BOSS spectrum; red is from SDSS, a spectrum taken 3377 days earlier); a star with our typical S/N and a  $z = 1.5$  quasar with our typical S/N. The feature at  $5577\text{\AA}$  in all spectra is a residual from a sky line.

as those selected by the single-epoch SDSS algorithms illustrated in Fig. 12 above. The ratio of the two measures the completeness of BOSS single-epoch quasar selection relative to known quasars in this well studied region, ranging from 40% to 70% over our critical redshift range  $2.2 < z < 3.5$ . Of course, this remains a lower limit to the true completeness at the BOSS magnitude limit, though in the  $2.2 < z < 3.5$  redshift range we anticipate that the BOSS Stripe 82 sample selected from co-added photometry and variability has high completeness (Palanque-Delabrouille et al. 2010).

Fig. 15 shows examples of BOSS spectra of quasar targets from the Year One data. From top to bottom: a  $z > 5$  quasar found by the Likelihood method (and not selected by any other method); a newly discovered  $z = 2.6$  quasar at a typical S/N; a  $z = 3.5$  quasar selected only by the KX method; a re-observed BAL quasar showing spectroscopic variability over 3377 days in the observed frame; a star at our typical S/N; and a  $z = 1.5$  quasar with our typical S/N.

## 5.2. Magnitude, Color and the $L - z$ Plane



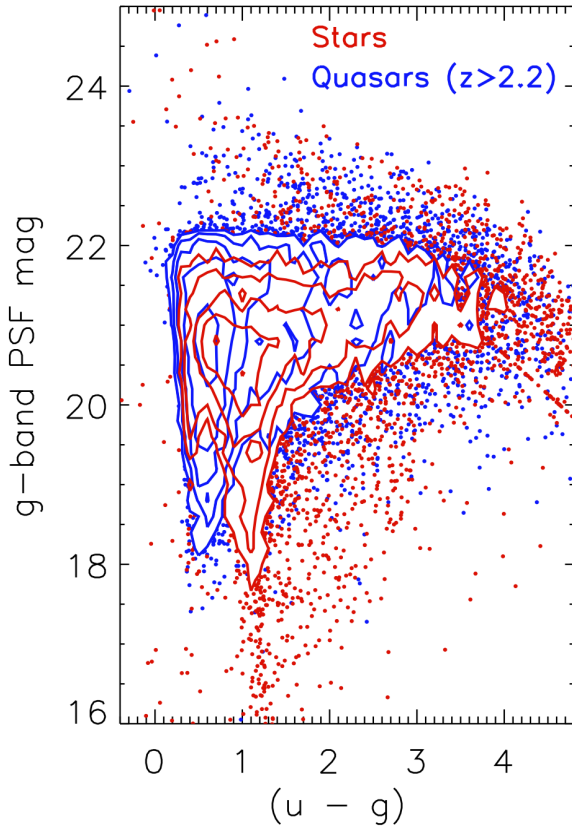


FIG. 16.— Color-magnitude diagram ( $(u-g)$  vs.  $g$ ) for objects spectroscopically classified as stars (red contours and points) and  $z > 2.2$  quasars (blue contours and points). Only objects with  $z\text{Warning}=0$  are shown. The quasars are systematically bluer; there are very few quasars with  $g < 18$ .

Fig. 16 shows the distribution of quasar targets from the BOSS first-year data which are spectroscopically confirmed as either stars or  $z > 2.2$  quasars, in the  $(u-g)$  vs.  $g$  color-magnitude plane. The distribution of stars at the bright end,  $g < 18$ , and the lack of bright  $z > 2.2$  quasars, led us to impose the bright  $i = 17.8$  limit. Objects fainter than  $g = 22$  are brighter than our  $r$  band limit of 21.85 mag.

Fig. 17 shows the SDSS  $(u-g)$ ,  $(g-r)$ ,  $(r-i)$ , and  $(i-z)$  colors as a function of redshift for the BOSS Year One data. Also shown are the mean color in redshift bins (thin solid line), and the model of Bovy et al. (2011b, in prep.; thick colored line). This model is systematically bluer than the data at low redshift; BOSS target selection systematically excludes UV-excess quasars, and thus those low-redshift quasars that happen to enter the sample are redder than the average quasar. The trends with redshift are due to various emission lines moving in and out of the SDSS broadband filters, and the onset of the Ly $\alpha$  forest and Lyman-limit systems (e.g., Fan 1999, Richards et al. 2002, 2003, Hennawi et al. 2010, Bovy et al. 2011 and Peth et al. 2011, but see also Prochaska et al. 2009 and Worseck & Prochaska 2011). McGreer et al. (2011, in preparation) will present a detailed analysis of this diagram, and its implications for our completeness.

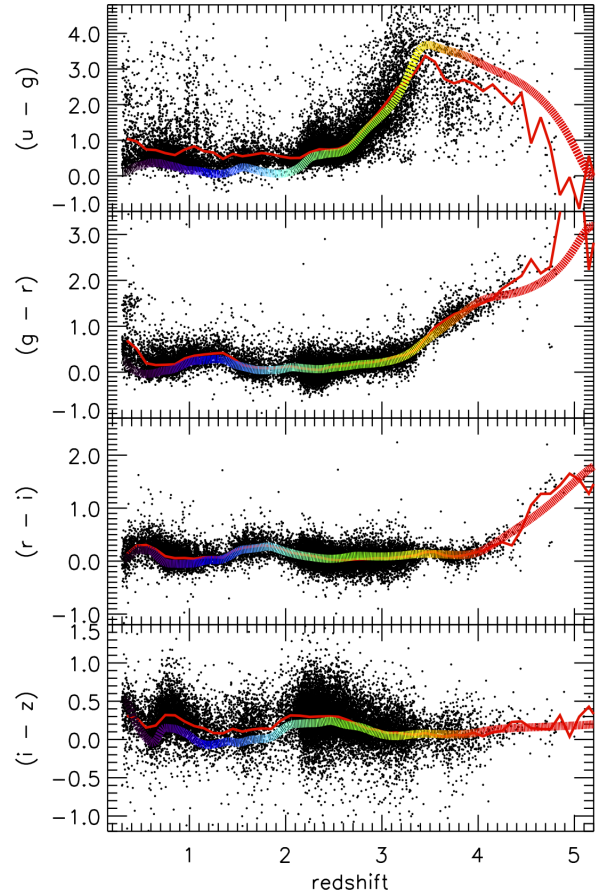


FIG. 17.— SDSS colors vs. redshift for quasars in the BOSS Year One data. The thin solid line is the mean color in bins of redshift, while the thick colorful line is from the model of Bovy et al. (2011, in preparation). The model is systematically bluer than the data at low redshift because BOSS systematically excludes UV-excess sources.

Fig. 18 shows the SDSS color-color diagrams for the first year BOSS quasars, for all quasars with good ( $z\text{Warning}=0$ ) redshifts above  $z = 2.2$ . This figure illustrates the redshift dependence of quasar colors as the Ly $\alpha$  emission line moves from the  $g$  band to the  $r$ -band at  $z \approx 3.5$ . Quasars with  $2.2 < z < 3.5$  lie in the range  $-0.3 < (g-r) < 0.6$ , while objects with  $z > 3.5$  generally have  $(g-r) > 0.8$ .

Fig. 19 shows the distribution of objects in the redshift-luminosity ( $L-z$ ) plane for three recent large quasar surveys: SDSS (black points), 2SLAQ (cyan) and BOSS (red). There are  $\approx 105,000$  objects in the SDSS DR7 catalog, and  $\approx 9,000$   $g \leq 21.85$  low-redshift quasars from the 2SLAQ Survey (Croom et al. 2009). We calculate the absolute  $i$ -band magnitudes,  $M_i$ , using the observed  $i$ -band PSF magnitudes and the  $k$ -corrections given in Table 4 of Richards et al. (2006). The three surveys together cover the  $L-z$  plane well, with a dynamic range in luminosity of  $\approx 4$  magnitudes at any given redshift up to  $z \sim 3.5$ . This coverage will be vital for calculating the evolution of the faint end of the quasar luminosity function, and placing strong constraints on the luminosity dependence of quasar clustering.

### 5.3. Comments on Several Chunks

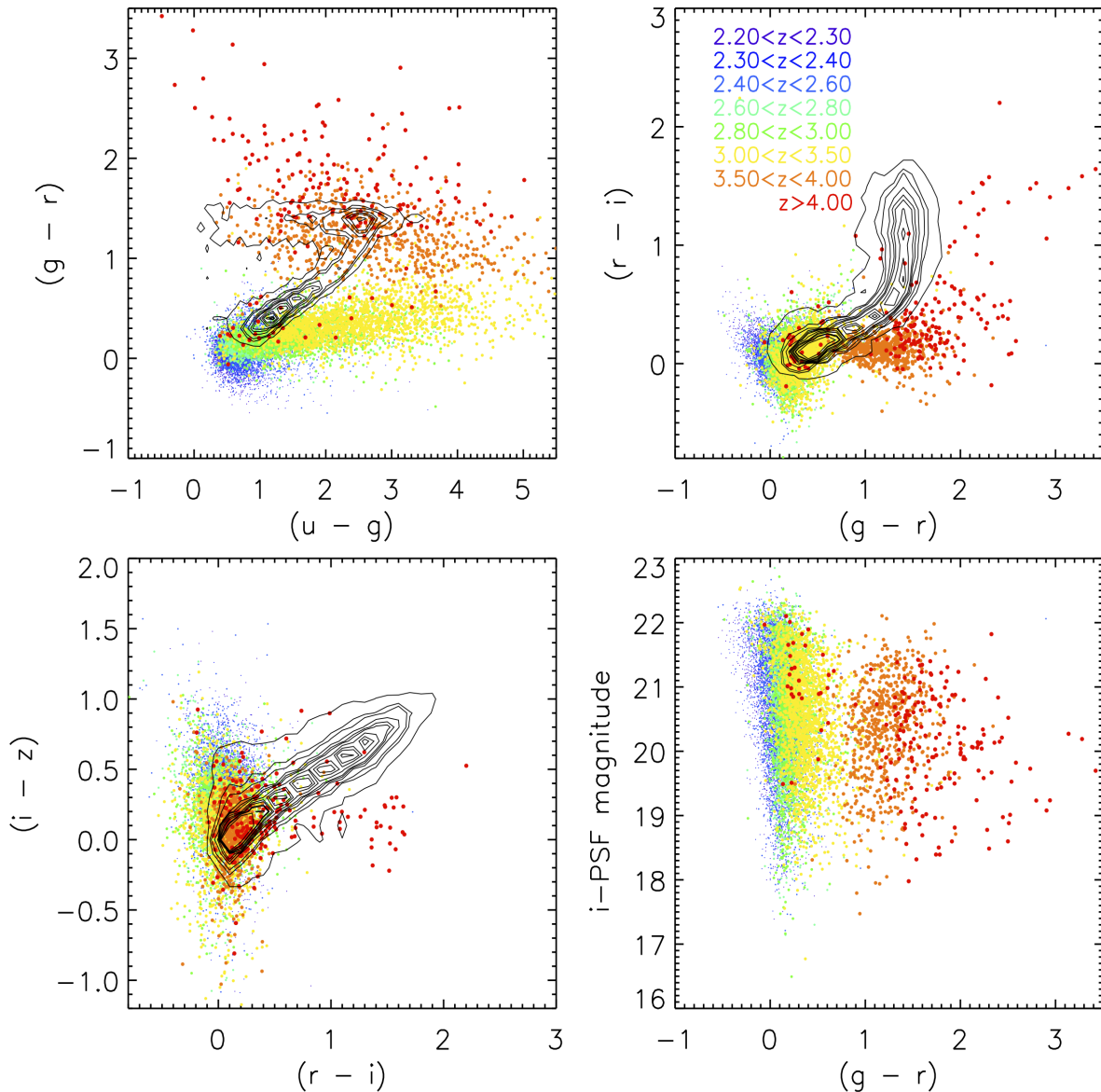


FIG. 18.— Color-color diagrams for the First Year data for all spectroscopically confirmed quasars with good ( $z\text{Warning}=0$ ) redshifts above  $z = 2.2$ . The stellar locus is shown as contours. *Top left*,  $ugr$ ; *top right*,  $gri$ , *bottom left*,  $riz$ . The horizontal swath of both stars and quasars at  $g - r \sim 1.5$  in the  $u - g, g - r$  color-color diagram is caused by the large  $u$ -band photometric errors in the reddest objects. The colors of points encode their redshifts; the sizes of the points vary for clarity. The lower right panel shows the  $i$  magnitude as a function of the  $g - r$  color.

Because of the BOSS hardware commissioning in Fall 2009, only  $37.4 \text{ deg}^2$  (out of a possible  $220 \text{ deg}^2$ ) were observed in Chunk 1 under survey-quality conditions after MJD 55169. Thus Stripe 82 was re-targeted, re-tiled and re-observed for Year Two as Chunk 11 (Palanque-DeLabrouille et al. 2010). However, the non-survey quality data from prior to MJD 55169 were visually inspected during the very early part of the survey, and used to inform subsequent QTS decisions.

In Chunks 1-6, the quasar target selection algorithm was generous, allocating  $60\text{-}80$  targets  $\text{deg}^{-2}$ . Chunk 7 was the first time we ran the BOSS QTS at the nominal  $40$  targets  $\text{deg}^{-2}$ . Of the  $4,506$  unique targets in this chunk,  $1,595$  (35%) are classified as  $z > 2.20$  objects with  $z\text{Warning}=0$  (Table 5). Although this does

not reach the BOSS efficiency goal of 50%, there are several reasons that this number can be considered a lower bound. First, Chunk 7 is in the region of sky known to have a high density of faint stellar sources, due to the presence of the tidal stream of the Sagittarius dwarf spheroidal galaxy (see Ibata et al. 1995, 1997; Belokurov et al. 2006, and our Fig. 4). Second, visual inspections of the spectra identified  $0.5\text{-}1$  more high- $z$  quasars per square degree than the pipeline, and while not all of these might be suitable for Ly $\alpha$ F analyses (e.g., due to BALs which cause the pipeline to fail), there should be a net gain upon production of the final BOSS quasar catalogs. Finally, and potentially most importantly, we know that our target selection methods and algorithms have continued to improve, with the incorporation of XDQSO and



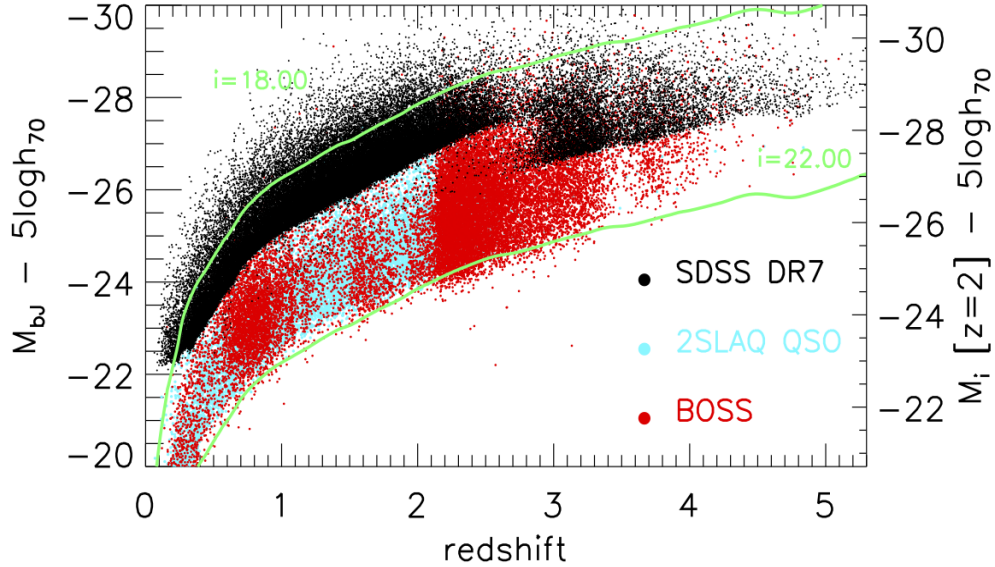


FIG. 19.— The  $L - z$  plane for three recent quasar surveys: SDSS-I/II, (black points), 2SLAQ (cyan) and BOSS (red). The luminosity assumes  $H_0 = 70 \text{ km s}^{-1} \text{ Mpc}^{-1}$ . There are  $\approx 105,000$  objects in the SDSS DR7 catalog and  $\approx 9,000$   $g \leq 21.85$  low-redshift quasars from the 2SLAQ Survey (Croom et al. 2009). The three surveys together give a dynamic range in luminosity of  $\approx 4$  magnitudes at any given redshift up to  $z \sim 3.5$ . The luminosity corresponding to magnitude limits of  $i = 22$  on the faint end and  $i = 18$  on the bright end are shown. The coverage here can be compared to Fig. 5 in Croton (2009).

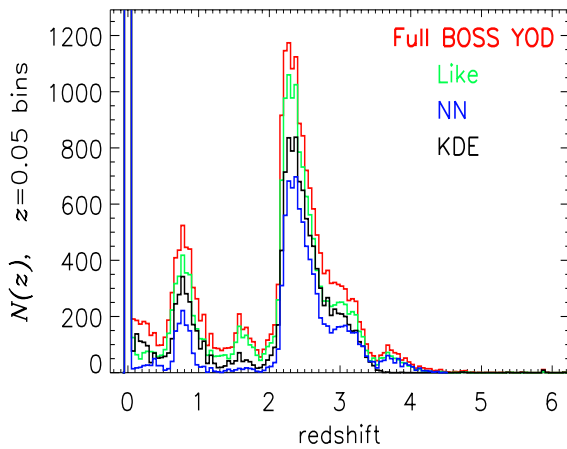


FIG. 20.— The BOSS quasar redshift distribution for objects with reliable redshifts ( $z\text{Warning}=0$ ), selected by our three main methods from Year One. The green, blue and black histograms give the redshift distributions for the Likelihood, NN and KDE methods, respectively. The red histogram is the full sample from Figure 11. These methods were not applied uniformly through Year One, so this plot is shown for *qualitative and informative* purposes only, and should not be used as a direct comparison between the methods. The KDE, NN and Likelihood algorithms are *not* mutually exclusive, with many objects selected by more than one method.

ancillary data such as UKIDSS and GALEX (see also the discussion on a variability based QTS in § 7).

In this context, the performance of QTS in Chunks 8 and 9, with only 11.5 and 9.5  $z > 2.2$  quasars  $\text{deg}^{-2}$  respectively, was disappointing. Chunk 8 lies at relatively low Galactic latitudes, and is affected by stellar contamination. Chunk 9 is in a region of sky where there was neither previously known quasars nor FIRST radio coverage. We continue to observe the rest of Chunks 8 and 9 in Year Two.

| Selection  | # Quasar targets | # with $z\text{Warning}=0$ | and with $z > 2.20$ | or are stars  |
|------------|------------------|----------------------------|---------------------|---------------|
| Totals     | 52,238           | 33,556                     | 13,580              | 11,149        |
| KDE        | 34,503 (4794)    | 20,993 (2693)              | 9,050 (229)         | 7,607 (1,856) |
| NN         | 16,747 (975)     | 13,267 (710)               | 7,743 (135)         | 3,604 (504)   |
| Likelihood | 29,150 (2325)    | 21,975 (1647)              | 11,244 (447)        | 4,483 (724)   |

TABLE 7

THE NUMBER OF UNIQUE QUASAR TARGETS FROM THE FIRST YEAR OF BOSS SPECTROSCOPY, BROKEN DOWN BY THE THREE KEY SELECTION METHODS. NUMBERS IN PARENTHESES INDICATE THE NUMBER OF OBJECTS SELECTED BY THE INDICATED METHOD *only*. BECAUSE THESE METHODS WERE APPLIED NON-UNIFORMLY, THIS TABLE IS PROVIDED AS AN *informational guide*, AND NOT AS A DIRECT COMPARISON BETWEEN METHODS (SEE TEXT FOR FURTHER EXPLANATION).

#### 5.4. Comparison of Algorithms

The original motivation for the implementation of multiple target selection algorithms was the lack of evidence prior to BOSS observations that a single method could select  $z > 2.2$  quasars down to  $g \approx 22$  with our required efficiency. With the Year One data now in hand, we can compare the effectiveness of our different methods. However, due to the continually changing nature of the BOSS QTS over this year, where different methods were used as CORE and BONUS, these comparison will be generally qualitative in nature. The interested reader is referred to the discussions in Bovy et al. (2011) for further comparisons.

As an aid for our discussions, we give a condensed version of Table 6 in Table 7, where we list the number of targets from this first year, broken down by the three key selection methods. Again, given the non-uniform selection over this year, this table is provided as an *informational guide* only; it should not be used as a direct comparison between methods.

The redshift distributions for objects with reliable redshifts selected by our three main methods (NN, KDE, and Likelihood) are given in Fig. 20. Again, because of the non-uniform manner in which these methods were applied during Year One, this plot should not be interpreted as a quantitative comparison between the methods. There is substantial overlap between the methods; many objects are selected by more than one technique. The three histograms have similar shapes over the range  $2.2 < z < 3.5$ . While NN avoids being confused by  $z \sim 1.5$  objects, and KDE avoids objects at  $z > 3.5$ , all three methods select a substantial number of objects at  $z \sim 0.8$ .

Figs. 21, 22 and 23 show the color-color and the color-magnitude distributions of  $z > 2.2$  quasars selected by the Likelihood, NN and KDE methods, respectively. The figures show in orange and black the ratio of numbers of objects selected by each method to the total number of Year One quasars, at each point in color space. This ratio is normalized to the global ratio of targets from Column 4 of Table 7; thus a point in color space with a value  $> 100\%$  is one where the method in question outperforms the total selection on average. The difference between the three methods is clear in the  $(u-g)$  vs.  $(g-r)$  diagrams. The contours for the Likelihood method are fairly flat away from the stellar locus. NN performs well at  $(u-g) \sim 0.6$ ,  $(g-r) \sim 0$  and in those regions of color-color space corresponding to higher-redshift quasars, but does more poorly elsewhere. KDE selects objects only over a very narrow range in  $(g-r)$ . From the  $(g-r)$  vs.  $i$ -band color-magnitude diagram (bottom right panels of the figures), we see that the Likelihood method was more efficient at selecting fainter,  $i \gtrsim 21.0$  quasars, while the NN tends to select the brighter  $i \lesssim 20.0$  objects at all  $(g-r)$  colors.

These trends can be understood given the methodology of these algorithms. The Likelihood method down-weights objects close to the stellar locus as the denominator of equation (5) gets large, which is why Likelihood selects few objects there. Otherwise, the Likelihood method traces the overall BOSS Year One sample in color-color and color-magnitude space. The Likelihood method did not place any cuts on photometric redshift, and hence samples the high redshift distribution of the BOSS data well, especially at  $(g-r) \gtrsim 1$  (corresponding to redshift  $z > 3.5$ ). We refer the interested reader to Kirkpatrick et al. (2011) for full details of the Likelihood performance.

At the crux of an artificial neural network is the sample of objects used to train it (see Yèche et al. 2010 and references therein, and Section 3.4). The training set for the NN we have used was based on the SDSS quasar catalog and the 2SLAQ surveys, and did *not* use data from the MMT pilot survey (Appendix C) or the AUS survey. Thus, this training set was geared towards brighter quasars ( $i < 20.2$ ), giving rise to the tendency for NN to select the brighter quasars.

The KDE training set included only  $2.2 < z < 3.5$  quasars, and thus the redshift histogram drops to zero at  $z = 3.5$  (Fig 20). This is related to the fact that KDE quasars inhabit a much narrower range of the  $(g-r)$  vs.  $(r-i)$  color-color plane than the other two methods. In summary, Figures 21-23 reflect the relative strengths and trainings of these methods; ultimately, the

three methods complemented each other well.

### 5.5. The Blind Test Area

After spectroscopy from the first few chunks had been analyzed, it became clear that the survey would have to decide on a single method for the CORE, and that we would have to restrict ourselves to the nominal target density of 40 targets  $\text{deg}^{-2}$ . Thus, we designed a test to decide which combinations of methods gave the best yields for the CORE and BONUS selections.

The “Blind Test Area” is a region of sky of  $\sim 1000 \text{ deg}^2$  in the NGC at high declination ( $\delta > +40^\circ$ ) and high Galactic latitudes, shown by the thin white line in Fig. 4. This area is used for tuning the threshold of each method to a particular target density. The resulting thresholds were then applied to existing data to determine the selection efficiency.

Table 8 summarizes these tests. This table gives the surface density of  $2.2 < z < 3.5$  quasars from early (Chunk 1, 2 and 3) BOSS spectroscopic data that would be recovered by various methods at various thresholds of their key parameters when they are tuned to yield a surface density of 20 or 40  $\text{deg}^{-2}$  in the blind survey region. The effectiveness of each quasar spectrum for Ly $\alpha$  forest studies depends on its redshift (and thus the spectral coverage of the forest) and its brightness (and thus the S/N of the spectrum). This “value” is quantified by a score of each quasar, motivated by the checks performed in McDonald & Eisenstein (2007); summing this over the expected quasars per square degree gives the numbers in Table 8. These scores do not include contributions from quasars outside the redshift range  $2.2 < z < 3.5$ . “Weighted Likelihood” was an adaption of the Likelihood method to maximize this score, as discussed in detail by Kirkpatrick et al. (2011).

We also tried selecting quasars using a simple color region isolating the region where  $z \sim 2.7$  quasars are found, akin to the mid- $z$  box used by Richards et al. (2002), but this did not deliver an efficiency close to our requirements.

Although Table 8 shows that the KDE method returns the most  $z > 2.2$  quasars ( $9.45 \text{ deg}^{-2}$ ) at the CORE target density of 20  $\text{deg}^{-2}$ , after much deliberation, we selected the Likelihood method as CORE for the latter stages of Year One, since it is a simpler algorithm to understand and explain, it has a more uniform spatial selection, and is easier to reproduce. Further tests showed that using the Neural Network in its “Combinator” mode for BONUS would yield the highest number of high- $z$  quasars overall. The difference when weighting by the Ly $\alpha$  forest score was too small to motivate us to include it; see the discussion in McQuinn & White (2011).

However, tests of the Year One data with the XDQSO method (Bovy et al. 2011) showed it selected about 1  $z > 2.2$  quasar  $\text{deg}^{-2}$  more than Likelihood. Thus in Chunks 12 and 13 (Section 4.5) the union of Likelihood and XDQSO was treated as CORE, allowing us to test them directly against one another (Bovy et al. 2011). In Chunks 12 and 13, 2426 out of 4710 XDQSO targets had spectra with  $z\text{Warning}=0$  and  $2.2 < z < 3.5$ , for an efficiency of 52%, while Likelihood obtained 2296 quasars from 5086 targets, for a 45% efficiency. This result is our

| Method              | Threshold<br>@ 20 deg <sup>-2</sup> | Threshold<br>@ 40 deg <sup>-2</sup> | $N_{\text{quasar}}$ (deg <sup>-2</sup> )<br>@ 20 deg <sup>-2</sup> | $N_{\text{quasar}}$ (deg <sup>-2</sup> )<br>@ 40 deg <sup>-2</sup> | Score (deg <sup>-2</sup> )<br>@ 20 deg <sup>-2</sup> | Score (deg <sup>-2</sup> )<br>@ 40 deg <sup>-2</sup> |
|---------------------|-------------------------------------|-------------------------------------|--|--|--|--|
| KDE                 | 0.904                               | 0.599                               | 9.45   | 11.35  | 4.79   | 5.71   |
| Likelihood          | 0.543                               | 0.234                               | 8.70   | 12.23  | 4.39   | 5.89   |
| Weighted Likelihood | 0.262                               | 0.108                               | 8.89   | 12.33  | 4.58   | 5.98   |
| NN                  | 0.852                               | 0.563                               | 7.62   | 10.84  | 4.00   | 5.51   |
| NN Combinator       | 0.853                               | 0.573                               | 9.37   | 12.81  | 4.69   | 6.26   |
| Color Box           | n/a                                 | n/a                                 | 6.45   |  | 3.41   |  |

TABLE 8

THE SURFACE DENSITY OF SPECTROSCOPICALLY CONFIRMED  $2.2 < z < 3.5$  QUASARS FROM EARLY (CHUNK 1, 2 AND 3) BOSS SPECTROSCOPIC DATA THAT WOULD BE RECOVERED BY VARIOUS METHODS, AND THE THRESHOLDS OF THE KEY PARAMETERS (TABLE 3) REQUIRED TO YIELD A SURFACE DENSITY OF 20 OR 40 DEG<sup>-2</sup> IN THE BLIND SURVEY REGION (§ 5.5). THE WEIGHTED LIKELIHOOD INCORPORATED A WEIGHTING FUNCTION WHICH OPTIMIZES THE S/N OF THE LY $\alpha$  FOREST CLUSTERING SIGNAL. THE REDSHIFT AND FLUX DISTRIBUTION OF THE RESULTING QUASAR SAMPLE DETERMINES THIS SIGNAL, AS QUANTIFIED BY THE SCORE IN THE LAST TWO COLUMNS.

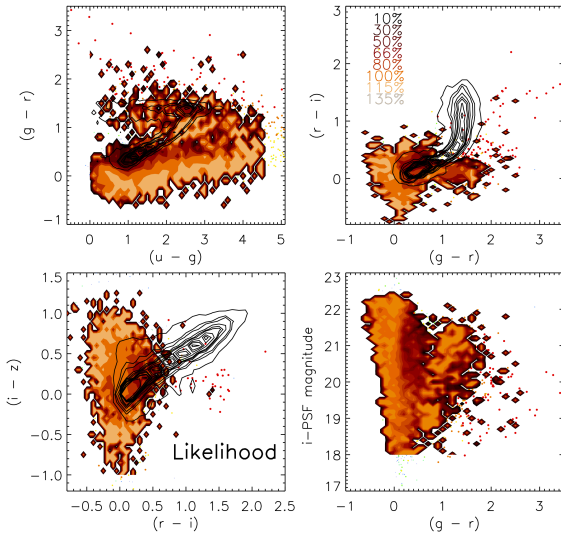


FIG. 21.— Distributions in color-color and color-magnitude space for  $z > 2.2$  quasars selected by the Likelihood method in Year One. The black contours give the location of the stellar locus, while the orange contours give the ratio, at each point of color space, of  $z > 2.2$  quasars selected by Likelihood to all Year One BOSS quasars, normalized to the global ratio of the two. Quasar numbers were smoothed with a tophat of width 0.10 mag in  $u - g$  and  $g - r$ , and 0.05 mag in  $r - i$  and  $i - z$ , before taking ratios.

motivation for declaring XDQSO to be CORE for the rest of the BOSS quasar survey.

## 6. THE COMPLETENESS OF CORE IN YEAR ONE

Studies of clustering in the Ly $\alpha$  forest are not biased by the distribution of background quasars used to illuminate Ly $\alpha$  forest absorption. Thus the Year One BOSS quasar sample can be used for these studies. Indeed, Slosar et al. (2011) have performed a first clustering analysis of Ly $\alpha$  forest flux from the BOSS Year One data.

However, given the changes in QTS throughout the first year, the quasar sample described in this paper is far from sufficiently uniform to be used directly for studies of the statistics of the quasars themselves, such as measurements of their luminosity function or clustering. The goals of the CORE sample is to have such a uniformly-selected sample of quasars, but as the definition of CORE changed several times during commissioning, CORE objects in the first year do not represent a statistical sample.

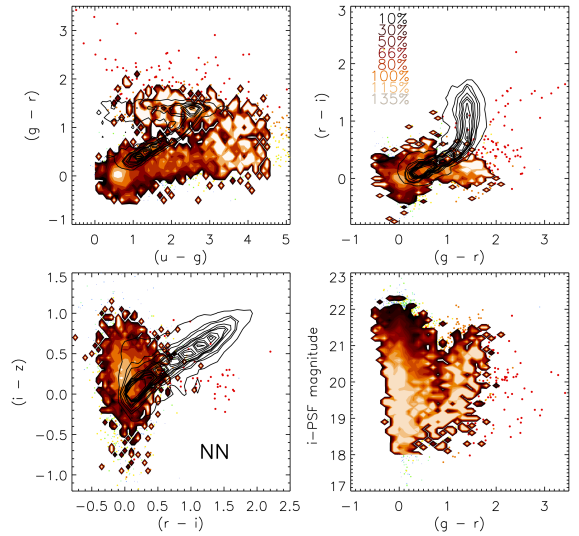


FIG. 22.— As in Figure 21, for the NN method.

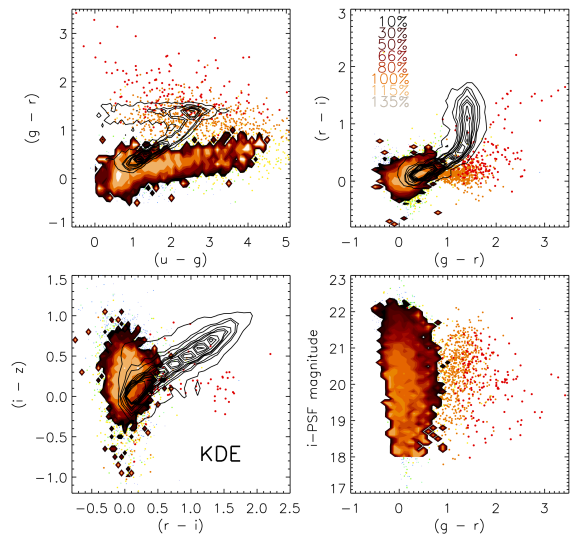


FIG. 23.— As in Figure 21, for the KDE method.

| Chunk | Effective                                 |   | Mean $C$ |
|-------|---|---|----------|
|       | Area (deg <sup>2</sup> )<br>$C \geq 0.75$ | Area (deg <sup>2</sup> )<br>$C \geq 0.75$ |          |
| 11    | 70.6                                      | 58.2                                      | 0.654    |
| 2     | 130.1                                     | 120.4                                     | 0.905    |
| 3     | 85.9                                      | 79.4                                      | 0.830    |
| 4     | 246.1                                     | 230.4                                     | 0.861    |
| 5     | 243.0                                     | 232.0                                     | 0.952    |
| 6     | 182.6                                     | 171.2                                     | 0.933    |
| 7     | 205.0                                     | 185.8                                     | 0.836    |
| 8     | 75.5                                      | 65.7                                      | 0.814    |
| 9     | 84.1                                      | 71.6                                      | 0.822    |
| 10    | 71.7                                      | 60.7                                      | 0.813    |

TABLE 9

FRACTION  $C$  OF OBJECTS THAT WOULD HAVE BEEN TARGETED BY THE *a posteriori* XDQSO CORE ALGORITHM, WHICH WERE ACTUALLY TARGETED, FOR EACH YEAR ONE CHUNK. CHUNK 11 HAS GREATER AREA COVERAGE THAN CHUNK 1, THUS WE LIST IT INSTEAD. THE SECOND COLUMN GIVES THE SOLID ANGLE (IN DEG<sup>2</sup>) OF THE REGION OF EACH CHUNK IN WHICH THE COMPLETENESS IS GREATER THAN 0.75, THE THIRD COLUMN LISTS THE SAME VALUE BUT FOR *effective area* (I.E. AREA  $\times$  COMPLETENESS) AND THE FOURTH COLUMN TABULATES THE MEAN COMPLETENESS OVER THE CHUNK. SEE ALSO FIG. 24.

The project settled on the XDQSO algorithm (§ 3.5; Bovy et al. 2011) for the CORE method at the end of Year One, and will use it for the rest of the survey. It is therefore useful to apply this algorithm to the photometry used in the Year One spectroscopy, and determine the completeness of the Year One targeted chunks. Table 9 and Fig. 24 give the results of this test. Given the placement and overlap of the spectroscopic plates, each chunk can be uniquely divided into sectors covered by a unique combination of plates. The completeness of the targeting: i.e., the fraction of the XDQSO CORE sources that were actually targeted in Year One, is measured for each sector separately. Encouragingly, these targeting completeness values are generally 80% or higher, which indicates that statistical analyses of the final CORE sample should be able to incorporate Year One data by introducing moderate weighting factors. The lower targeting completeness (65%) on Chunk 11 highlights a subtle point: the completeness for CORE-selected *quasars* should be higher than the completeness for CORE targets as a whole, because the true quasars are the most likely to also be selected by one of our other algorithms. In the case of Chunk 11, the deeper Stripe 82 photometry eliminates many noisy stellar contaminants in the single-epoch XDQSO target list, but it probably selects nearly all of the true quasars selected by CORE.

*For Year Two and the remainder of the BOSS quasar Survey, the core sample is defined by boss\_target1 flag QSO\_CORE\_MAIN (bit 40) and QSO\_CORE\_ED for Chunks 12 and 13, and QSO\_CORE\_MAIN (bit 40) only for later chunks (Table 10).*

For calculations of the quasar luminosity function, one must also account for the incompleteness of the XDQSO CORE sample relative to the full population of quasars. This can be quantified, for example, using the extensive targeting on Stripe 82 (Palanque-Delabrouille et al. 2010). Similarly, to determine completeness as a function of position on the sky for quasar clustering work it is necessary to determine the fraction of quasars hiding among the unclassifiable spectra (see Appendix D). Ongoing visual inspections of these spectra will address this

| Chunk          | Bits to Select |
|----------------|----------------|
| 12, 13         | 40 AND 42      |
| 14 and onwards | 40             |

TABLE 10

THE BOSS\_TARGET1 FLAG VALUES THAT NEED TO BE SET IN ABLE TO SELECT A CORE SAMPLE FROM YEAR TWO OBSERVATIONS ONWARD.

question to some extent.

## 7. CONCLUSIONS AND FUTURE PROSPECTS

This paper describes the BOSS quasar target selection algorithms during the first two years of BOSS observations. BOSS aims to obtain spectra of a sample of  $\sim 150,000$   $z > 2.2$  quasars, in order to probe structure in the Ly $\alpha$  forest to provide a percent-level measurement of the expansion history of the Universe, by measuring baryon oscillations in the Ly $\alpha$  forest clustering. This first year was a commissioning period for quasar target selection, and the algorithms for identifying quasar candidates varied significantly over the year.

Our key results are:

- We have performed quasar target selection (QTS) over 10,200 deg<sup>2</sup> of the SDSS-III imaging footprint, producing a list of 488,000 targets. These objects are selected to be at redshift  $z > 2.2$ , motivated by the need to observe the Ly $\alpha$  forest in the BOSS wavelength coverage.
- After a year of testing and evolution of the BOSS QTS, we settled on the Extreme Deconvolution method as our uniformly-selected subsample (CORE) and a neural network Combinator for the BONUS sample.
- Having the BONUS selection allows us to implement improvements throughout the survey, e.g., through auxiliary photometric data. This has already been achieved with the inclusion of NIR *YJHK* photometry from the UKIDSS and UV data from GALEX, increasing our  $z > 2.2$  quasar yields by  $\sim 2 - 3$  deg<sup>-2</sup>.
- We obtained spectra of 54,909 objects selected by the quasar target selection algorithms over a footprint of 878 deg<sup>2</sup> during the first year of observations, the mean target density is 63.8 targets deg<sup>-2</sup>.
- Of these 54,909 spectra, 33,556 were unique objects and had high quality spectra. 11,149 had redshifts  $z < 0.02$ , and 13,580 had redshifts of  $z > 2.20$  (of which 11,263 were not previously known).
- Our mean  $z > 2.2$  quasar surface density was 15.46  $z > 2.20$  quasar deg<sup>-2</sup>, with a global efficiency of 26.0%.
- The  $z > 2.2$  objects selected by the three main methods used during Year One are found in different regions in color-color and color-magnitude space, reflecting in part the fact that the methods were trained for different redshift ranges. The three methods complemented each other well, and

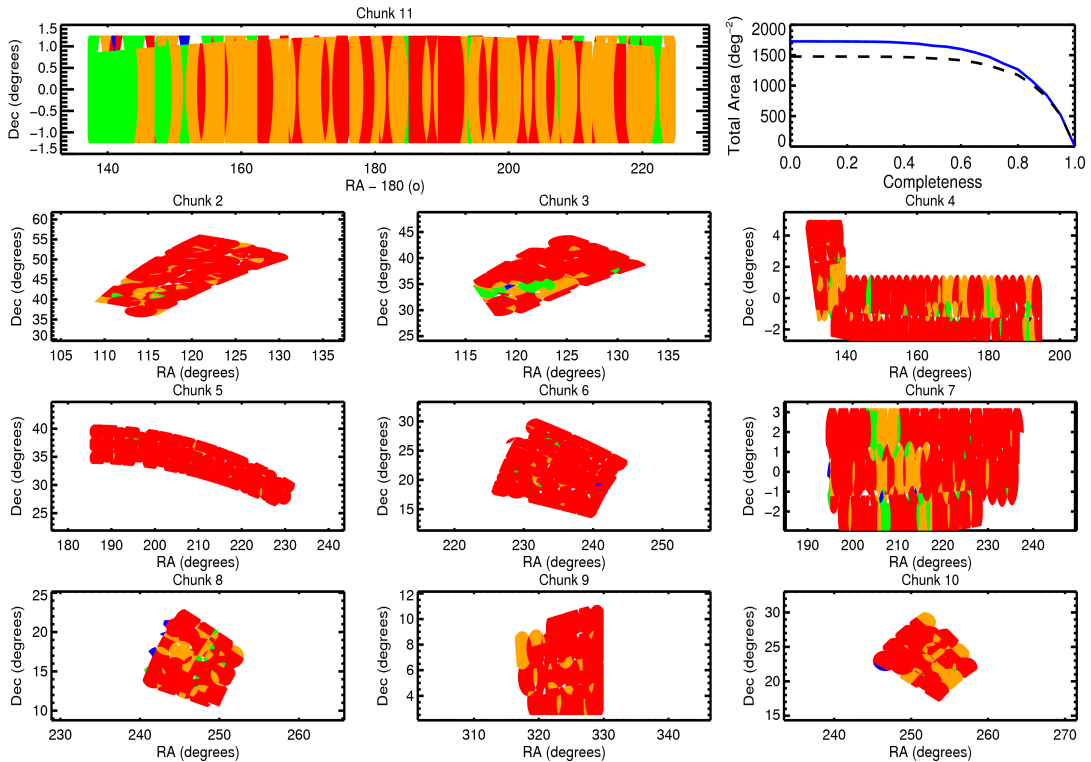


FIG. 24.— The fraction of the objects would be targeted using the final version of the XDQSO CORE quasar target selection, that were actually targeted in Year One. Each panel shows the area covered by a Chunk (2-11) from Year One. We use Chunk 11 on Stripe 82 in place of Chunk 1 (top-left panel) as Chunk 11 has superior areal coverage. Note that in some chunks, the scales on the RA and Dec axes are quite different. Color coding shows the spectroscopic completeness of the *a posteriori* XDQSO CORE sample for each area. Those areas in red have a targeting completeness above 0.75, orange have a completeness of 0.5–0.75, green have a completeness of 0.25–0.5 and the few areas in blue have a completeness below 0.25. The top right panel shows the cumulative area (blue solid line) and effective area (area  $\times$  completeness; black dashed line) above a given level of targeting completeness for the XDQSO CORE sample.

together select 60-70% of *all* quasars in our magnitude range with  $2.2 < z < 3.5$ .

- Working with single-epoch SDSS data, our current target selection algorithms slightly exceed the BOSS technical goal of selecting 15  $z > 2.2$  quasars  $\text{deg}^{-2}$  from 40 targets  $\text{deg}^{-2}$  (Eisenstein et al. 2011). The tests on Stripe 82 indicate an efficiency of 15.4 quasars  $\text{deg}^{-2}$ , of which 11.2  $\text{deg}^{-2}$  come from known quasars plus the CORE selection at 20 targets  $\text{deg}^{-2}$  (Fig. 12). We anticipate that use of auxiliary imaging data, including GALEX, UKIDSS, and additional SDSS epochs in overlap regions, will boost our efficiency by 1 – 4 quasars  $\text{deg}^{-2}$ , significantly increasing the statistical power of BOSS Ly $\alpha$  forest clustering measurements.
- All BOSS spectra from the first two years of observations, August 2009 through to July 2011, will be made publicly available in the next SDSS data release, DR9.

We continue to investigate ways to improve quasar target selection. We have already described the incorporation of data from ultraviolet (GALEX) and near-IR (UKIDSS). Data from the Wide-field Infrared Survey Explorer (WISE; Wright et al. 2010) will provide photometry at mid-infrared wavelengths for our targets; it is deep enough to detect at least the brighter quasars in the BOSS sample. Variability as measured from repeat scans

is an important method, independent of colors, to separate quasars from stars. Building on the SDSS Stripe 82 study by Sesar et al. (2007), recent investigations by Palanque-Delabrouille et al. (2010), Butler & Bloom (2011), MacLeod et al. (2011), Richards et al. (2011), Kozłowski et al. (2011) and Sarajedini et al. (2011), have re-invigorated the field of AGN identification through variability selection.

In addition to Stripe 82, roughly 50% of the SDSS imaging footprint has been imaged more than once (Aihara et al. 2011), primarily in overlaps between adjacent stripes. However, most of this area is observed only a few times, over timescales of days, rather than the desired month or year baselines that lead to efficient AGN selection.

In this regard, the Palomar Transient Factory (PTF; Law et al. 2009)<sup>38</sup> could be a natural dataset to use for this purpose. The PTF is an automated, wide-field imaging survey aimed at the exploration of the optical transient sky. PTF uses the 1.2m Schmidt telescope at Palomar Observatory with a 8  $\text{deg}^2$  field-of-view to perform large area transient searches. An area of several hundred  $\text{deg}^2$  can be imaged in one night, typically in the Mould *R*-band but also in the SDSS *g*-band. We are actively investigating the inclusion of PTF imaging data into BOSS QTS.

PTF could also potentially aid BOSS QTS by improv-

<sup>38</sup> <http://www.astro.caltech.edu/ptf/>



ing star/galaxy separation at the faint end. Potentially any of the PTF variability methods could work with other transient/variability based surveys as well, e.g. the Pan-STARRS survey, (Kaiser et al. 2002).

We kindly thank Nurten Filiz Ak for providing us with the variable BAL information and spectra shown in Fig. 15. This work was partially supported by the National Science Foundation grant AST-0607634 (N.P.R. and D.P.S.). A.D.M. was partially supported by NASA (grant NNX08AJ28G) and is a research fellow of the Alexander von Humboldt Foundation. J.B. was partially supported by NASA (grant NNX08AJ48G) and the NSF (grant AST-0908357). M.A.S. acknowledges the support of NSF grant AST-0707266. N.P.R. thanks Gabor Worsack, Nick Mostek and Anna Rosen for helpful discussions.

The observations reported here were obtained in part at the MMT Observatory, a facility operated jointly by the Smithsonian Institution and the University of Arizona. Some MMT telescope time was granted by NOAO (program 2008B-0282), through the Telescope System Instrumentation Program (TSIP). TSIP is funded by

NSF.

Funding for SDSS-III has been provided by the Alfred P. Sloan Foundation, the Participating Institutions, the National Science Foundation, and the U.S. Department of Energy. The SDSS-III web site is <http://www.sdss3.org/>. SDSS-III is managed by the Astrophysical Research Consortium for the Participating Institutions of the SDSS-III Collaboration including the University of Arizona, the Brazilian Participation Group, Brookhaven National Laboratory, University of Cambridge, University of Florida, the French Participation Group, the German Participation Group, the Instituto de Astrofísica de Canarias, the Michigan State/Notre Dame/JINA Participation Group, Johns Hopkins University, Lawrence Berkeley National Laboratory, Max Planck Institute for Astrophysics, New Mexico State University, New York University, Ohio State University, Pennsylvania State University, University of Portsmouth, Princeton University, the Spanish Participation Group, University of Tokyo, University of Utah, Vanderbilt University, University of Virginia, University of Washington, and Yale University.

*Facilities: SDSS, MMT*

## APPENDIX

### APPENDIX A: QUASAR TARGETING LOGIC CUTS

This Appendix describes the various quality cuts that objects from the SDSS photometric pipeline must satisfy to be considered for selection using the algorithms described in § 3. Target selection is restricted to sources that are unresolved in SDSS imaging, as determined by the difference between the model and PSF magnitudes (Stoughton et al. 2002); such objects are flagged with `OBJC_TYPE = 6` in the outputs of the SDSS photometric pipeline (Lupton et al. 2001).

To reduce processing time, we precalculate a number of combinations of flags from the photometric pipeline and the photometric calibration (Padmanabhan et al. 2008). These flags are used in different ways for different target selection algorithms, as summarized in Table 11: for example, we are not as stringent for objects selected as FIRST radio sources (§ 3.6) as we are for those objects which are selected by their colors. In the main text, we refer to various combinations of the six flag combinations described in this Appendix.

#### *Is the Photometry Clean?*

The photometric pipeline sets a series of flag bits for each detected object which identify problems with the processing of the SDSS photometry, ranging from the presence of bad columns to issues with deblending (Stoughton et al. 2002). These are particularly useful in recognizing when the photometry might be poor, and therefore color selection of targets unreliable. The detailed meaning of the specific flag bits in what follows is described in Stoughton et al. (2002) and the SDSS-III web page<sup>39</sup>; the logic behind these flag combinations is given in Richards et al. (2002).

Note that unlike the latter paper, we did not calculate and apply the flag checks on each band separately, and just use the flags associated with the union of the detections in the five SDSS bands. While this could cause us to reject some genuine quasars, checks on Stripe 82 (where the flag checking on the coadded data was significantly less strict; see below) showed only a statistically insignificant 1% difference in the number of quasars identified.

We first define a combination of flag bits that denotes whether the source in question was adversely affected by interpolation across bad pixels, bad columns, or bleed trails:

```
INTERP_PROBLEMS = (PSF_FLUX_INTERP && (gerr > 0.2 || rerr > 0.2 || ierr > 0.2)) || BAD_COUNTS_ERROR || (INTERP_CENTER && CR),
```

a combination that identifies objects in which the deblending of overlapping images may be questionable:

```
DEBLEND_PROBLEMS = PEAKCENTER || NOTCHECKED || (DEBLEND_NOPEAK && (gerr > 0.2 || rerr > 0.2 || ierr > 0.2))
```

and a combination which identifies objects with detectable proper motion between the exposures in the different SDSS filters (asteroids):

<sup>39</sup> [http://www.sdss3.org/dr8/algorithms/photo\\_flags.php](http://www.sdss3.org/dr8/algorithms/photo_flags.php)



| Flag Name           | Bitmask | Description                                     | CORE/BONUS | FIRST | KNOWN |
|---------------------|---------|---|------------|-------|-------|
| GOOD                | 11      | Target has clean SDSS photometry                | ✓          | ×     | ×     |
| GMAG_BITMASK        | 11      | Target meets the magnitude limits               | ✓          | ×     | ×     |
| GMAG_BITMASK_NOB    | 12      | Used when no bright cut is required             | ×          | ✓     | ×     |
| RESOLVE_BITMASK     | 13      | Target is a primary target in SDSS photometry   | ✓          | ✓     | ✓     |
| BOUNDS_BITMASK      | 16      | Target lies within the SDSS target footprint    | ×          | ✓     | ✓     |
| FIRST_COLOR_BITMASK | 17      | Color cut for objects that match a radio source | ×          | ✓     | ×     |

TABLE 11  
 FLAGS USED BY BOSS QUASAR TARGET SELECTION.

$$\text{MOVED} = \text{DEBLENDED\_AS\_MOVING} \ \&\& \ (\text{rowv}/\text{rowverr})^2 + (\text{colv}/\text{colverr})^2 > 3^2.$$

Here, the symbols (&&, ||, !) have their standard meanings from Boolean logic. The quantities rerr, gerr, and ierr are the quoted uncertainties in the PSF photometry in  $g$ ,  $r$ , and  $i$  respectively, rowv and colv are the measured proper motion along the rows and columns of the CCD, and rowverr and colverr are their errors.

A source is considered to have clean photometry if it satisfies the following:

$$\text{GOOD} = \text{BINNED1} \ \&\& \ \text{!BRIGHT} \ \&\& \ \text{!SATURATED} \ \&\& \ \text{!EDGE} \ \&\& \ \text{!BLENDED} \ \&\& \ \text{!NODEBLEND} \ \&\& \ \text{!NOPROFILE} \ \&\& \ \text{!INTERP\_PROBLEMS} \ \&\& \ \text{!DEBLEND\_PROBLEMS} \ \&\& \ \text{!MOVED}.$$

### Magnitude Limits

The GMAG\_BITMASK records whether a target satisfies the magnitude limits required to be targeted as a quasar. Magnitude cuts are made on PSF magnitudes measured by the SDSS, corrected for Schlegel et al. (1998) Galactic extinction. These limits are encoded in a flag:

$$\text{GMAG\_BITMASK} = (g \leq 22 \ \parallel \ r \leq 21.85) \ \&\& \ i \geq 17.8.$$

This includes a cut at the bright end, reflecting the fact that bright  $z > 2.2$  quasars are extraordinarily rare. We also define a variant of this flag:

$$\text{GMAG\_BITMASK\_NOB} = (g \leq 22 \ \parallel \ r \leq 21.85),$$

to be used when no bright cut is required—such as when retargeting known quasars or FIRST objects.

### Resolving Image Overlaps

The DR8 paper (Aihara et al. 2011) describes the algorithm used to define the primary detection of a given object, if it lies in the  $\sim 50\%$  of the SDSS footprint covered by more than one scan. The RESOLVE\_BITMASK records whether a source is a primary target in the SDSS photometry.

### Boundary Logic

The BOUNDS\_BITMASK records whether a source is within the footprint of the SDSS imaging, which is useful for keeping track of data from the ancillary surveys (FIRST, UKIDSS, GALEX) used in the target selection.

### FIRST Color Logic

We saw in § 3.6 that we could limit the number of  $z < 2.2$  sources targeted by FIRST with  $u - g$  color cut. Thus we define:

$$\text{FIRST\_COLOR\_BITMASK} = (u - g > 0.4).$$

### Conditions for Generation of Stripe 82 Coadded Photometry

The single-epoch photometry used for coaddition on Stripe 82 is first vetted by a series of quality cuts. All fluxes used in the coaddition are limited by the following conditions:

- They must be primary, i.e., RESOLVE\_BITMASK must be true;
- They must be observed under photometric conditions (an important issue from Stripe 82, as it was repeatedly observed under non-photometric conditions as part of the SDSS Supernova Survey; see Frieman et al. 2008);
- They must have a positive estimated inverse flux variance (zero values are indicative of problems with the data);
- They must pass various flag cuts:  
 (!DEBLEND\_TOO\_MANY\_PEAKS && !SATUR && !BADSKY && !SATUR\_CENTER && !INTERP\_CENTER && !DEBLEND\_NOPEAK && !PSF\_FLUX\_INTERP).

| Area Name     | Target Selection Version label | Tiling Priority  |
|---------------|--------------------------------|--|
| Chunk 1       | comm                           | all quasar targets before galaxy targets                   |
| Chunk 2       | comm2                          | "  |
| Chunks 3, 4   | main002                        | all galaxy targets before quasar targets                   |
| Chunks 5, 6   | main005                        | "  |
| Chunks 7, 8   | main006                        | "  |
| Chunk 9       | main006-masksgc1               | "  |
| Chunk 10      | main006-collate-maskngc        | KNOWN before galaxies; galaxies before CORE, BONUS, FIRST. |
| Chunk 11      | vcat-2010-07-02                | "  |
| Chunks 12, 13 | main008-sgc40                  | "  |
| Chunk 14      | main008-edcore-maskngc40       | KNOWN, CORE, FIRST over galaxies; galaxies before BONUS.   |
| Chunk 15      | main008-edfinal-maskngc40      | "  |
| Chunk 16      | main010-maskngc40              | "  |
| Chunk 17      | main011-maskngc40              | "  |
| Chunk 18      | main012-nosuppz-maskngc40      | "  |

TABLE 12

THIS TABLE LISTS THE INTERNAL LABEL OF THE VERSION OF TARGET SELECTION CODE USED IN EACH CHUNK, AND ALSO EXPLAINS THE RELATIVE PRIORITY OF DIFFERENT CLASSES OF TARGET IN THE CASE OF FIBER COLLISIONS.

## APPENDIX B: FLOWCHART FOR YEAR ONE QTS AND TARGET SELECTION VERSIONS

Figure 2 is a flowchart which describes quasar target selection as it was carried out in Year Two and beyond. Fig. 25 gives the equivalent for Year One. The red numbers give the bitwise value for the `boss_target1` flag. Those values with asterisks have target flags that were obsolete after the first year of target selection.

Table 12 gives the BOSS quasar target selection version code label for each chunk. Sheldon et al. (2011, in prep.) will describe in detail the differences between these versions.

Because of the 62'' diameter of the cladding around each optical fiber, two objects with separation smaller than that angle cannot both be observed on a given spectroscopic plate, which means that an algorithm to decide which of two objects in such a collision should take precedence is needed. Our thinking on this evolved throughout Year One; the rules for each chunk are given in Table 12. By Chunk 14, we settled on giving KNOWN, CORE, and FIRST quasar targets higher priority than galaxy targets, with BONUS at lower priority.

## APPENDIX C: QUASARS FROM THE MMT PILOT PROGRAM

Prior to the commencement of BOSS spectroscopy, we carried out spectroscopy of quasar candidates selected from coadded photometry in SDSS Stripe 82 to increase the number of faint quasars available in the BOSS redshift range for testing and training of BOSS targeting algorithms. Candidate quasars for these observations were selected in two ways: first, using very inclusive cuts in the  $(\chi^2_{\text{phot}}, \chi^2_{\text{star}})$  plane, where these  $\chi^2$  statistics are as defined in Hennawi et al. (2010), and second, using the methods outlined in Richards et al. (2009a,b). These observations were intended to include as large a sample of  $z > 2.2$  quasars as possible, but do not represent a statistically well-defined sample, so we do not describe their selection in greater detail.

Observations of these candidates were carried out in queue mode between 2008 September and 2009 January using the Hectospec multi-fiber spectrograph (Fabricant et al. 2005) on the 6.5m Multiple Mirror Telescope (MMT). The data were reduced using Juan Cabanela's ESPECROAD<sup>40</sup> pipeline, an external version of the SAO SPECROAD pipeline (Mink et al. 2007). Quasars were identified by eye, and redshifts were measured using IRAF.

The MMT program was conducted before the release of the SDSS DR7 quasar catalog. In addition, BOSS targets all confirmed quasars from the MMT program for re-observation (§ 3.7). Thus, most of the MMT observations have been superseded by subsequent SDSS DR7 or BOSS spectroscopy at better resolution, wavelength coverage and signal-to-noise ratio. In Tables 13–14, we provide positions, PSF photometry (as observed, uncorrected for Galactic extinction), and redshifts for confirmed quasars from the MMT survey. Objects that are not flagged Primary in the CAS are listed separately. Over 99% of quasars that *were* observed a second time have redshifts in agreement (to  $\Delta z < 0.05$ ) between the MMT survey and the SDSS/BOSS pipelines.

## APPENDIX D: PERFORMANCE OF ZWARNING

Here we present the fraction of spectroscopically observed quasar targets which are flagged with `zWarning`  $\neq 0$  by the spectroscopic pipeline. As described in Adelman-McCarthy et al. (2008), this is an indication that the automatically derived redshift and classification are not reliable.

Table 15 gives the three most common of the `zWarning` flag bits for quasar targets, a short description of each, and the number of objects with these bits set. 1851 objects have both bits 2 and 6 set. All other `zWarning` bits are set in 200 or fewer objects, representing less than 1% of the sample.

Fig. 26 gives the fraction of objects with good, `zWarning=0`, spectra as a function of *i*-band magnitude and spectroscopic S/N per pixel (median over the spectrum). The (black) histogram shows the distribution of all objects to give a sense of where the majority of the signal arises from. The most common flag is `SMALL_DELTA_CHI2`, indicating that

<sup>40</sup> <http://iparrizar.mnstate.edu/~juan/research/ESPECROAD/index.php>

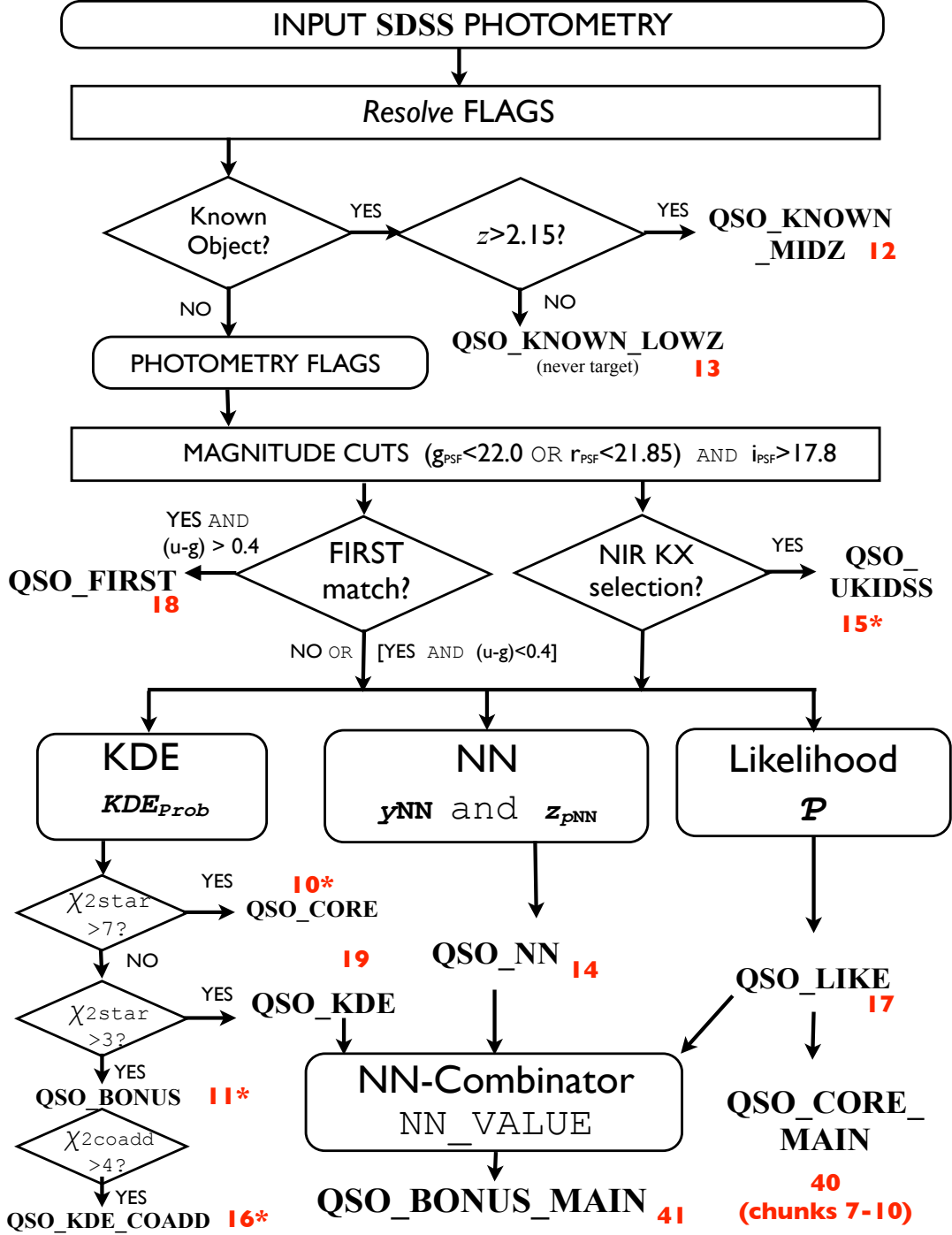


FIG. 25.— Schematic flowchart for the BOSS quasar target selection during the first year of observations, to be compared with the Year Two version in Figure 2. The red numbers give the bitwise value for the `boss_target1` flag (see Table 2). The red numbers with asterisks have target flags that were obsolete after the first year of target selection. The input SDSS photometry is described in Section 2 and the algorithm to resolve overlapping images is explained in Aihara et al. (2011). Previously known objects are described in Section 3.7 and the FIRST radio selection is given in Section 3.6. The photometry flags are discussed in Section 2.2 and in Appendix A. The three target selection methods (KDE, NN, and Likelihood) are described in Richards et al. (2009a, and references therein), Yèche et al. (2010) and Kirkpatrick et al. (2011), respectively, and are outlined in Section 3. Each of these methods produces one or more continuous parameters that quantify the confidence that the object in question is a high-redshift quasar:  $\mathcal{P}$  for the Likelihood method;  $KDE_{Prob}$  and  $\chi^2_{star}$  for the KDE method;  $y_{NN}$  and  $z_{p,NN}$  for the first Neural Network and `NN_VALUE` for Neural Network Combinator. The target selection flag bits are also shown, with descriptions in Table 2. Objects with  $i < 17.8$  with FIRST counterparts are selected for spectroscopy.

| RA          | DEC         | u      | u <sub>err</sub> | g      | g <sub>err</sub> | r      | r <sub>err</sub> | i      | i <sub>err</sub> | z      | z <sub>err</sub> | redshift | z |
|-------------|-------------|--------|------------------|--------|------------------|--------|------------------|--------|------------------|--------|------------------|----------|---|
| 00 46 00.48 | +00 05 43.7 | 23.488 | 0.384            | 22.241 | 0.070            | 21.775 | 0.062            | 21.365 | 0.060            | 20.455 | 0.119            | 2.460    |   |
| 00 46 31.22 | -00 11 46.2 | 22.802 | 0.381            | 21.535 | 0.048            | 20.541 | 0.032            | 20.217 | 0.041            | 19.445 | 0.062            | 2.451    |   |
| 00 46 42.32 | -00 07 53.7 | 20.947 | 0.074            | 20.282 | 0.028            | 20.031 | 0.027            | 19.882 | 0.039            | 19.719 | 0.072            | 2.234    |   |
| 00 46 47.93 | -00 06 17.4 | 20.005 | 0.044            | 19.296 | 0.023            | 19.140 | 0.021            | 19.070 | 0.035            | 19.002 | 0.047            | 2.850    |   |
| 00 47 20.78 | +00 18 06.7 | 21.252 | 0.091            | 20.969 | 0.034            | 20.747 | 0.036            | 20.544 | 0.039            | 20.919 | 0.198            | 1.610    |   |
| 00 47 21.06 | +00 09 32.3 | 25.176 | 0.529            | 21.628 | 0.045            | 20.690 | 0.030            | 20.393 | 0.033            | 20.272 | 0.104            | 3.573    |   |
| 00 47 32.61 | -00 16 35.7 | 23.181 | 0.300            | 22.038 | 0.062            | 21.825 | 0.067            | 21.606 | 0.076            | 20.872 | 0.160            | 2.610    |   |
| 00 47 43.04 | -00 23 32.0 | 23.872 | 0.475            | 22.251 | 0.074            | 22.077 | 0.084            | 21.928 | 0.100            | 21.560 | 0.281            | 2.837    |   |
| 00 47 51.18 | -00 15 44.9 | 21.865 | 0.111            | 21.065 | 0.031            | 20.686 | 0.038            | 20.524 | 0.038            | 20.174 | 0.089            | 2.477    |   |
| 00 47 55.49 | +00 14 42.3 | 23.320 | 0.546            | 21.762 | 0.053            | 21.431 | 0.056            | 21.214 | 0.064            | 20.483 | 0.138            | 0.822    |   |

TABLE 13

QUASARS DISCOVERED IN THE MMT SURVEY. MANY OF THESE OBJECTS WERE SUBSEQUENTLY CONFIRMED IN THE SDSS DR7 QUASAR CATALOG OR IN THE BOSS. IMAGING INFORMATION IS TAKEN FROM THE SDSS DR8 CATALOG ARCHIVE SERVER. THE FIRST 10 OBJECTS ARE GIVEN TO SHOW THE FORMAT OF THE TABLE. THIS TABLE IS AVAILABLE IN ITS ENTIRETY IN MACHINE-READABLE AND VIRTUAL OBSERVATORY (VO) FORMS IN THE ONLINE JOURNAL.

| RA          | DEC         | u      | u <sub>err</sub> | g      | g <sub>err</sub> | r      | r <sub>err</sub> | i      | i <sub>err</sub> | z      | z <sub>err</sub> | redshift | z |
|-------------|-------------|--------|------------------|--------|------------------|--------|------------------|--------|------------------|--------|------------------|----------|---|
| 00 46 39.91 | -00 05 03.7 | 21.784 | 0.184            | 21.572 | 0.075            | 21.498 | 0.096            | 21.396 | 0.114            | 20.750 | 0.264            | 2.235    |   |
| 00 57 16.14 | +00 21 04.7 | 21.896 | 0.153            | 21.700 | 0.090            | 21.649 | 0.226            | 21.116 | 0.316            | 22.734 | 0.385            | 2.110    |   |
| 02 33 23.79 | -00 02 11.1 | 23.946 | 0.659            | 21.480 | 0.054            | 22.083 | 0.138            | 21.755 | 0.151            | 22.929 | 0.861            | 2.402    |   |
| 03 37 10.37 | +00 23 55.1 | 20.082 | 0.074            | 19.279 | 0.123            | 18.978 | 0.150            | 18.922 | 0.166            | 18.938 | 0.129            | 2.920    |   |
| 03 37 33.89 | -00 03 04.7 | 21.458 | 0.120            | 20.264 | 0.259            | 19.667 | 0.021            | 19.282 | 0.024            | 19.127 | 0.050            | 0.671    |   |
| 22 58 58.68 | -00 20 38.0 | 21.924 | 0.317            | 21.373 | 0.078            | 21.077 | 0.085            | 20.967 | 0.105            | 20.497 | 0.294            | 2.421    |   |
| 23 07 33.34 | -00 17 58.9 | 21.981 | 0.186            | 21.884 | 0.088            | 22.491 | 0.209            | 21.815 | 0.163            | 21.323 | 0.334            | 2.765    |   |

TABLE 14

QUASARS DISCOVERED IN THE MMT SURVEY THAT ARE NON-PRIMARY IN SDSS DR8 IMAGING

| zWarning flag     | bit | Description  | No. of objects in Year One (unique) |
|-------------------|-----|--|-------------------------------------|
| No flag set       | -   | Spectrum has no known problems.  | 35,305 (33,556)                     |
| SMALL_DELTA_CHI2  | 2   | $\chi^2$ best fit is too close to that of second best ( $< 0.01$ in reduced $\chi^2$ ) | 16,765 (15,982)                     |
| NEGATIVE.EMISSION | 6   | a quasar line exhibits negative emission.  | 620 (597)                           |

TABLE 15

ZWARNING FLAG BITS AND YEAR ONE QUASAR SPECTROSCOPY

there is more than one template that fits the spectrum. This is most commonly seen in low S/N spectra. We hope that planned visual inspections of those objects with zWarning  $\neq 0$  will allow positive identification of many of these objects, boosting the number of confirmed high-redshift quasars.

## REFERENCES

- Abazajian K., et al., 2004, AJ, 128, 502  
Abazajian K. N., et al., 2009, ApJS, 182, 543  
Adelman-McCarthy J. K., et al., 2006, ApJS, 162, 38  
Adelman-McCarthy J. K., et al., 2008, ApJS, 175, 297  
Aihara H., et al., 2011, ApJS, 193, 29  
Barenboim G., Fernández Martínez E., Mena O., Verde L., 2010, Journal of Cosmology and Astro-Particle Physics, 3, 8  
Becker R. H., White R. L., Helfand D. J., 1995, ApJ, 450, 559  
Belokurov V., et al., 2006, ApJ Lett., 642, L137  
Blake C., Glazebrook K., 2003, ApJ, 594, 665  
Blanton M. R., Lin H., Lupton R. H., Maley F. M., Young N., Zehavi I., Loveday J., 2003, AJ, 125, 2276  
Bond J. R., Efstathiou G., 1984, ApJ Lett., 285, L45  
Bond J. R., Efstathiou G., 1987, MNRAS, 226, 655  
Bovy J., et al., 2011, ApJ, 729, 141  
Bovy J., Hogg D. W., Roweis S. T., 2009, AOAS, in press, arXiv:0905.2979v1  
Butler N. R., Bloom J. S., 2011, AJ, 141, 93  
Casali M., et al., 2007, Astron. & Astrophys., 467, 777  
Chiu K., Richards G. T., Hewett P. C., Maddox N., 2007, MNRAS, 375, 1180  
Cole S., et al., 2005, MNRAS, 362, 505  
Croom S. M., et al., 2005, MNRAS, 356, 415  
Croom S. M., et al., 2009, MNRAS, 392, 19  
Croom S. M., Smith R. J., Boyle B. J., Shanks T., Miller L., Outram P. J., Loaring N. S., 2004, MNRAS, 349, 1397  
Croom S. M., Warren S. J., Glazebrook K., 2001, MNRAS, 328, 150  
Croton D. J., 2009, MNRAS, 394, 1109  
Dye S., et al., 2006, MNRAS, 372, 1227  
Eisenstein D. J., et al., 2005, ApJ, 633, 560  
Eisenstein D. J., Hu W., 1998, ApJ, 496, 605  
Eisenstein D. J., Weinberg D. H., et al., 2011, arXiv:1101.1529v1  
Fabricant D., et al., 2005, PASP, 117, 1411  
Fan X., 1999, AJ, 117, 2528  
Frieman J. A., et al., 2008, AJ, 135, 338  
Fukugita M., Ichikawa T., Gunn J. E., Doi M., Shimasaku K., Schneider D. P., 1996, AJ, 111, 1748  
Gray A. G., Moore A. W., 2003 Third SIAM International Conf. on Data Mining eds. D. Barbara and C. Kamath, p. 203  
Gray A. G., Riegel A. W., 2006 Computational Statistics Eds. A. Rizzi and M. Vichi, p. 845  
Gunn J. E., et al., 1998, AJ, 116, 3040  
Gunn J. E., et al., 2006, AJ, 131, 2332  
Hambly N. C., et al., 2008, MNRAS, 384, 637  
Hennawi J. F., et al., 2010, ApJ, 719, 1672  
Hewett P. C., Warren S. J., Leggett S. K., Hodgkin S. T., 2006, MNRAS, 367, 454  
Hodgkin S. T., Irwin M. J., Hewett P. C., Warren S. J., 2009, MNRAS, 394, 675  
Hogg D. W., Finkbeiner D. P., Schlegel D. J., Gunn J. E., 2001, AJ, 122, 2129  
Holtzman J. A., 1989, ApJS, 71, 1  
Hopkins P. F., Richards G. T., Hernquist L., 2007, ApJ, 654, 731  
Ibata R. A., Gilmore G., Irwin M. J., 1995, MNRAS, 277, 781  
Ibata R. A., Wyse R. F. G., Gilmore G., Irwin M. J., Suntzeff N. B., 1997, AJ, 113, 634  
Ivezic Ž., et al., 2004, Astronomische Nachrichten, 325, 583

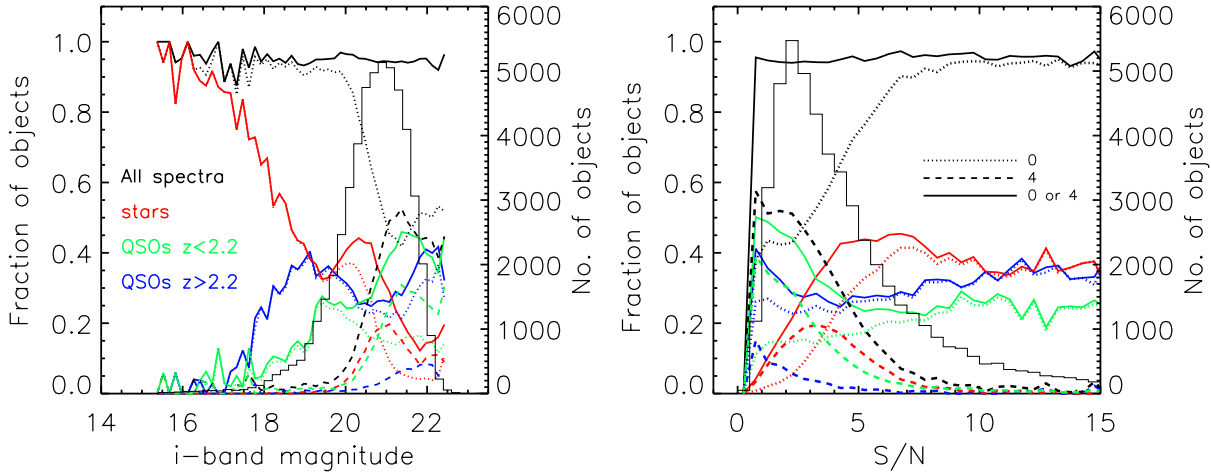


FIG. 26.— The fraction of Year One quasar targets with good redshifts ( $z\text{Warning}=0$ ) as a function of  $i$ -band magnitude (*left*) and median spectroscopic  $S/N$  (*right*). Objects with  $z\text{Warning}=0$  are given by the dotted lines, objects with  $z\text{Warning}=4$  are given by the dashed lines, and objects with  $z\text{Warning}=0 \parallel z\text{Warning}=4$ —representing 95% of our sample—are given by the solid lines (i.e. dashed+dotted = solid). Also shown separately are objects classified spectroscopically as stars (red) and high (blue) and low (green)-redshift quasars, as indicated. Their sum is given by the black lines. Also shown as the histogram and the right-hand y-axis is the distribution function of objects.

- Jiang L., et al., 2006, *AJ*, 131, 2788  
Kaiser N., et al., 2002, in J. A. Tyson & S. Wolff ed., *Society of Photo-Optical Instrumentation Engineers (SPIE) Conference Series Vol. 4836, Pan-STARRS: A Large Synoptic Survey Telescope Array*, pp 154–164  
Kirkpatrick J. A., Schlegel D. J., Ross N. P., Myers A. D., Hennawi J. F., Schneider D. P., Weaver B. A., 2011, arXiv:1104.4995v1  
Komatsu E., et al., 2011, *ApJS*, 192, 18  
Kozłowski S., Kochanek C. S., Udalski A., 2011, arXiv:1102.0703v1  
Larson D., et al., 2011, *ApJS*, 192, 16  
Law N. M., et al., 2009, *PASP*, 121, 1395  
Lawrence A., et al., 2007, *MNRAS*, 379, 1599  
Loverde M., Marnerides S., Hui L., Ménard B., Lidz A., 2010, *Phys. Rev. D*, 82, 103507  
Lupton R., Gunn J. E., Ivezić Z., Knapp G. R., Kent S., 2001, in F. R. Harnden Jr., F. A. Primini, & H. E. Payne ed., *Astronomical Data Analysis Software and Systems XVI* Vol. 238 of *Astronomical Society of the Pacific Conference Series, The SDSS Imaging Pipelines*, p. 269  
Lupton R. H., Gunn J. E., Szalay A. S., 1999, *AJ*, 118, 1406  
MacLeod C. L., et al., 2011, *ApJ*, 728, 26  
Maddox N., Hewett P. C., Warren S. J., Croom S. M., 2008, *MNRAS*, 386, 1605  
Martin D. C., et al., 2005, *ApJ Lett.*, 619, L1  
McDonald P., Eisenstein D. J., 2007, *Phys. Rev. D*, 76, 063009  
McDonald P., et al., 2006, *ApJS*, 163, 80  
McQuinn M., White M., 2011, arXiv:1102.1752v1  
Meiksin A., White M., Peacock J. A., 1999, *MNRAS*, 304, 851  
Mink D. J., Wyatt W. F., Caldwell N., Conroy M. A., Furesz G., Tokarz S. P., 2007, in R. A. Shaw, F. Hill, & D. J. Bell ed., *Astronomical Data Analysis Software and Systems XVI* Vol. 376 of *Astronomical Society of the Pacific Conference Series, Automating Reduction of Multifiber Spectra from the MMT Hectospec and Hectochelle*, p. 249  
Myers A. D., et al., 2006, *ApJ*, 638, 622  
Norman M. L., Paschos P., Harkness R., 2009, *Journal of Physics Conference Series*, 180, 012021  
Oke J. B., Gunn J. E., 1983, *ApJ*, 266, 713  
Osmer P. S., 1982, *ApJ*, 253, 28  
Padmanabhan N., et al., 2008, *ApJ*, 674, 1217  
Palanque-Delabrouille N., Yèche C., Myers A. D., Petitjean P., Ross N. P., Sheldon E., Aubourg E., Delubac T., Le Goff J., Paris I., Rich J., Dawson K. S., Schneider D. P., Weaver B. A., 2010, ArXiv e-prints  
Peebles P. J. E., Yu J. T., 1970, *ApJ*, 162, 815  
Peth M. A., Ross N. P., Schneider D. P., 2011, *AJ*, 141, 105  
Pier J. R., Munn J. A., Hindsley R. B., Hennessy G. S., Kent S. M., Lupton R. H., Ivezić Z., 2003, *AJ*, 125, 1559  
Prochaska J. X., Worseck G., O’Meara J. M., 2009, *ApJ Lett.*, 705, L113  
Richards G. T., et al., 2002, *AJ*, 123, 2945  
Richards G. T., et al., 2003, *AJ*, 126, 1131  
Richards G. T., et al., 2004, *ApJS*, 155, 257  
Richards G. T., et al., 2006, *AJ*, 131, 2766  
Richards G. T., et al., 2009a, *ApJS*, 180, 67  
Richards G. T., et al., 2009b, *AJ*, 137, 3884  
Richards J. W., et al., 2011, arXiv:1101.1959v1  
Riegel R., Gray A., Richards G., 2008 *SIAM International Conference on Data Mining (SDM)* Ed. N. Abe et al., p. 208  
Sarajedini V. L., Koo D. C., Klesman A. J., Laird E. S., Perez Gonzalez P. G., Mozena M., 2011, ArXiv e-prints  
Schlegel D., White M., Eisenstein D., 2009, in *Astro2010: The Astronomy and Astrophysics Decadal Survey Vol. 2010 of Astronomy, The Baryon Oscillation Spectroscopic Survey: Precision measurement of the absolute cosmic distance scale*, p. 314  
Schlegel D. J., et al., 2007, in *BAAS Vol. 38, SDSS-III: The Baryon Oscillation Spectroscopic Survey (BOSS)*, p. 966  
Schlegel D. J., Finkbeiner D. P., Davis M., 1998, *ApJ*, 500, 525  
Schmidt M., Schneider D. P., Gunn J. E., 1995, *AJ*, 110, 68  
Schneider D. P., et al., 2010, *AJ*, 139, 2360  
Seo H.-J., Eisenstein D. J., 2003, *ApJ*, 598, 720  
Sesar B., et al., 2007, *AJ*, 134, 2236  
Sharp R. G., Sabbey C. N., Vivas A. K., Oemler A., McMahon R. G., Hodgkin S. T., Coppi P. S., 2002, *MNRAS*, 337, 1153  
Slosar A., et al., 2011, arXiv:1104.5244v1  
Slosar A., Ho S., White M., Louis T., 2009, *Journal of Cosmology and Astro-Particle Physics*, 10, 19  
Smail I., et al., 2008, *MNRAS*, 389, 407  
Smith J. A., et al., 2002, *AJ*, 123, 2121  
Stoughton C., et al., 2002, *AJ*, 123, 485  
Sunyaev R. A., Zeldovich Y. B., 1970, *Ap&SS*, 7, 3  
Tucker D. L., et al., 2006, *Astronomische Nachrichten*, 327, 821  
Warren S. J., Hewett P. C., Foltz C. B., 2000, *MNRAS*, 312, 827  
White M., 2003, in *The Davis Meeting On Cosmic Inflation The Ly- $\alpha$  forest*  
White M., Pope A., Carlson J., Heitmann K., Habib S., Fasel P., Daniel D., Lukic Z., 2010, *ApJ*, 713, 383  
Worseck G., Prochaska J. X., 2011, *ApJ*, 728, 23  
Wright E. L., et al., 2010, *AJ*, 140, 1868  
Wu X., Jia Z., 2010, *MNRAS*, 406, 1583  
Yèche C., Petitjean P., Rich J., Aubourg E., Busca N., Hamilton J., Le Goff J., Paris I., Peirani S., Pichon C., Rollinde E., Vargas-Magaña M., 2010, *Astron. & Astrophys.*, 523, A14  
York D. G., et al., 2000, *AJ*, 120, 1579